AD-A179 500 SUPERSONIC BOUNDARY LAYER STABILITY OVER A ROUGH WALL (U) MONTANA STATE UNIV BOZEMAN DEPT OF MECHANICAL ENGINEERING A DEMETRIADES JAN 85 AFOSR-TR-87-0445 1/1

UNCLASSIFIED AFOSR-80-0267 F/G 20/4 NL

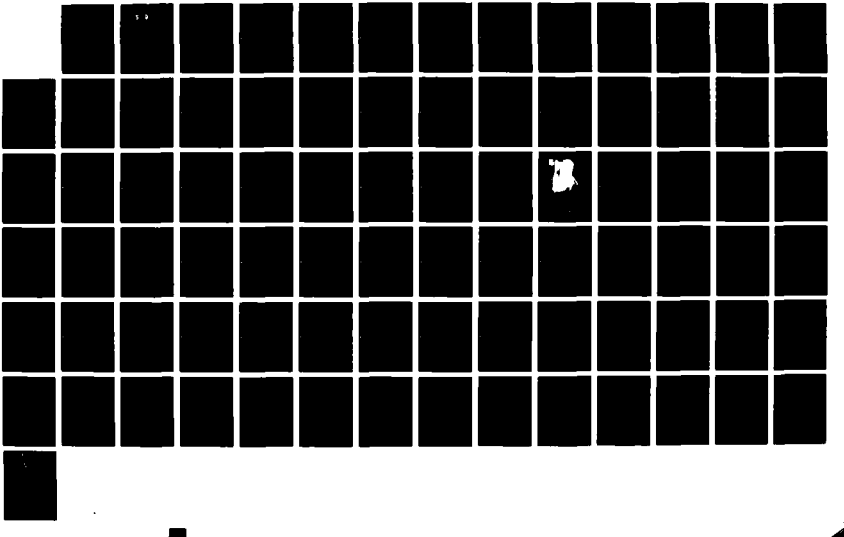

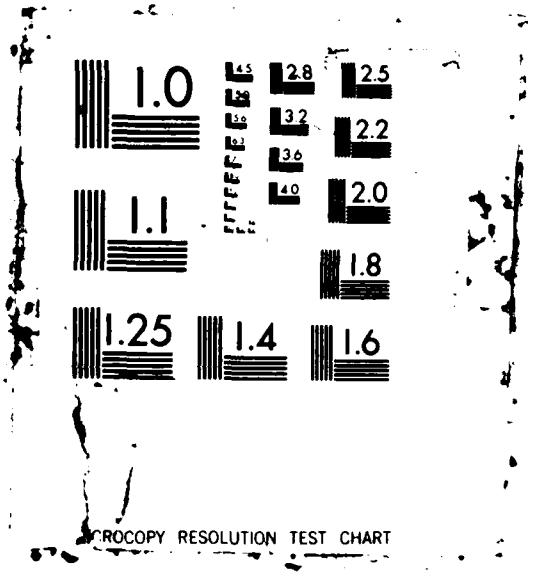
1.0
1.1
1.25
1.4
1.6
2.8
3.2
3.6
4.0
2.5
2.2
2.0
1.8
CROCOPY RESOLUTION TEST CHART

AD-A179 580

REPORT DOCUMENTATION PAGE

1a. REPORT SECURITY CLASSIFICATION: UNCLASSIFIED	1b. RESTRICTIVE MARKINGS
2a. SECURITY CLASSIFICATION AUTHORITY	3. DISTRIBUTION/AVAILABILITY OF REPORT: APPROVED FOR PUBLIC RELEASE DISTRIBUTION IS UNLIMITED
2b. DECLASSIFICATION/DOWNGRADING SCHEDULE	
4. PERFORMING ORGANIZATION REPORT NUMBER(S)	5. MONITORING ORGANIZATION REPORT NUMBER(S): AFOSR-TR- 87-0445
6a. NAME OF PERFORMING ORGANIZATION: MONTANA STATE UNIVERSITY; 6b. OFFICE SYMBOL (If applicable)	7a. NAME OF MONITORING ORGANIZATION: AFOSR/NA
6c. ADDRESS (City, State and ZIP Code): BOZEMAN, MONTANA 59717	7b. ADDRESS (City, State and ZIP Code): BUILDING 410, BOLLING AFB, DC 20332-6448
8a. NAME OF FUNDING/SPONSORING ORGANIZATION: AFOSR/NA; 8b. OFFICE SYMBOL (If applicable): NA	9. PROCUREMENT INSTRUMENT IDENTIFICATION NUMBER: AFOSR GRANT 80-0267
8c. ADDRESS (City, State and ZIP Code): BUILDING 410, BOLLING AFB, DC 20332-6448	10. SOURCE OF FUNDING NOS: PROGRAM ELEMENT NO 61102F; PROJECT NO. 2307; TASK NO. A2; WORK UNIT NO.
11. TITLE (Include Security Classification): (U) SUPERSONIC BOUNDARY LAYER STABILITY OVER A ROUGH WALL	
12. PERSONAL AUTHOR(S): A. DEMETRIADES	
13a. TYPE OF REPORT: FINAL; 13b. TIME COVERED: FROM 1Aug 80 TO 30Sep 84; 14. DATE OF REPORT (Yr., Mo., Day): JANUARY 1985; 15. PAGE COUNT: 81	
16. SUPPLEMENTARY NOTATION: A. DEMETRIADES	

17. COSATI CODES		
FIELD	GROUP	SUB GR

18. SUBJECT TERMS (Continue on reverse if necessary and identify by block number): BOUNDARY LAYER, ROUGHNESS, SUPERSONIC

19. ABSTRACT (Continue on reverse if necessary and identify by block number):

Measurements of the growth or damping of natural disturbances in a laminar boundary layer at Mach 3 have been made. Unit Reynolds number and roughness effects have been documented. A primary mode, 3-dimensional unstable region was identified which has a minimum critical Reynolds number of 180. Amplification rates within this region agree well with theory except that show higher amplification than expected. A second unstable region was discovered between this region and the transition onset defined by the first departure from laminar similarity. Much higher frequencies and amplification rates are found in this region. Increasing unit Reynolds number decreases overall amplification rates and increases transition distance. Random roughness was found unsuitable for stability studies.

20. DISTRIBUTION/AVAILABILITY OF ABSTRACT: UNCLASSIFIED/UNLIMITED ☒ SAME AS RPT ☐ DTIC USERS ☐	21. ABSTRACT SECURITY CLASSIFICATION: UNCLASSIFIED
22a. NAME OF RESPONSIBLE INDIVIDUAL: JAMES M MCMICHAEL	22b. TELEPHONE NUMBER (Include Area Code): 202-767-4935; 22c. OFFICE SYMBOL: AFOSR/NA

DD FORM 1473, 83 APR EDITION OF 1 JAN 73 IS OBSOLETE

SECURITY CLASSIFICATION OF THIS PAGE

SUPERSONIC BOUNDARY LAYER STABILITY OVER A ROUGH WALL

Final Report
AFOSR Grant No. 80-0267
For the Periods 9/80 - 8/82 and 9/83 - 8/84

Prepared by
A. Demetriades, Principal Investigator
Professor, Department of Mechanical Engineering
Montana State University
Bozeman, Montana

January 1985

SUPERSONIC BOUNDARY LAYER STABILITY OVER A ROUGH WALL

Final Report, AFOSR Grant No. 80-0267
For the Periods 9/80 - 8/82 and 9/83 - 8/84

A. Demetriades, Principal Investigator
Montana State University
Bozeman, Montana

ABSTRACT

Measurements of the growth or damping of natural distubances at Mach 3 have been made in the laminar boundary layer over an adiabatic, constant-pressure flat-plate surface, from the leading edge to the transition onset point. The effect was studied on the flow stability of the stream unit Reynolds number, plate surface roughness and wind-tunnel sidewall boundary layer turbulence radiation. A first-mode, 3-dimensional unstable region was identified which has a minimum critical Re_θ of about 180 and a maximum amplified frequency of F = 0.00023. The amplification rates within this region fit available theoretical predictions, but they, as well as the low-frequency end of the lower neutral branch, show greater and earlier amplification than expected. A second unstable region was discovered between this region and the transition onset defined by the first departure from laminar self-similarity. This second region produces higher amplification rates, and at much higher frequencies, than the first. The effect of increasing unit Reynolds number is to decrease the overall amplification rates and to increase the transition distance without affecting the location of the neutral branches or of the maximum-amplitude line. When noise radiation from sidewall turbulence was allowed to impinge on the plate, the stream disturbance amplitude increased by about 60 percent and the amplification rates within the layer increased slightly, obliterating many regions of damping. Random-distributed sand grain roughness was found to be unsuitable for stability studies in supersonic flows, and the roughness effect

was studied by using a two-dimensional periodic ridge-groove roughness arrangement. This roughness was effective in moving transition forward, primarily by increasing the rates in the second unstable region and moving the latter forward. In all circumstances, the onset of boundary layer transition required the stream disturbances to amplify by a factor of about 25, but of that only a factor of 2 - 3 was supplied by the boundary layer instability. The mechanism accounting for the other major portion of the gain is thought related to some forcing process.

FOREWORD

The present program, AFOSR Grant 80-0267, was initiated in 1980. The 1980-82 period was devoted to work on the stability of an axi-symmetric model laminar boundary layer, on which a graduate thesis was written; and on preliminary work with the two-dimensional boundary layer. In the 1982-83 period, this program was interrupted to divert attention to free shear layer mixing problems of interest to the USAF Weapons Lab. The stability work was completed in the 1983-84 period. A paper entitled "The Two-Dimensional Laminar Wake with Initial Asymmetry" describing work under this Grant was published in the AIAA Journal (Vol. 21, No. 9, Sept. 1983, pp. 1347-1349). A second journal paper, dealing mainly with results described herein, is under preparation. Two graduate students in Mechanical Engineering did their theses on the present research.

The following Technical Reports describing research under the present grant have been so far disseminated to the cognizant technical people and agencies:

1) Demetriades A.: "The Compressible Laminar Two-Dimensional Wake with Initial Asymmetries", MSU/SWT Report 81-3, July 1981.

2) Demetriades A.: "The Hydrodynamic Stability of a Supersonic Laminar Boundary Layer over a Rough Wall", AFOSR TR 83-1287, ADA 137056, Sept. 1983.

3) Demetriades A. and Brower T.L.: "Experimental Study of Transition in a Compressible Free Shear Layer", AFOSR TR 83-0144, ADA 126450, MSU/SWT TR 82-05, Dec. 1982.

4) D'Sa J.M.: "Characteristics of a Supersonic Laminar Boundary Layer over a Rough Wall", M.S. Thesis, MSU, July 1982.

5) Brower T.L.: "Experiments on the Free Shear Layer Between Adjacent Supersonic Streams", M.S. Thesis, MSU, March 1983.

Contact has been continuously maintained between this laboratory and government agencies in order to discuss, cross-check, and disseminate the results of this research. The principal contact points were the AFWL (Paul J. Ortwerth, Bruce Masson) and the NASA-Air Force Transition Committee (L. Mack, J. Kendall, NASA Langley).

It must be stressed that the stability results obtained in this program are voluminous and still under reduction and analysis; this document is therefore, in essence, only a summary of the principal results. A full Technical Report is under preparation and will be soon submitted to the sponsor.

CONTENTS

1. Introduction and Motivation

It is common experience that surface roughness destabilizes the laminar boundary layer. Nearly every text on boundary layers includes a summary of the numerous experiments done to date, by which transition to turbulence was found to move upstream when the surface is roughened. The body of available literature is necessarily large because of the large variety of possible roughness geometries and their distribution on the surface, i.e., of the spectrum of the surface contour. For example, there are several prevalent notions of turbulence generation by roughness: one is that the turbulent wakes of a few isolated surface protrusions agitate the boundary layer into a turbulent state; another, that the roughness distorts the mean flow field into a hydrodynamically unstable shape. The latter view is attractive when the surface is uniformly covered by "distributed" (statistically stationary) roughness of height much smaller than (the layer thickness).

Ideally, one would hope to calculate the mean velocity profile distortion due to small-scale, uniformly distributed roughness, and then subject this profile to hydrodynamic stability analysis; a rational connection between the roughness and transition would thus be found. Practically, this is an immense task because of the difficulty of the flowfield calculation and the need to repeat it for every conceivable type of roughness. As an alternative, Reshotko (Reference 1) and Kendall (Reference 2) attempted to measure the velocity profile instead, with a view of perhaps using the measured profile as an input to stability analysis. One could then make parallel stability (e.g. disturbance amplification) measurements, and compare the latter with stability characteristics predicted from the measured mean flowfield.

The Reshotko and Kendall tests were done at low speeds. The work described here is the analogue for supersonic flows. Specifically, the purpose here was to measure both the mean profile and the amplification rates (stability diagram)

of a supersonic laminar boundary layer, when the wall surface is rough. Under the best of circumstances, it was hoped that eventual use of the measured profile could be made by stability theory and that the stability characteristics so calculated would in turn be compared with the measured stability characteristics. No information exists to date on the amplification of small disturbances in a supersonic boundary layer over a rough wall; such information would be in any way invaluable toward the understanding of the role of roughness in promoting transition. Thus, the data could play a dual role as checks of the stability theory and as practical guides to transition prediction.

At the inception of the present program, it was clearly understood that previous knowledge on the supersonic boundary layer stability with a smooth wall should be the necessary base on which the measurements with roughness should rest. It soon became apparent that such knowledge was overestimated. A survey of the experiments done on smooth-wall stability showed a number of reports dealing with subsonic edge Mach Number M_e (e.g. References 3 and 4), a series of experiments at $1.5 < M_e < 2.2$ (Reference 5) and a rather heavy concentration at $6 < M_e < 8.5$ (References 6 through 12). Kendall (Reference 7) made another series of measurements at $M_e = 3$ and 4.5, but his presentation deals mainly with the issue of boundary layer response to the free-stream noise, with little information on the disturbance behavior within the boundary layer especially at Mach 3.

Those with some experience in amplification measurements at $M_e = 3$ have given discouraging accounts of its suitability as a test-bed of linear stability theory. Laufer and Vrebalovich (Reference 5) limited their published account of stability to $M_e = 1.6$ and 2.2 because "...at M = 3 the detection of self-excited oscillations was much more difficult and less reliable." Kendall notes that in his supersonic experiments "fluctuations of all frequencies were observed to grow monotonically larger in the region of a boundary layer extending from the

flat plate leading edge to the predicted location of instability, i.e., in a region where no growth was expected" (Reference 7, p. 291). This statement portends grave difficulties for stability experiments aiming at the observation of neutral boundaries for checking the linear stability theory. Such experiments, furthermore, also depend on amplified "Tollmien-Schlichting waves" as a reliable indicator of on-going instabilty, and indeed the accidental discovery of such waves by Schubauer and Skramstadt in the 1940's (Reference 3) supplied the major impetus for modern-day stability research. Even at hypersonic speeds, laminar instability waves are so pronounced that they are routinely visible even to unsophisticated sensors. This selectivity of the boundary layer disappears at $M_e = 3$, however, giving the experimenter no immediate evidence of disturbance amplification.

An interesting theoretical explanation of the exceptional non-selectivity and low amplification in the vicinity of $M_e = 3$ is supplied by Mack (Reference 13, p. 282). It turns out that $M_e = 3$ lies at the minimum of curves one can plot of maximum spatial amplification rate vs. M_e. This minimum marks the intersection of 3-D, first-mode amplification rates, and the rates due to 2-D second-mode disturbances. Thus $M_e = 3$ occupies a unique spot in boundary-layer stability, one which should present difficulties to the experimentalist and the theoretician alike.

As a result of the ideas expressed above, the objective of measuring the growth of damping of natural disturbances over the smooth wall, rather than being a simple tare measurement, became quite prominent. The smooth-wall stability measurement provided, in the end, most of the measurements described and conclusions reached here. A complete account will appear shortly in a more detailed Technical Report.

2. Wind-Tunnel Facility

All measurements described here were done in the continuous supersonic wind-tunnel at MSU (MSU/SWT) at Mach number 3.0. A detailed description of the facility appears in Reference 14. The relevant attributes of this facility are its ability to run for long periods (e.g. 8 hours) at constant supply (stagnation) pressures and temperatures, its steadiness and uniformity of flow, its convenience of access to the test section, its broad expanse of optical view of the flow, its automated probe control and data acquisition, and the ease of controlling the sidewall boundary layer transition zone.

3. Early Experiments with the Axi-Symmetric Model

This program began as a M.S. thesis experiment to look at the rough-wall flowfield, stability and transition on an axi-symmetric (ogive-cylinder) model at Mach 3. This geometry was chosen mainly to alleviate possible problems of model-wall interference common with flat-plate models. This phase of the program is presented in detail in Reference 15.

The model consisted of a 20.3 cm. long, 2 cm. diameter cylinder attached to an 11.7 cm long ogive with a sharp tip of 5.2 half angle. The rear end of the ogive screwed on and blended smoothly with the front end of the cylinder, while the latter was supported in the back by a sting. This model was always operated at zero angle of attack, in the tunnel stagnation pressure P_o range of 200-600 torr (unit Reynolds number range $20{,}000 < Re' < 60{,}000/cm$), and stagnation temperature range 75-125 F. Numerous photos of the tunnel, model, and of the flow over it are shown on Reference 15.

The boundary-layer flowfield over this model was first examined when the cylindrical afterbody had a smooth surface (the ogive was always configured with a smooth surface). The transition behavior dependence on P_o was measured, and it was next attempted to determine the surface roughness suitable for

stability measurements by introducing roughness on the cylinder and studying changes in the transition location. Accordingly, duplicates of the cylindrical afterbody were built which were covered by uniformly distributed sand-type roughness; tests were then made to find the transition location dependence on roughness height. In the process, we verified the Schiller-Smith criterion that the minimum critical roughness Reynolds number for tripping transition is about 120 but only if based on the flow conditions at the roughness top (References 16 and 17). This was discovered when it was found that transition on the model remained unaffected unless the roughness height became excessive (40- or 60-grit sandpaper). Such a roughness height was much too large a fraction of the boundary layer thickness and made the flowfield measurements ill-defined and awkward, as it would for any similar experiment with transition-tripping roughness at high speeds. Work with the sand-grain roughness method was therefore stopped.

Better results were achieved with a two-dimensional roughness made up of the periodic grooves and ridges ("teeth") shown on Figure 1. The major advantages of this roughness configuration were that 1) the boundary-layer profile was found independent of position relative to the ridge or groove, 2) an equivalent surface (i.e., the plane of the tops of the ridges) could be defined from the data and 3) transition moved upstream over such a surface. Therefore, this special kind of roughness became the one to use for studying the boundary layer stability.

At about this time, it also became clear that the boundary layer development over the ogive-cylinder had certain disadvantages. For example, the boundary layer growth was not of the Blasius type, and especially at and downstream of the shoulder the measured momentum Reynolds numbers Re_θ were too large. Such behavior is typical of axi-symmetric flows but is not conducive to

the study of stability. This phase having exhausted its usefulness, the experiments were continued with a flat plate geometry.

4. Flat Plate Experiment Geometry

Beginning in 1982, the program was continued with the design and fabrication of a 2-dimensional sharp-tipped flat plate model for the stability measurements. Like its axi-symmetric predecessor, this model, pictured on Figure 2, had provisions for changing its top surface from a smooth to a roughened one. This was done by the use of interchangeable inserts, one of which was smooth, and the other roughened by parallel "teeth" of the same geometry as used for the axi-symmetric model (Figure 1). All discussion will henceforth pertain to this flat plate model only.

5. Mean Flowfield in the Boundary Layer

Detailed surveys of the flow in the boundary layer over the model were first performed over a range of P_o (i.e. Reynolds number) for both the smooth and the rough wall. The plate installation in the SWT for these measurements is shown on Figure 2. Three specific values of P_o were taken, P_o = 350, 475, and 600 torr which, at a supply temperature of 100 F (125 F for P_o = 350) gave nominal unit Reynolds numbers of 30,000, 40,700, and 51,400 per cm. These surveys showed that, for the smooth wall (Figure 3) the flow conformed well with the Blasius theory ahead of transition, and the "first departure" of the laminar toward the turbulent velocity profile was noted with unusual care to serve as the downstream limit of the linear stability region.

On changing from the smooth to the rough surface, the transition zone advanced upstream, typically from a "first departure" Re_θ = 400 to about $Re_\theta \simeq$ 330. It is remarkable, however, that the velocity profiles over the rough wall (Figure 4) showed no departure from the laminar (Blasius) theory for $y/\delta > 0.15$. It is conjectured that either (a) the profile change due to roughness occurred

in the lower 10 percent of the boundary layer where data were not taken or (b) whatever caused the roughness to trip the boundary layer produced a profile change too small to be detected.

6.0 Measurements of Disturbance Growth

6.1 Instrumentation and Procedures

Data of the fluctuations were taken with the hot-wire anemometer for the three stagnation pressures mentioned above, two surface configurations (rough and smooth) and also along two paths over the plate surface, for a total of 3 x 2 x 2 = 12 data "sets". One of the two paths lay on the $y/\delta \simeq 0.6$ line above the surface where the wideband r.m.s. fluctuations were found to peak; the second lay on a plane outside the layer parallel to the surface and 0.6 cm above it, where the instrument responded only to the stream turbulence. For each of these 12 sets, the hot-wire recorded the fluctuation spectrum every tenth of an inch (0.25 cm.) beginning very near the leading edge and marching downstream well beyond the point of "first departure". This provided the opportunity to study the fluctuation development throughout the linear, non-linear, and transitional zones. The number of spectra (i.e., of positions x along the flow) varied from one set to another and averaged around 60.

The three tunnel pressures P_o chosen covered all possible cases of noise radiation from the tunnel sidewalls onto the plate. At P_o = 350, transition on the sidewalls was so far downstream that radiation from them never reached the plate surface. At P_o = 600 torr, the entire sidewall surface was covered by a turbulent boundary layer; in this case, the plate received the maximum amount of noise radiation. At P_o = 475 torr, noise impinged on the plate starting at about 5 cm. downstream of the leading edge.

The hot-wire signals for all sets were first processed by a Fast-Fourier-transform computer, with each transform averaged 1024 times, and with a

resolution of 1.6 KHZ in the range 0-320 KHZ (200 Fourier components). These 200 x 60 x 12 = 144,000 Fourier amplitudes or "spectral densities" A(f;x) or e(f;x) were stored as a data file in the IBM 9000 computer along with a very large menu-driven program (STABLEØ2) which produced the following on demand:

1) The raw spectrum at each x of the set, i.e., A or e as a function of frequency f or non-dimensional frequency $F = 2\pi f/U_e Re'$ ("raw" means noise-inclusive, and the units of A (or e) are r.m.s. voltage per 1.6 KHZ window).

2) Same as (1) but corrected for noise; henceforth, these are the only amplitudes and spectra considered.

3) The wideband r.m.s. voltage $e_{rms}(x)$, given in terms of x or of the following functions of x: Re_x (wetted Reynolds number), $R = (Re_x)^{0.5}$, nominal Re_θ and actual Re_θ. The nominal momentum Reynolds number Re_θ obtains from the Blasius theory, while the actual includes a correction dictated by the measured θ. The quantity e_{rms} is provided both with and without noise subtraction.

4) The amplitude A(f;x) or e(f;x) (r.m.s. spectral density as in (1)) but now for any chosen f, as a function of x or its dependencies (R, Re_x, etc.) The curve A(x;f) is called the amplitude change and is the basic source for computing amplification rates.

5) A "dressing room" for choosing any desired A(x;f) from (4), and seeing what polynomial degree will fit the best variation A(x;f) vs. x. This is a key issue; it turns out that in this experiment the phenomena in the linear range are most faithfully fitted with a 7th-degree polynomial. This computation then also produces, for every frequency of each set, the non-dimensional amplification rate

$$\alpha_i = -\frac{1}{2A}\frac{dA}{dR}$$

versus x or its dependencies.

6) The "poles" and "zeroes" of the amplification rate curves for all f's of a particular set. That is, viewing the 3-dimensional stability diagram ($-\alpha_i$, F, R), this algorithm finds and stores the coordinates (F, R) of the neutral branches and the amplification rate maxima and minima.

7) The amplification rate spectrum for any desired x (or R or Re_θ, etc.) of each set. This first computes $-\alpha_i(x;f)$ vs. x for all f, then computes and stores the variation $-\alpha_i(f)$ or $-\alpha_i(F)$ for each desired x or R.

8) The total amplification spectrum between two desired x (or R), that is the amplitude spectrum $A(f;x_2)$ at x_2 divided by the amplitude spectrum $A(f;x_1)$ at x_1. To smooth things out a bit, this was done indirectly by first choosing a frequency, curve-fitting the variation A(x;f) with a 7th-degree polynomial, forming $A_c(x_2;f)/A_c(x_1;f)$ (where A_c means the fitted amplitude from the curve-fit) and repeating for each frequency.

9) The boundary layer response spectra. This consists simply of first picking a representative point in the free stream from the "free stream" set of data and storing the spectrum $A_o(f)$ at that point; then picking a spectrum A(f;x) from a "boundary layer" set and computing $A(f;x)/A_o(f)$ at that point x.

It is important to note that the hot-wire anemometer responds jointly to fluctuations in the fluid speed, its temperature, density and pressure. The process by which the latter fluctuations are extracted from the wire AC voltage is called "modal analysis". In practice (References 5, 7, and 9 for example) modal analysis is put aside in stability experiments because of its great complexity, because of the theoretically-confirmed insensitivity of the stability to the precise mode of fluctuation (Reference 13) and because of recent experimental confirmation of such insensitivity by Stetson (Reference 10). Therefore, in this work the quantity A(f;x), while in reality the spectral density of the AC anemometer output, is equated to the r.m.s. spectral density of a typical fluctuation.

6.2 Results

6.2.1 Wideband Signals on the Smooth and Rough Walls

Figures 5, 6, and 7 set the stage by showing the observed relation among velocity profiles, friction coefficient and wideband hot-wire output for the smooth-wall P_o = 350 and 450 data and for the rough wall, P_o = 350 data. Note that the abscissa is the nominal Re_θ (the actual one is higher; see Figure 3). The "first departure" of the velocity profile, and the departure of C_f from the laminar values are clear. Note that as P_o (and Re′) increases, the first departure is somewhat delayed from just under Re_θ = 400 to about Re_θ = 420, possibly due to the unit Re′ effect. These numbers should not be casually compared with "transition" data obtained from sources which take no pains to define the term precisely. The present data represent a very careful look at the very beginning of the process, and from Figures 5, 6, and 7 in fact it seems that arrival at the turbulent state is a long way off, to the right of the graphs.

Also observe the wideband r.m.s. voltage variation. Note how it begins growing far ahead of the "first departure" and how it is impossible to pinpoint the latter from the wideband magnitude alone. It is important to the subsequent discussion to note that the r.m.s. signal begins increasing in the laminar flow far ahead of the first departure point.

The effect of P_o and surface roughness on the wideband r.m.s. magnitudes is shown on Figures 8 and 9. Attention is drawn here to the low free-stream level compared to the level inside the boundary layer, a significant point as regards stability. Reynolds number similarity of the fluctuating field is shown on Figures 10 and 11.

6.2.2 Spectra of the Boundary-Layer Fluctuations

Typical spectra of the fluctuations for various sets (i.e., different surface configurations, different Re′ and various x stations) appear in Figures

12 through 14, where the ordinate is the quantity A(f;x) here called "amplifier output". Nearly in all cases the tendency appears for the signal at low frequencies to increase going downstream, while the high-frequency signals decrease. This is in accord with notions of linear stability theory.

In hypersonic (Reference 8) and low supersonic (Reference 5) Mach numbers, spectra such as shown here would exhibit a sharp "peak" of intensity increasing and of frequency decreasing as x increases. With the smooth wall, no such peak appears clearly before Re_θ (nominal) reaches 370, which is just before the first departure (Figure 5). This non-selectivity is obviously due to the special niche occupied by $M_e = 3$ in the linear stability theory (e.g. see Reference 13).

With the rough wall, the selectivity increases, as seen by the presence of such peaks in Figures 12, 13, etc. (compare the x = 5.4 cm., $Re' = 56{,}100$ with rough and smooth walls). This is mainly due to the displacement of the first departure upstream when the wall is roughened; actually, however it was also noted that the inherent selectivity of the boundary layer increased for the rough wall.

6.2.3 The Maximum Amplitude Line

Figure 15 shows the position, on the stability diagram (F, Re), of the spectrum peaks discussed above. The locus is often called "maximum amplification" line in the literature, which should not be confused with the "maximum amplification rate" line in the ($-\alpha_i$, F, Re) space. The data shown on this Figure were taken directly from the spectrum peaks found from Figures such as 12, etc.

The point made by Figure 15 is that, first, the maximum amplitude line is fairly independent of Re'; second, there seems to be no effect of the roughness; third, the data agree with those of Laufer (Reference 5) in that they form with the latter a logical progression in the range $M_e = 1.5 - 3$. In this respect, note that the agreement improves when the actual Re_θ is considered. This

argument implies that the observed spectrum peaks at $M_e = 3$ are due to a first-mode type of instability (the first mode, presumably a 3-D mode, thus gives maximum-amplitude wavelengths of order 25δ, as can be computed from Figure 15. By contrast, the second-mode instabilities prevalent in hypersonic flows (References 8, 9, 10, etc.) give $\lambda \simeq 2.5\delta$).

6.2.4 The Amplification Rates

The next step in the process was to find the amplification rates $-\alpha_i$ (see Section 6.1) by cross-plotting the amplitudes A(f;x) versus x at constant f. It has been already noted that the polynomial fit used was uniformly set to 7th degree; this statement hides the substantial labor devoted to, and continuing concern about, finding the proper polynomial degree. One can make serious mistakes in the amplification factors and the location of neutral branches, for instance, by using the wrong polynomial degree. Figures 16 and 17 show examples of what we found in this issue. In Figure 16, a fixed range of data points on amplitude (called here "spectral density") is fitted by a variety of polynomials; in Figure 17, the degree is fixed and the effect on the fit is found of the range of points fitted. Both effects are important since resulting amplification rates computed on the right can vary widely. In the present case, we did almost all analysis by fitting the points $0 < x < 10$ cm. with 7th degree polynomials.

Selected amplitude variations and amplification rates are shown on Figures 18 through 20. Here we show, too, on Figure 21 a direct copy of the computer CRT screen display of such results to illustrate the data-reduction program capability.

Figures 22 through 25 show amplification rates at typical frequencies. It is clear that for $P_o = 350$ and 475, there is always damping at low R and amplification at high R (the location of the "first departure" on these graphs will be presented later). Almost always there is a clearly defined maximum in

the $-\alpha_i$ curves at R of order 200 - 400, which is either submerged below the $-\alpha_i = 0$ line to become a damping region or emerges above it to become an amplified region. In many cases, there is also a second maximum in the $-\alpha_i$ curves, possibly due to a second unstable region, but at $P_o = 600$ and also at the lowest frequencies there seems to be no damping present between these two "modes". Around R = 600 the "first departure" occurs, but prior to that the amplification rates suddenly "blow up", especially at the higher frequencies.

The amplification rates at P_o (Figure 25) are especially interesting because they show very little damping regardless of frequency, distance from the leading edge and surface type (smooth or rough). This is the case where the entire interior surface of the nozzle was covered by a turbulent boundary layer which was in turn irradiating the plate model. And yet the maxima, mentioned above, are quite visible and systematic. It looks as if reasonable neutral boundaries would emerge from Figure 25 if one could judiciously move the $-\alpha_i = 0$ line upwards for each frequency. This idea, which implies that each amplification curve is burdened with some extraneous gain, invites the hypothesis that the incident sound increases the gain of the boundary layer.

Three-dimensional views of $-\alpha_i$ vs. F and R are shown on Figures 26 through 28. It is clear that roughness accentuates the gain phenomena. It is also clear, again, that $-\alpha_i$ begins rising long before the first departure (R = 600 for smooth wall) is achieved. Also clear is the fact that the so-called first instability region extends to lower R than expected at low F.

Figures 29 and 30 are an attempt to discern unit Reynolds number effects on the amplification rates. It is seen from Figure 29 that for the smooth wall the rates for $P_o = 350$ and 475 are in fair mutual agreement, while for the rough wall there is hardly a comparison. A comparison of the rates between the smooth and rough wall is shown on Figures 31, 32, and 33. Especially for $P_o = 350$ it appears that the maximum rates increase slightly when the wall is rough.

6.2.5 The Amplification-Rate Spectra

The amplification rate spectra of $-\alpha_i$ vs. F are experimental landmarks most easily compared with theory. For the smooth wall, such spectra are shown for typical R on Figure 34. Accompanying the data are theoretical curves from information supplied to this writer by L. Mack for the first unstable mode of 3-dimensional disturbances with $\psi > 0^\circ$ where ψ is the wavefront inclination. Specifically, the range $55^\circ < \psi < 65^\circ$ is considered to represent the most unstable wavefront orientation. At this point, the short line segments shown on Figure 34 are the sum total of the theoretical results available to Mack for the flow conditions at hand.

It is evident from Figure 34 that theory and experiment are located in a mutually consistent manner if one was to isolate the unexpected amplification visible at low frequencies. The low-frequency amplification rates are out of place with what the data, together with the theory, seem to indicate. This phenomenon is typical of $M_e = 3$, and in fact both Laufer (Reference 5) and Kendall (Reference 7) have observed a continuous increase of the low-frequency signal strength from the leading edge going downstream. The data of Figure 34 is the first documentation of this phenomenon known to this writer. Additional amplification spectra are shown on Figures 35 and 36.

The data for R = 500 in Figure 36 show $-\alpha_i$ levels as high as 0.003, and an overall shape of the spectrum which now begins departing from any reasonable extrapolation of the theoretical curve shown on the same graph. The value R = 500 is stil below R = 600 marking the "first departure" toward transition and is still therefore in the laminar self-similar region. Thus there are occurrences in the laminar flow not accounted for by stability theory. In this work, we will refer to this large amplitude, large amplification region as the "non-linear region".

The collection of amplification rate spectra of Figures 35 and 36 should, in principle, permit some judgement to be made on the effect of roughness and of Re′. In general, for the smooth wall the spectra for Re′ = 29,400 and 43,900 seem to coincide except at R = 250 and 450. These departures are on the side favoring lower amplification for the higher of the two Re′, and is consistent with the slight transition delay seen for the latter, i.e., the "unit Reynolds number effect".

An effect of roughness can also be gleaned from Figures 35 and 36. For R < 300 no statement about the rate spectra over the rough wall can be made, for reasons soon apparent; but for R > 300, it is clear that amplification rates higher for the rough than smooth wall begin building up, even though the rates for the rough wall start out at R = 300, below those for the smooth wall (this latter effect might involve a measurement problem which is presently unclear). In any way, the spectra for the rough wall reach a rate as high as 0.004 at R = 500 while at the same R the smooth wall rates are 0.0025 - 0.003.

6.2.6 The Stability Diagrams

At the outset it should again be borne in mind that $M_e = 3$ occupies a rather unique position in boundary layer stability because of low selectivity and the suppression of amplification rates. No stability diagrams at $M_e = 3$ have been presented to date. Previous investigators (References 5 and 7) warn of a generally confused state of affairs at this Mach number and stress their finding that the stability picture gets obscured by "continuously growing disturbances". Regions of damping have apparently not been found before.

The smooth wall neutral branches (F, Re_θ) are shown on Figure 37. The outstanding features are (a) there is no Re′ effect, (b) an upper unstable frequency limit of $F \simeq 0.00023$ is indicated, (c) with the exception of the low frequencies (F < 0.0001) the shape of the unstable region is as expected. Furthermore, there is a very reasonable placement of the data relative to the

M_e = 2.2 data of Laufer. It should be recalled also that the present maximum amplitude locus is very close to that found by Laufer (Figure 15).

The upper part of the lower neutral branch is more credible at this point, an it gives a minimum critical Reynolds number of about $Re_\theta = 180$. The lower part of this branch lies at excessively low Re_θ, and is here showing the effect reported elsewhere of amplification at the lower frequencies ($F < 0.0001$) and at low Reynolds numbers. Aside from that, however, the situation here is much clearer than expected regarding this amplified region, presumably the "first mode".

Figure 37 has been slightly edited, only as regards data points far from the main neutral branches of the first mode. The complete unedited collection of neutral points and also amplification rate maxima and mimima for all cases (sets) generated is shown on Figures 38 and 39. A striking aspect of the six graphs shown is the appearance of a second amplified region to the right of the first mode (this is not so much inferred by the second set of "lower neutral branch" points shown, as much as the appearance of lines of amplification rate minima past the first mode). In other words, there appears a second mechanism, perhaps non-linear, but still in the laminar, self-similar flow, which provides further disturbance amplification. Thus the stability diagram looks quite complex.

Another feature of Figures 38 and 39 is the excessive scatter of points at $P_o = 600$, which is when the plate model is wholly immersed in the radiation field of the sidewalls. For this reason, further analysis of the $P_o = 600$ cases has been stopped.

For the rough wall, the stable and unstable regions stand out with great clarity at $Re' = 29{,}400/cm.$ ($P_o = 350$). Figure 39 shows how the first mode, again disfigured at the lower frequencies, has moved bodily to the lower Re_θ ;

furthermore, the highest unstable frequency has also increased to about F = 0.0003. This caused some excitement at first, until it was realized that the roughness section on the model did not begin until 3 cm. from the leading edge (R = 300 at Re′ = 29,400/cm.). The origin of this unstable region is therefore hard to interpret. On the other hand, Figure 39 shows that another unstable region appears at $R_\theta \simeq 350$ for the rough wall (the minima in the amplification rates at P_o = 350, Figure 39).

Figures 40, 41, and 42 show a general view of the boundary-layer stability findings in a geographic sense, plotting everything versus the nominal Re_θ. The idea here is to give the viewer the location of the various phenomena relative to one another, especially relative to the first departure ("transition") location. The latter is accurately pinpointed by the top two graphs, especially the friction plot. It is important to note that, as already mentioned, there exist several features in the stability diagram (bottom graphs in these Figures) which antedate the onset of transition.

6.2.7 The Boundary Layer Response

Since amplitude information was available all the way to the first departure, it is natural to ask about the maximum amplitude change experienced by the fluctuations before they became large enough to cause turbulence. Some answers are shown on Figures 43 through 48.

Rather than integrate the amplification rates to get final amplitudes, the spectra A(f;x) at various locations were simply divided by the spectrum at a typical "most forward" position, such as at R = 150 (or $Re_\theta \simeq 100$). On Figures 43 and 45 are shown such results for the smooth wall, picking spectra at important landmarks of the stability diagram. For example, it is interesting to see by how much disturbances amplified by the end of the "linear region", which is marked (Figures 40, 41, etc.) by the appearance of an amplification rate minimum line just beyond the first unstable region. According to our data, this

occurs at about R = 400 (Re_θ = 265) for the smooth wall and at about R = 350 (Re_θ = 230) for the rough wall.

Also, how much have the disturbances amplified upon reaching the first departure point beyond which C_f increases and the boundary layer loses laminar self-similarity? As a reminder, this occurs at about R = 600 ($Re_\theta \simeq 400$) for the smooth and R = 500 (Re_θ = 335) for the rough wall (recall that these are nominal values of Re_θ).

Some surprising answers appear. For example, for the smooth wall at P_o = 350 (Figure 43), the first mode has caused an indifferent 10 percent increase in the fluctuation magnitude and that only for a very small frequency band below F < 0.00005. At P_o = 475, there is net attenuation for all frequencies up to R = 500! And in the entire zone upstream of transition, the maximum amplification observed with the smooth wall did not exceed a factor of 3 for P_o = 350 and 2 for P_o = 475, again for a limited frequency band only. For the rough wall, similarly, the maximum amplification is about 2.3 (Figure 44).

These results have important implications to the mechanism of turbulence generation in the boundary layer. It seems highly unlikely to this writer that such modest gains could be responsible for transition and quite likely that some other mechanism is at play, stemming perhaps from the idea that the layer is "forced" (Reference 13). Kendall (Reference 7) pursued this idea by plotting the spectrum of the ratio $A/A_o(f)$ where A_o is the spectral density in the free stream. Similar plots appear here on Figures 46, 47, and 48 (values R = 330, 470 ... on these plots were picked to correspond to Kendall's values). Now we can draw some conclusions by comparing Figures 43, 44, etc. which show events within the boundary layer with Figures 46, 47, etc. which compare events inside and outside of the boundary layer. The former show that between the neighborhood of the leading edge and transition onset, disturbances amplify typically by a factor of 2. But the latter say that the disturbances have

gained, say, a factor of 5 "upon entering" the boundary layer. Therefore most of the disturbance growth appears to have little to do with linear stability theory.

Experimentalists like this writer have observed, in fact, that an amount of "noise" much larger than can be found in the free stream is always found inside a laminar boundary layer no matter how close to the leading edge one gets. Spurred by findings as the one above, it has been suggested that the disturbances enter the boundary layer "near the leading edge"; until such statements can be quantified, however, it must be recalled that fluid is entrained into the layer continuously along its length. Thus it appears that a "jump" in disturbance strength occurs upon crossing into the boundary layer at any event, as opposed to the role of the leading edge above.

7. Discussion and Conclusions

This program has addressed two separate questions, the first being the stability of the boundary layer over a smooth, adiabatic wall at Mach 3. The classical method was followed of measuring the evolution of the hot-wire anemometer signal Fourier components along the plate from the vicinity of the leading edge to the transition zone. The latter was fixed securely by careful observations of the velocity profiles. "First departure" was the term used to define the position (at each stagnation pressure) where the profiles showed a change over the theoretical Blasius profile.

In the upstream half of the laminar boundary layer, we have identified a region of amplification surrounded by a region of damping in the F, R plane. The upper part of this "stability loop" would be easily seen from the data and fits preconceptions formed by previous test data at lower Mach numbers ($1.5 < M_e < 2.2$) and by early stability theory (e.g. Reference 18). The same can be said about the "line of maximum amplitude". For the first time known to this writer, the maximum amplified frequency could also be clearly seen (at $F \simeq 0.00023$).

The lower neutral branch of the amplified loop does not fit earlier notions from linear stability, however. Specifically, the lower neutral branch seems to occur at a nearly constant Reynolds number. Laufer (Reference 5) also obtained the lower neutral branch quite clearly; but he used artificial disturbances and, more significantly, he used edge Mach number where the amplification rates were considerably higher. In fact, interpreting literally the comments by References 5 and 7, the existence of the entire lower neutral branch at $M_e = 3$ would be in doubt since disturbances were previously found to "increase monotonically from the leading edge on". If the discernment of that branch is any standard of quality at all, we should be fairly satisfied that the branch was visible here at the lower frequencies.

There appears to be a small but definite unit Reynolds number Re′ effect on stability. For the largest of the two Re′ employed, transition moved slightly downstream. The neutral branches did not move, but at the higher Re′ the amplification rates within them decreased slightly also. In fact at this Re′, the total result between the leading edge and R = 500 is a net decrease of the amplitude at all frequencies.

Quantitatively, the amplification rates in the linear region (here defined as ending by R = 400 or 450 at most) are in seeming agreement with theoretical predictions for first mode 3-D instabilities ($\psi = 55^\circ - 65^\circ$). The qualification arises from the need to ignore the low frequency amplification phenomenon mentioned above and from the incompleteness of the available theoretical results.

The above remarks concern primarily those data obtained with a laminar sidewall boundary layer. Data were also recorded (at $P_o = 600$) with a turbulent sidewall boundary layer, which would irradiate the entire working surface with sound waves. The data show that in this case the amplification loop maintained its position and shape but that an "amplification increment" was added to each

Fourier component. The principal result is that all amplification rate curves are raised, leaving very little damping anywhere. Data were also taken with an intermediate pressure (P_o = 475) where irradiation occurred only in the non-linear region (R > 400). One could see no abrupt change in the disturbance history along this plate due to this effect. Furthermore, it is interesting that transition was still delayed, even though the irradiation would normally accelerate it.

It was found that amplification activity in the region preceding the first departure is not limited to the "loop" identified in the previous paragraphs as the first 3-D amplification mode. The data invariably show that soon after Re_θ = 300, the upper neutral branch turns upward vertically and becomes a "lower" neutral branch. This phenomenon actually sets in as early as Re_θ = 250 at P_o = 350 (at $Re_\theta \simeq 300$ at P_o = 475) where one notes that outside and past the first mode loop the damping reaches a maximum while inside the loop the amplification rates, while still positive, also reach a minimum. The interesting feature of this new amplification region is the involvement of the higher frequencies (F > 0.00015) and at higher Reynolds numbers. It must be stressed that this is not related to the familiar, sudden activity generated at high frequencies after transition occurs.

It should be noted that the possibility of unstable regions at high F and R is quite real. We know from theory that around M_e = 3.5 the 2-D second instability mode appears; the hypersonic data show multiple unstable regions in the range of $0 < F < 0.0005$ and $1000 < R < 2000$. It is not yet known where such regions will fall extrapolated to lower R. There may well be 2-D or 3-D unstable regions visible in the $300 < R < 1000$ range which are not related to the first mode but connected to it in the stability diagram (these comments are not meant to imply validity of recent numerical results by Wazzan et al.,

(Reference 19) which have been disputed by Mack (Reference 20) and which, besides, predict amplifications at very high frequencies).

The second question addressed in this work was the influence of wall roughness on stability. The rough wall results have been a mixture of interesting and disappointing incidents. The early history of this program began with some important experimental lessons. The criterion for minimum roughness height needed to trigger transition was confirmed with the axi-symmetric geometry. For supersonic/hypersonic flows, the height is so large that different laminar flow profiles obtain from one point to another on the surface. This loss of similarity makes this writer suspect that no general profile shape will ever be obtained at these speeds, theoretically or experimentally, for transition-effective random-distributed roughness.

The chosen roughness of periodic grooves and ridges did the job of destabilizing the boundary layer but by a mechanism which is presently obscure. It was frustrating that no profile distortion caused by the roughenss could be found for $y/\delta > 0.15$. It is possible that the destabilizing distortion occurred very near the surface where the experiment scale prevented measurements. It is more likely, though, that the distortion extended farther out but was too weak to be captured by the diagnostic probes. (At low speeds, Kendall (Reference 2) implies that both possibilities are valid.)

An interesting finding with the rough wall was that the disturbance history became clearer, i.e., the inflections became more pronounced and less dependent on the subtleties of the curve-fits. This behavior was reminiscent of the ease with which artificial disturbances behave (e.g. Reference 5). It is implied here that some peculiarity of the roughness geometry (such as instabilities radiating sound waves from the shear layers separating over every ridge) provided a forced oscillation much clearer than the natural disturbances. Thus, the "linear" region with the first mode loop shows up distinctly; this,

unfortunately, is discounted as an effect of the roughness because it appears ahead of the roughened zone. Even so, it may be stated here that the neutral boundaries of the first mode are unaffected by the roughness. For example, the location of the maximum amplitude line on the stability diagram is unaffected by the roughness.

The effect of roughness comes into its own in the range $300 < R < 500$, the former limit signifying the beginning of the roughness patch and the latter the first departure point. The amplification rates increase quickly with roughness and substantially exceed the smooth wall rates.

From the data, it appears that whether the wall is smooth or rough, the total "boost" given disturbances by boundary layer instability occurs only at low frequencies and consists of a factor of about 2 (high frequencies experience a net decrease by the boundary layer action alone, between the leading edge and the first departure). The transition-triggering mechanism must therefore be sought elsewhere, such as an amplification experienced by the disturbances while entering the boundary layer. A comparison with the disturbances magnitude in the free stream indeed shows a large increase in amplitude between free stream and the formative (low R) stages of the layer. The data show that first departure occurs when the disturbances have grown to about 25 times their stream value.

The conclusions drawn from this research can be summarized as follows:

1) Three different regions of boundary layer behavior at $M_e = 3$ have been established: "linear" ($R < 400$), "non-linear" ($400 < R < 600$), and "transitional" ($R > 600$).

2) An unstable region ("loop") fitting theoretical ideas of linear stability has been found in the linear region of the stability diagram, with a maximum amplified frequency $F \simeq 0.00023$ and a minimum critical Reynolds number of 180. The landmarks of this unstable loop are also consistent with earlier

stability data at $1.5 < M_e < 2.2$. The experimental amplification rates furthermore conform to the available theoretical predictions. The lower neutral branch of the loop is severely distorted at the low frequencies but not in the extreme manner observed elsewhere.

3) The effect, on the above findings, of irradiating the plate surface with sound emanating from the sidewall boundary layers was, in the main, to increase the amplification rate uniformly so that regions of damping shrank or vanished.

4) The effect of increasing the unit Reynolds number was to decrease slightly the amplification rates without changing the neutral boundary position. Transition to turbulence also moved slightly downstream.

5) A second region of amplification was discovered in the "non-linear region" downstream of the "first mode" loop, while still upstream of the first evidence of transition. This second region extends to higher frequencies ($F > 0.0002$ and beyond) and involves higher amplification rates than found in the linear region. The causative disturbance mode and geometry for this phenomenon are unknown.

6) At $M_e = 3$, random distributed sandgrains were found unsuitable for the study of roughness-induced instability in general. A special type of 2-dimensional roughness was discovered and used which caused transition to move upstream, but a causative distortion of the mean velocity profile was not found. Stability measurements with this roughness showed that the linear-range amplified region shifted in an undetermined manner; and in the non-linear range the newly-discovered second region of amplification became much clearer, set in earlier and had larger amplification rates than the rates with the smooth surface.

7) A final accounting of disturbance amplitude development in the boundary layer shows that in the linear range ($R < 400$) the amplitude increases very

little irrespective of frequency and may actually decrease. In the non-linear range ($400 < R < 600$ for the smooth, $300 < R < 500$ for the rough wall) the amplitude increases by no more than a factor of 3 at most (at the low frequencies) and often by no more than a factor of 2. However, a factor of 5 in gain was observed when the disturbances entered the boundary layer (the stream amplitudes needed a factor of 25 or so to "cause" transition). Thus it is proposed that linear boundary layer stability in itself is incapable of causing transition and that the major contribution must be sought elsewhere.

References

1. Reshotko E. and Leventhall L.: "Disturbances in a Laminar Boundary Layer Due to Distributed Surface Roughness", AIAA Paper No. 81-1224, Palo Alto, CA, June 1981.

2. Kendall J.M. Jr.: "Laminar Boundary Layer Velocity Distortion by Surface Roughness: Effect Upon Stability", AIAA Paper No. 81-0195, St. Louis, MO, January 1981.

3. Schubauer G.B. and Skramstad H.K.: "Laminar Boundary-Layer Oscillations and Transition on a Flat Plate", NACA TR 909, 1948.

4. Bennett H.W.: "An Experimental Study of Boundary Layer Transition", Kimberly-Clark Corp. Rept., Neenah, WI, 1953.

5. Laufer J. and Vrebalovich T.: "Stability and Transition of a Supersonic Laminar Boundary Layer on an Insulated Flat Plate", J.F.M. Vol. 9, No. 2, 1960, p. 257.

6. Demetriades A.: "Hypersonic Viscous Flow Over a Slender Cone, Part III: Laminar Instability and Transition", AIAA Paper No. 74-535, Palo Alto, CA, June 1974.

7. Kendall J.M. Jr.: "Wind-Tunnel Experiments Relating to Supersonic and Hypersonic Boundary Layer Transition", AIAA J. Vol. 13, No. 3, March 1975, p. 290.

8. Demetriades A.: "Boundary Layer Stability Observations at Mach No. 7", J. of App. Mech., ASME, Vol. 99, No. 1, January 1977, p. 7.

9. Demetriades A.: "New Experiments on Hypersonic Boundary Layer Stability Including Wall Temperature Effects", Proceedings of the 1978 Heat Tr. and Fl. Mech. Inst., Stanford Univ., 1978, p. 39.

10. Stetson K.F., Thompson E.R., Donaldson J.C. and Siler L.G.: "Laminar Boundary Layer Stability Experiments on a Cone at Mach 8, Part 1: Sharp Cone", AIAA Paper No. 83-1761, July 1983.

11. Stetson K.F., Thompson E.R., Donaldson J.C. and Siler L.G.: "Laminar Boundary Layer Stability Experiments on a Cone at Mach 8, Part 2: Blunt Cone", AIAA Paper No. 84-0006, January 1984.

12. Stetson K.F., Thompson E.R., Donaldson J.C. and Siler L.G.: "Laminar Boundary Layer Stability Experiments on a Cone at Mach 8, Part 3: Sharp Cone at Angle of Attack", AIAA Paper No. 85-0492, January 1985.

13. Mack L.M.: "Linear Stability Theory and the Problem of Supersonic Boundary-Layer Transition", AIAA J. Vol. 13, No. 3, March 1975, p. 278.

14. Drummond D., Rogers B., and Demetriades A.: "Design and Operating Characteristics of the Supersonic Wind-Tunnel", MSU TR 81-1, Montana State Univ., January 1981.

15. D'Sa J.M.: "Characteristics of a Supersonic Laminar Boundary Layer Over a Rough Wall", Thesis, Mech. Engr. Dept., Montana State Univ., 1982.

16. Schiller L.: Handbook of Exper. Physics, Vol. IV, Part 4, Leipzig 1932, pp. 1 - 207.

17. Smith A.M.O. and Clutter D.W.: "The Smallest Height of Roughness Capable of Affecting Boundary-Layer Transition", J. of Aero Sciences, Vol. 26, No. 4, April 1959, p. 229.

18. Lees L. and Lin C.C.: "Investigation of the Stability of the Laminar Boundary Layer in a Compressible Fluid", NACA TN-1115, September 1946.

19. Wazzan A.R., Taghavi H. and Keltner G.: "The Effect of Mach Number on the Spatial Instability of Adiabatic Flat Plate Flow to Oblique Disturbances", Physics of Fluids, Vol. 27, No. 2, February 1984, p. 331.

20. Mack L.M.: "Remarks on Disputed Numerical Results in Compressible Boundary-Layer Stability Theory", Physics of Fluids, Vol. 27, February 1984, p. 342.

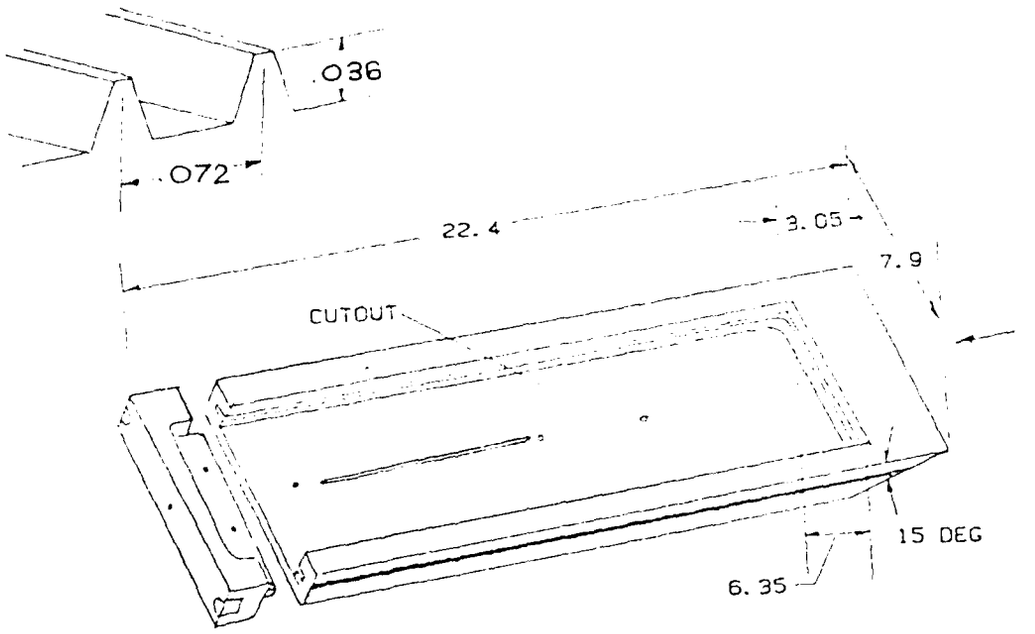

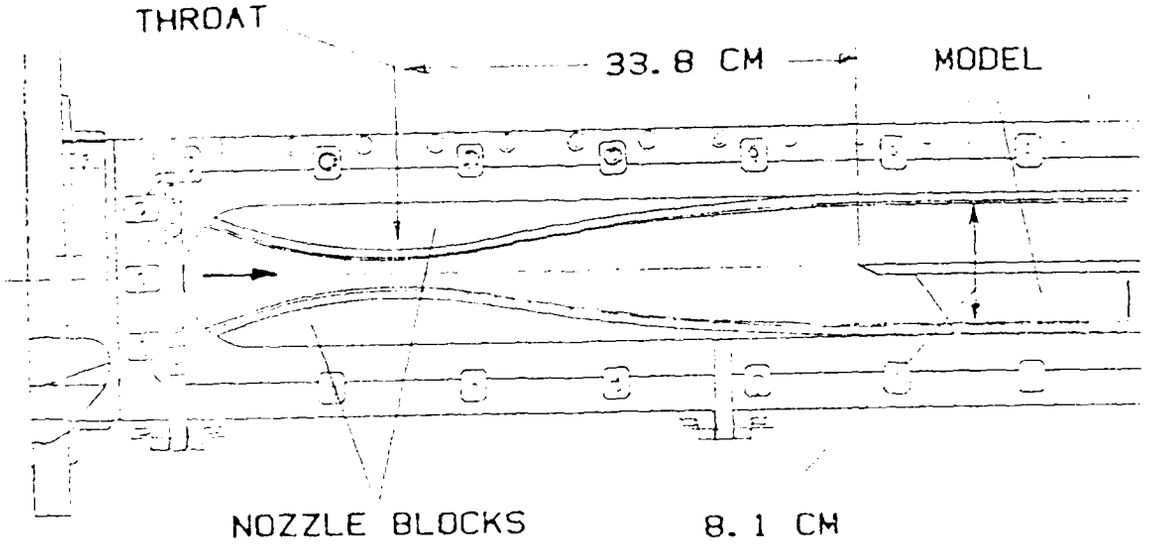

Figure 1. Top: Schematic of flat plate model, showing "tooth" geometry at upper left. All dimensions in cm.
Bottom: Installation of model in the wind-tunnel.

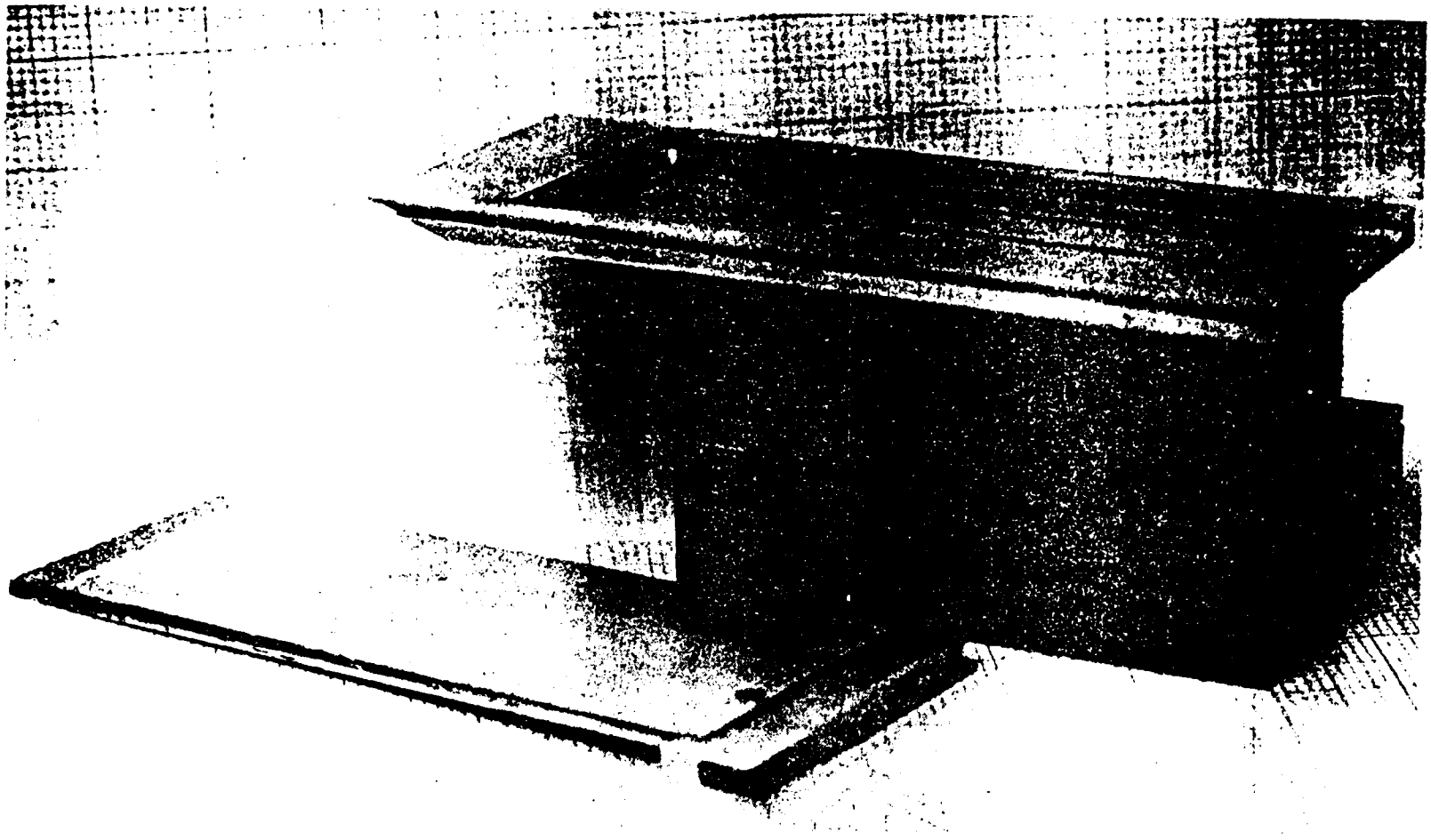

Figure 2. Flat plate model. Smooth-wall insert in foreground.

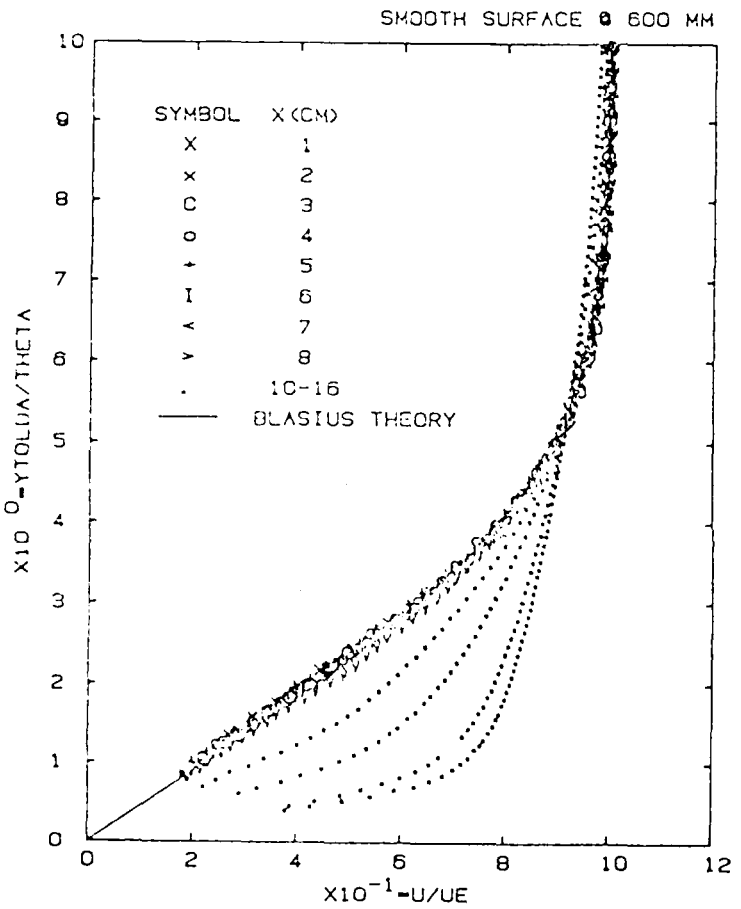

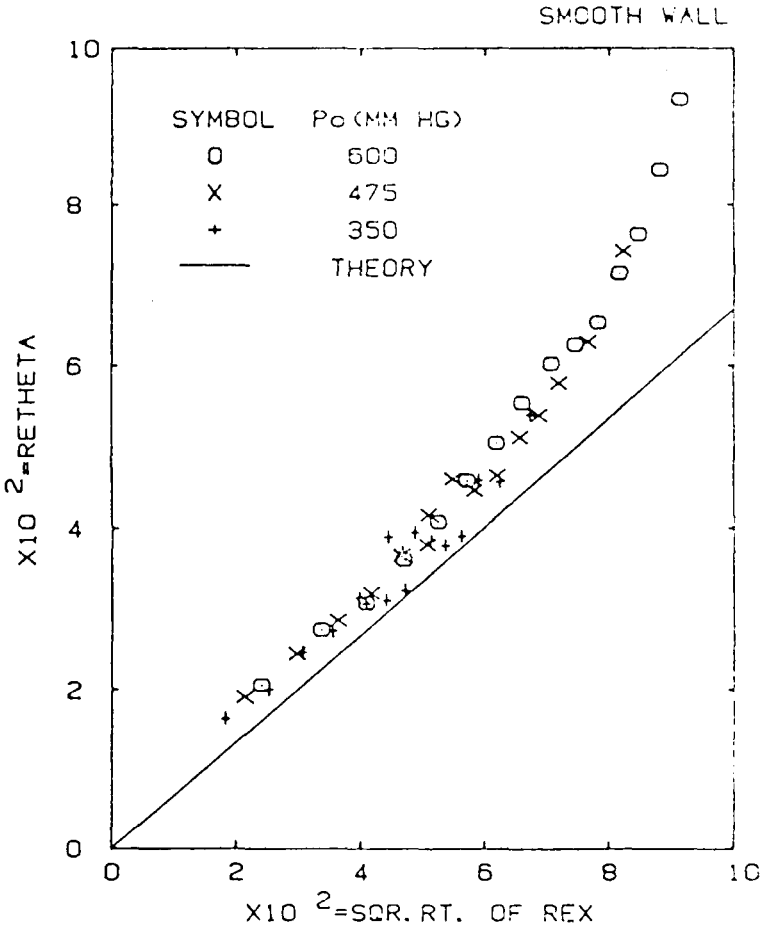

Figure 3. Typical smooth-wall velocity profiles (left) and the Re_θ variations with Re_x.

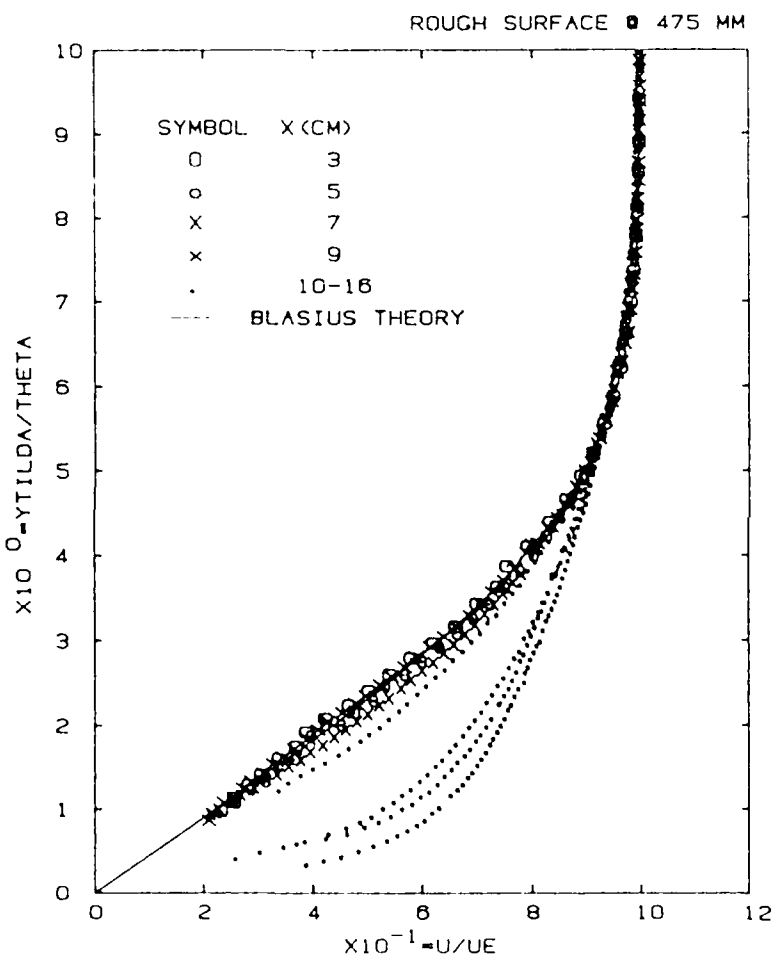

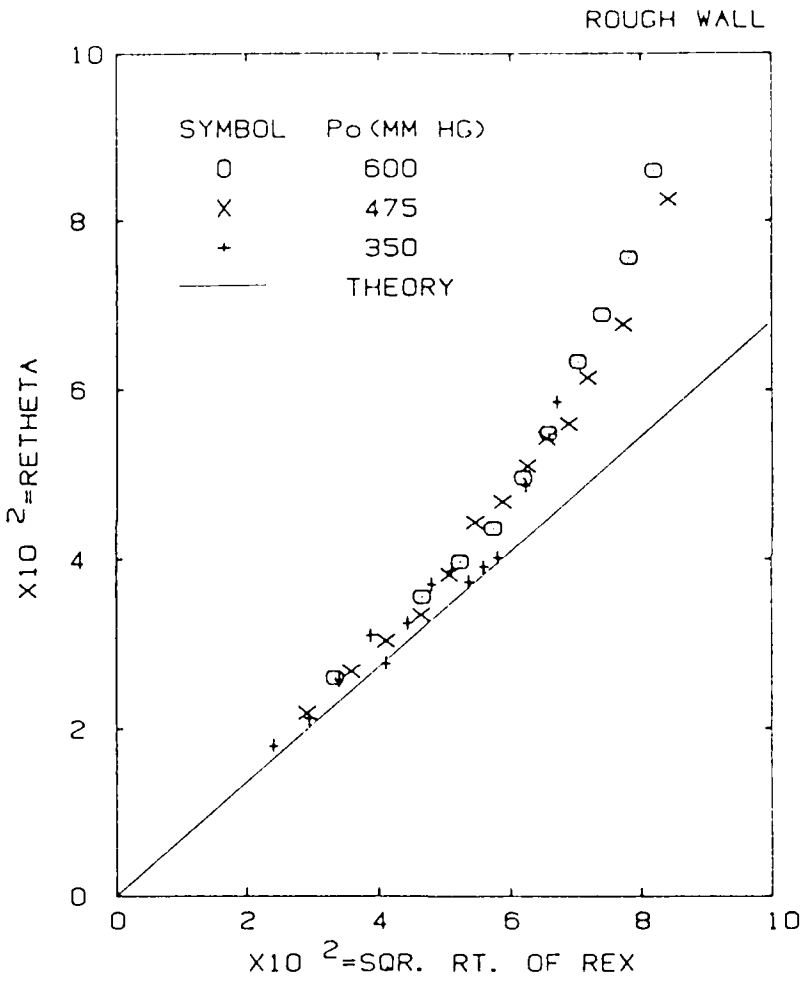

Figure 4. Typical rough-wall velocity profiles (left) and the variation of Re_θ with Re_x.

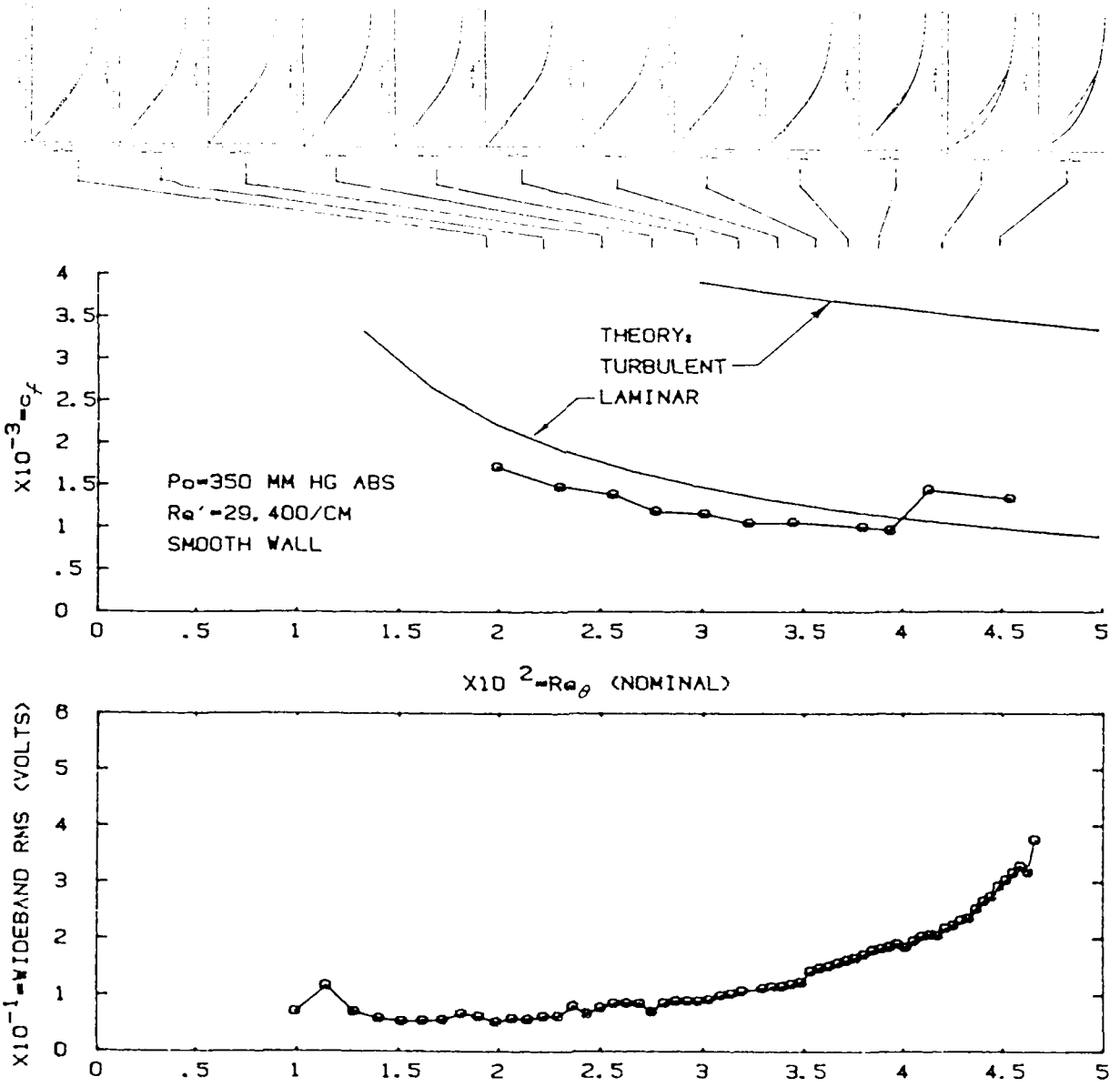

Figure 5. Velocity profiles (top), friction coefficient (middle) and the hot-wire rms wideband output (bottom) along the smooth wall, p_0=350.

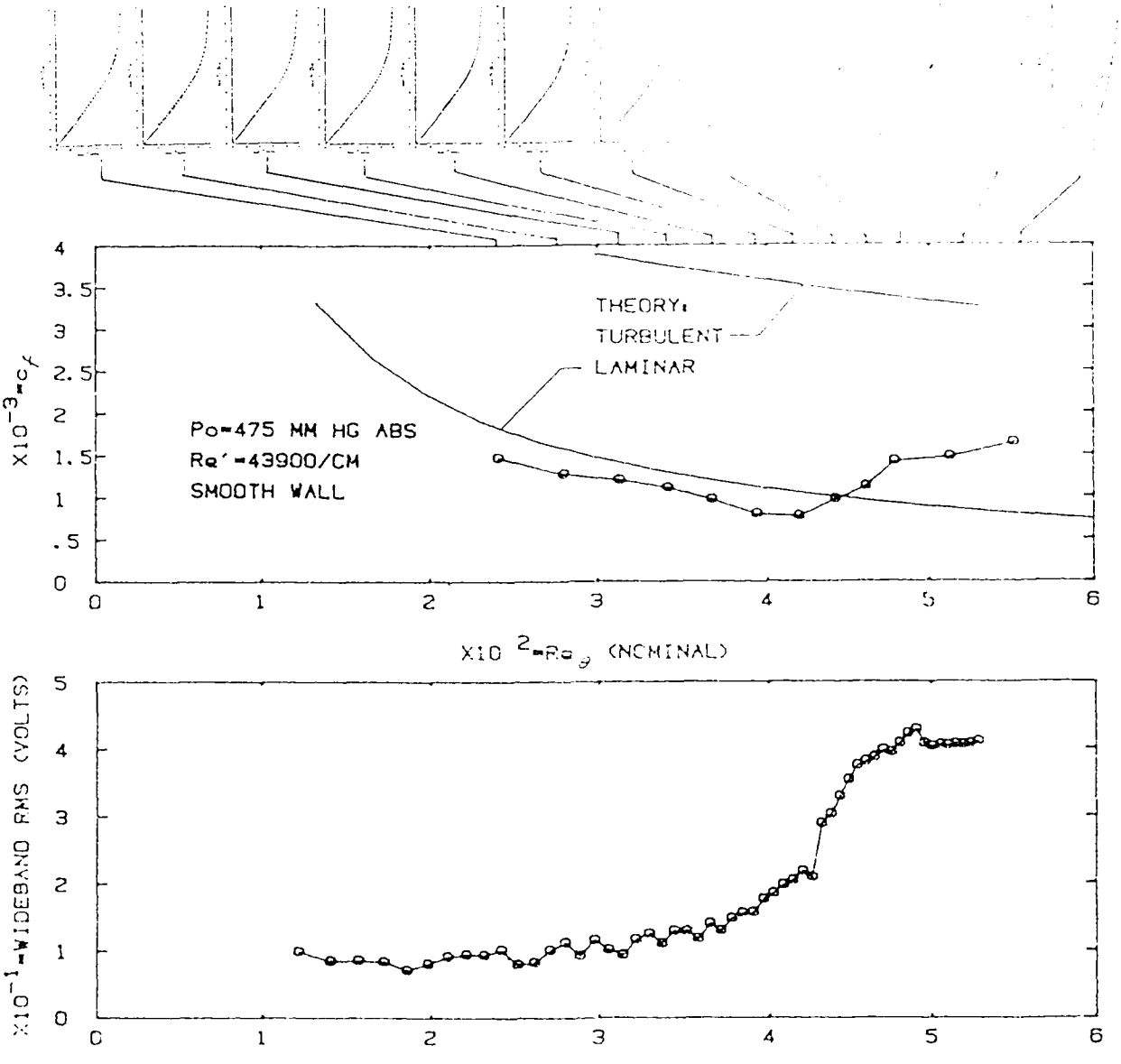

Figure 6. Velocity profiles (top), friction coefficient (middle) and the hot-wire wideband rms output (bottom) along the smooth wall, p_0=475.

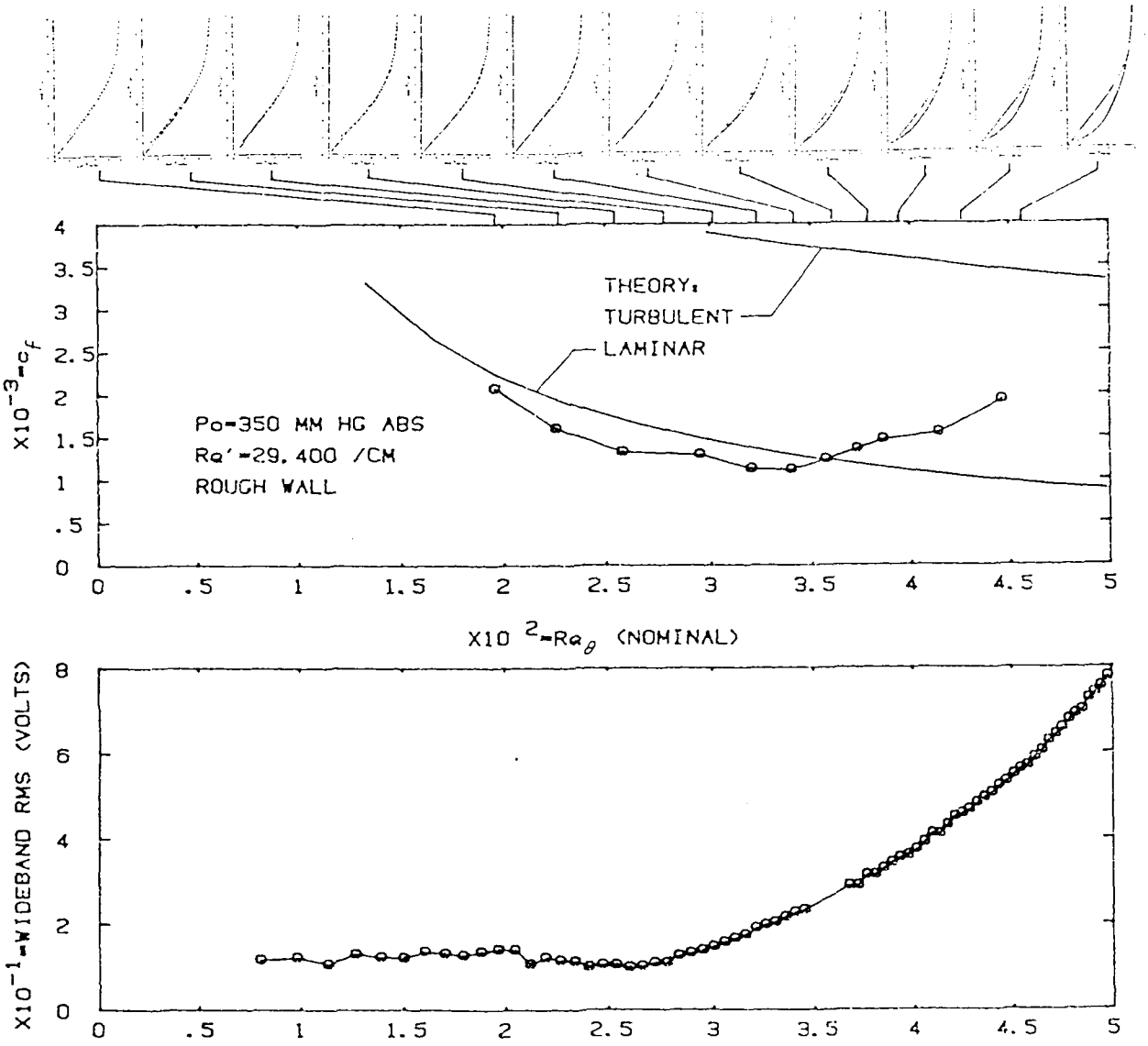

Figure 7. Velocity profiles (top), friction coefficient (middle) and the hot-wire wideband rms output (bottom) along the rough wall, p_o=350.

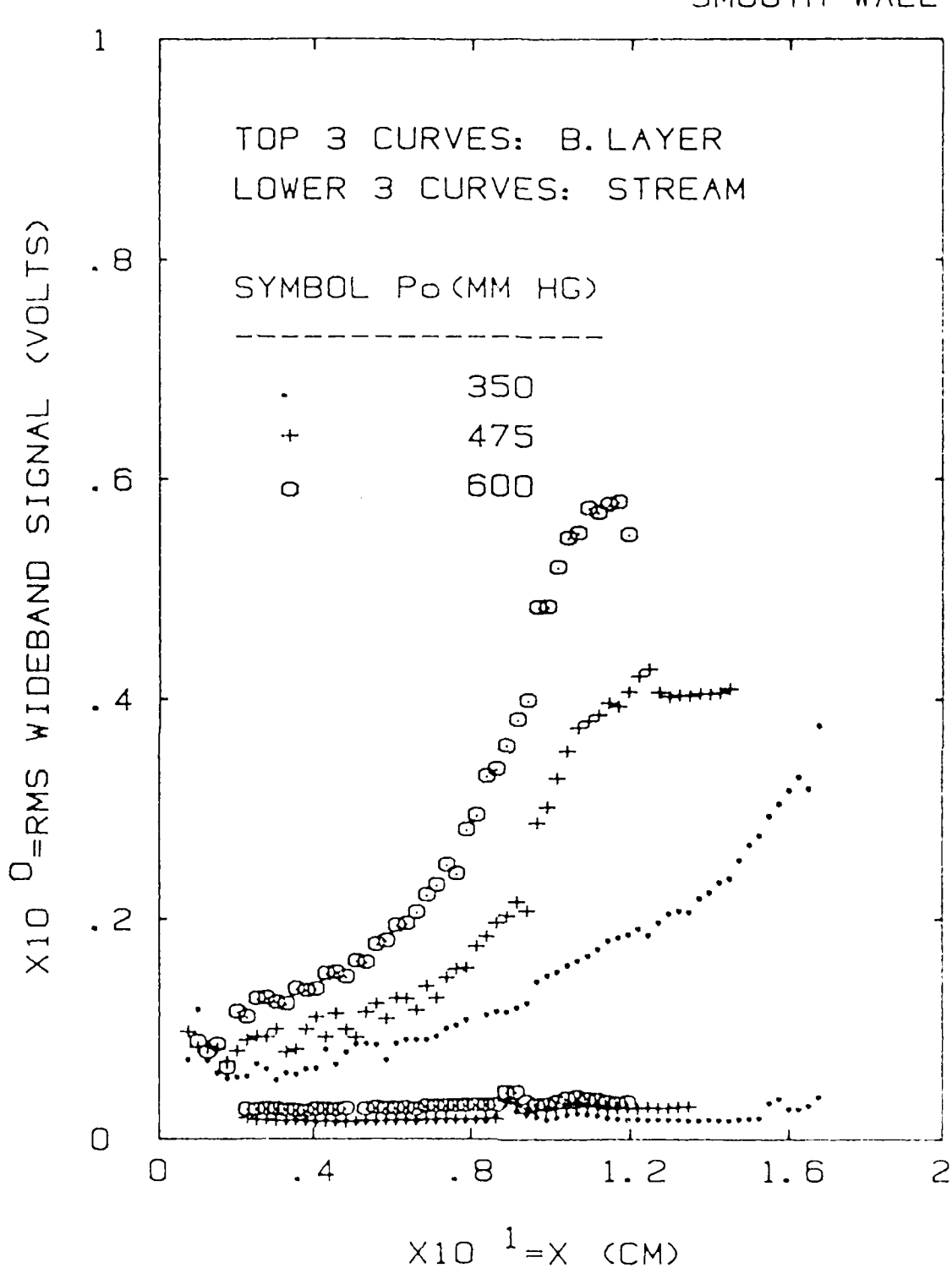

Figure 8. Wideband rms output along the smooth wall.

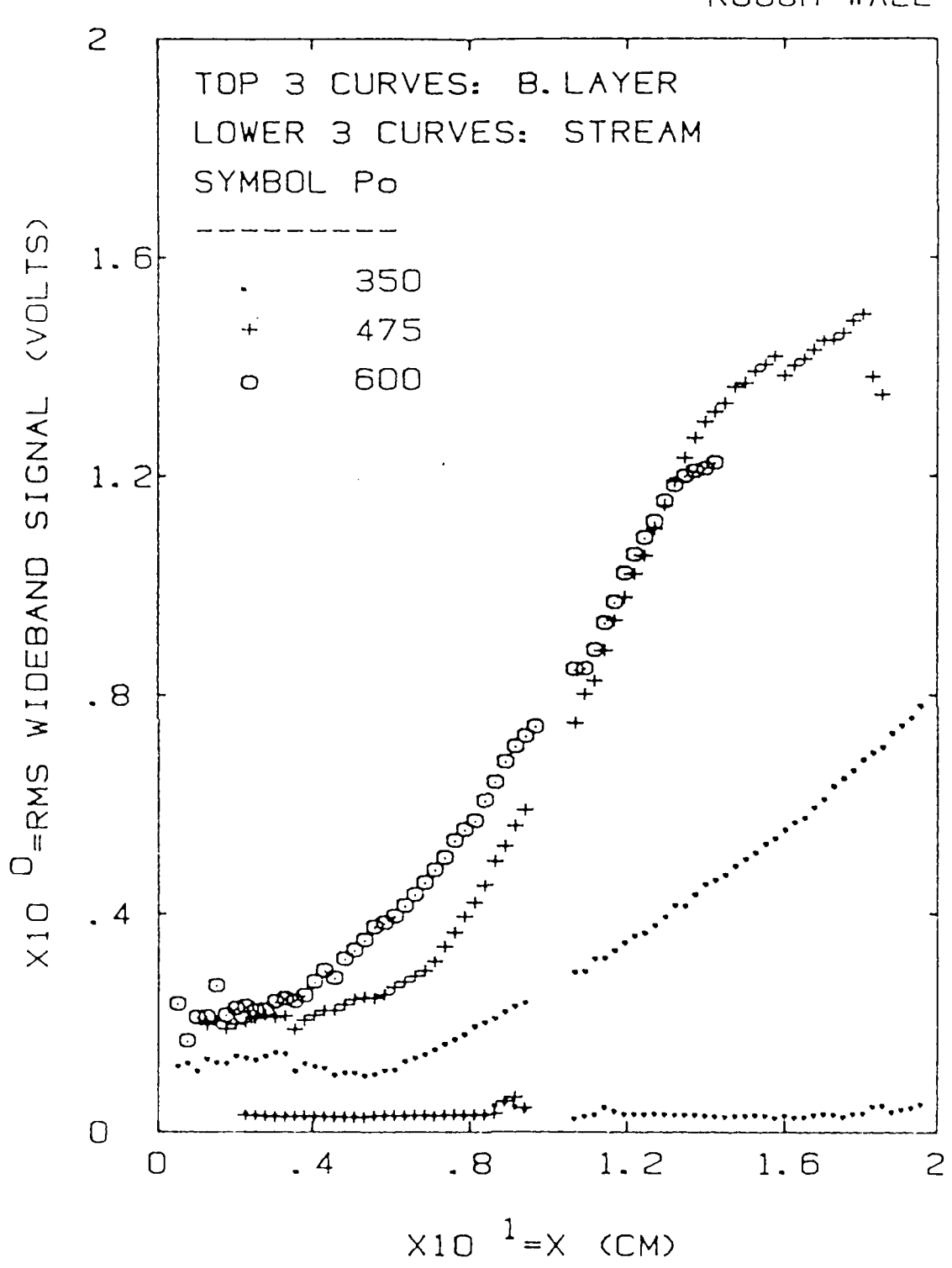

Figure 9. Wideband rms output along the rough wall.

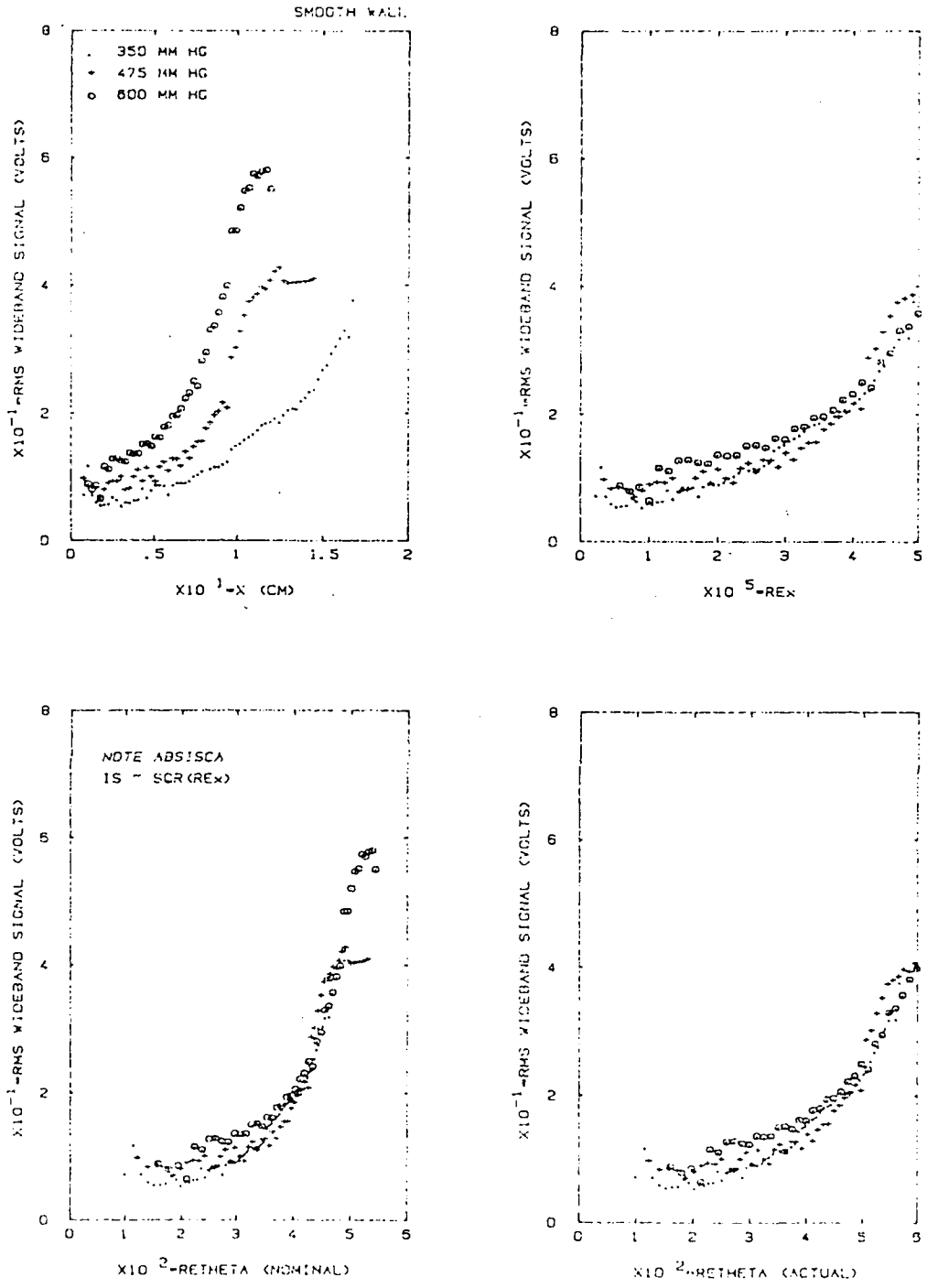

Figure 10. Reynolds-number scaling of the wideband rms variation, smooth wall.

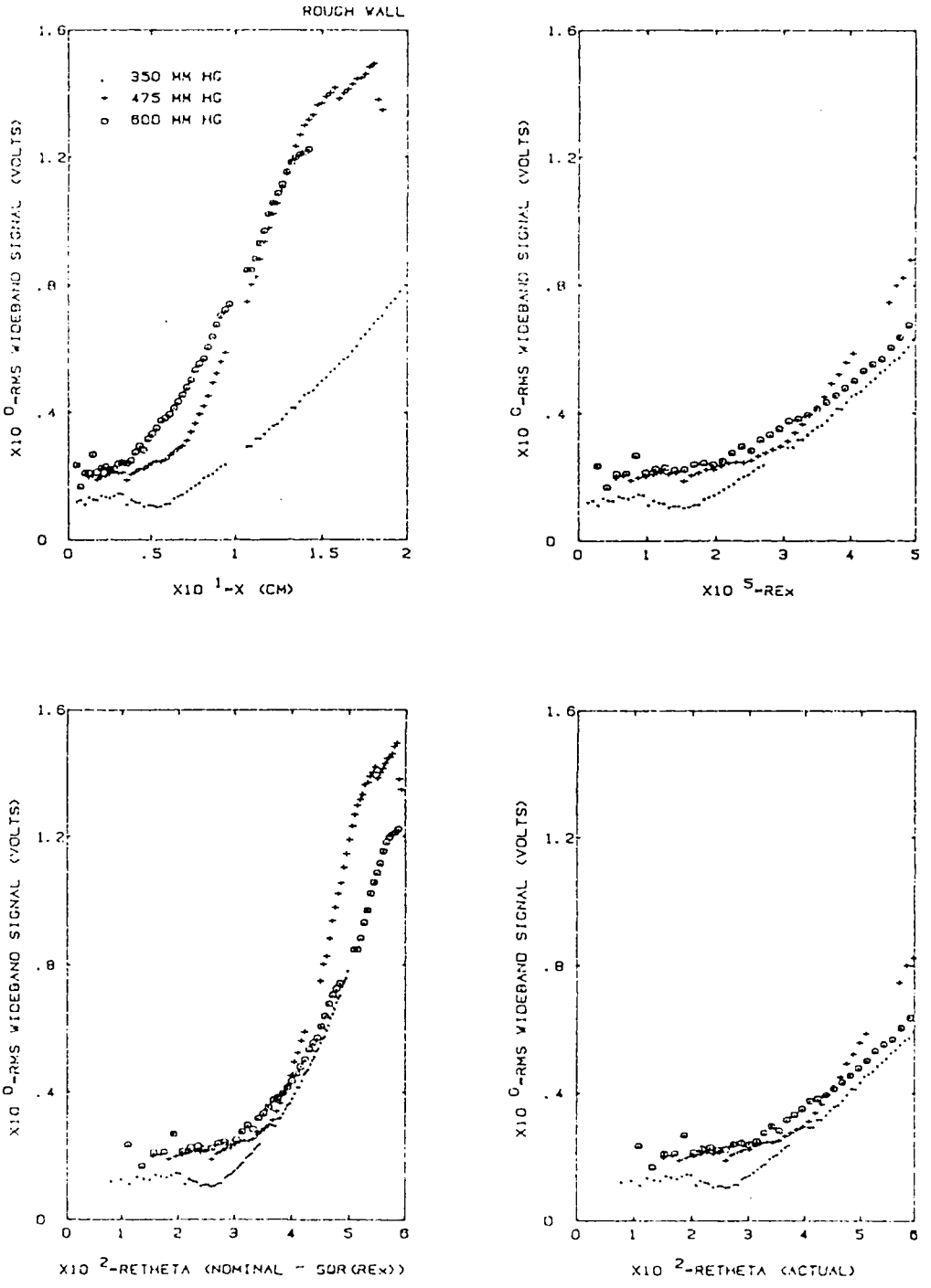

Figure 11. Reynolds-number scaling of the wideband rms variation, rough wall.

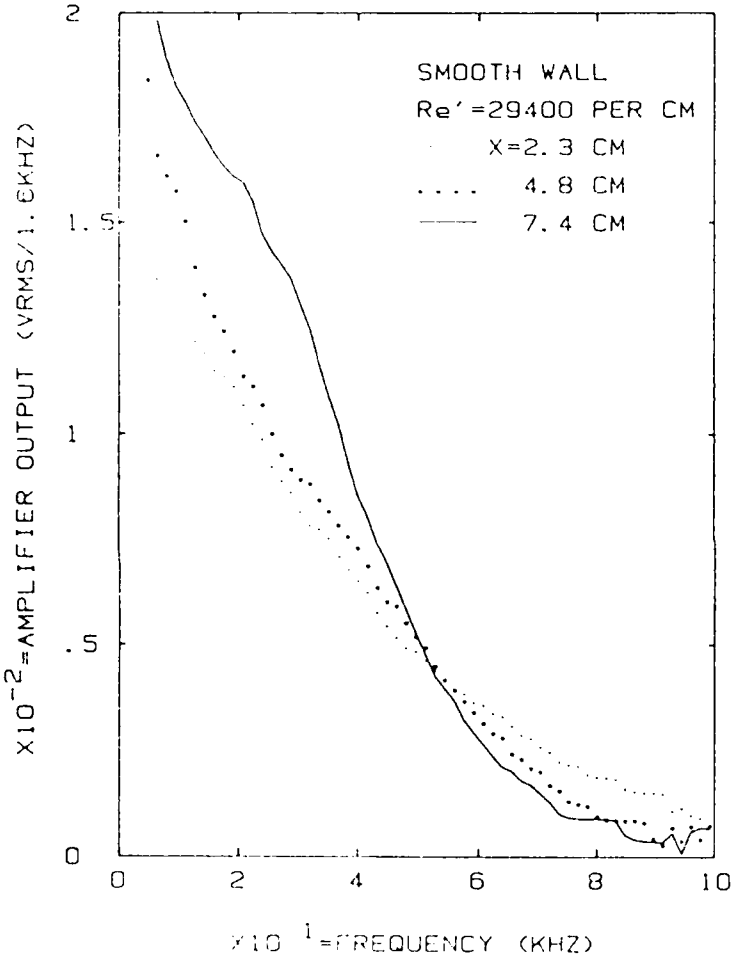

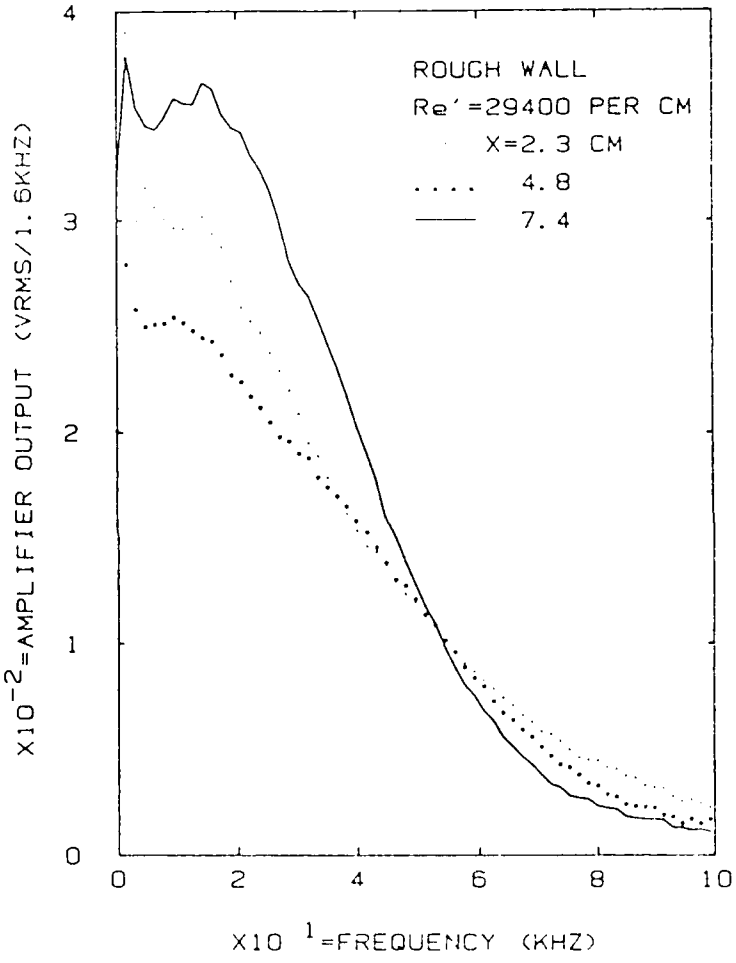

Figure 12. Typical fluctuation spectra, p_o= 350 torr.

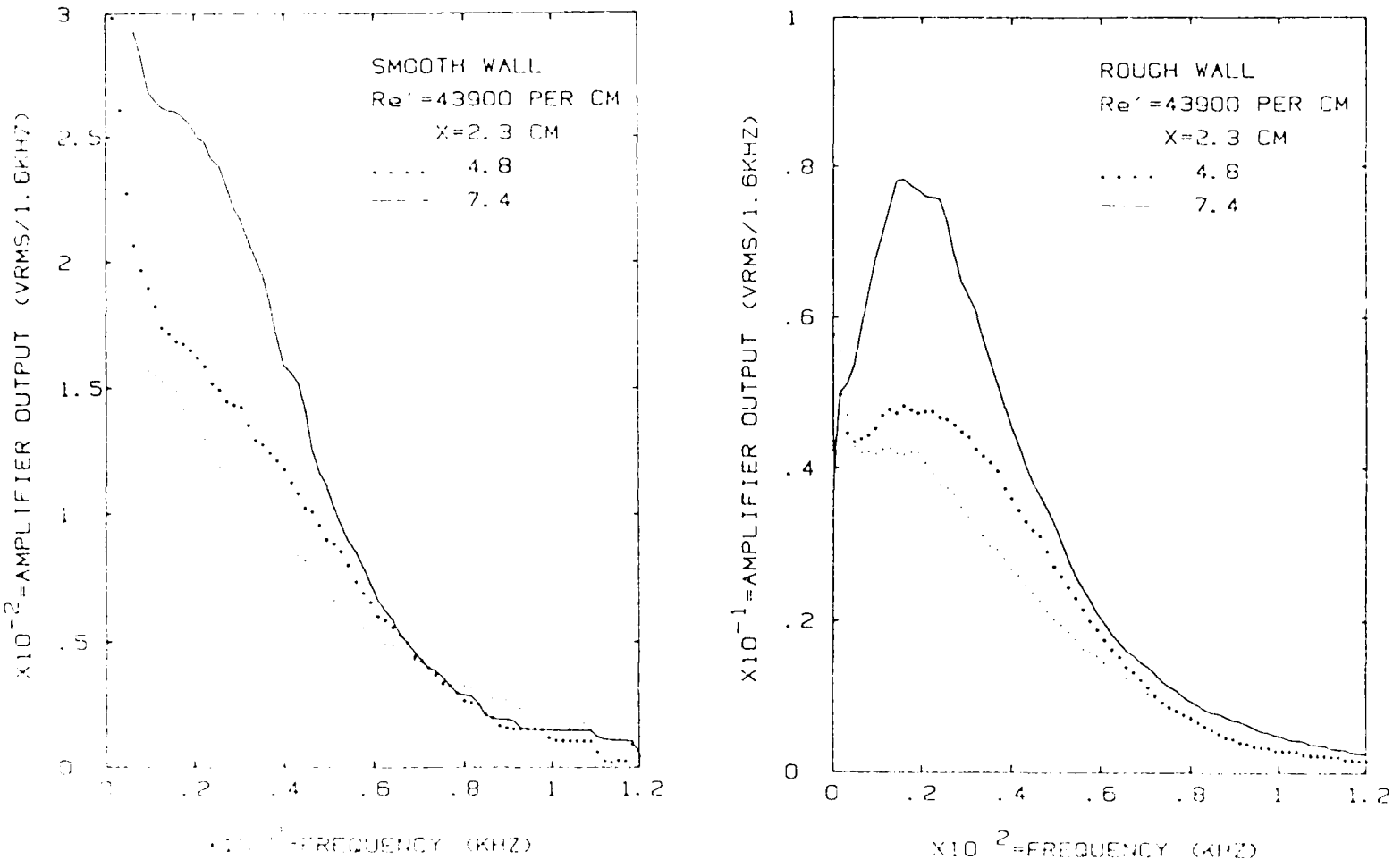

Figure 13. Typical fluctuation spectra, p_o=475 torr.

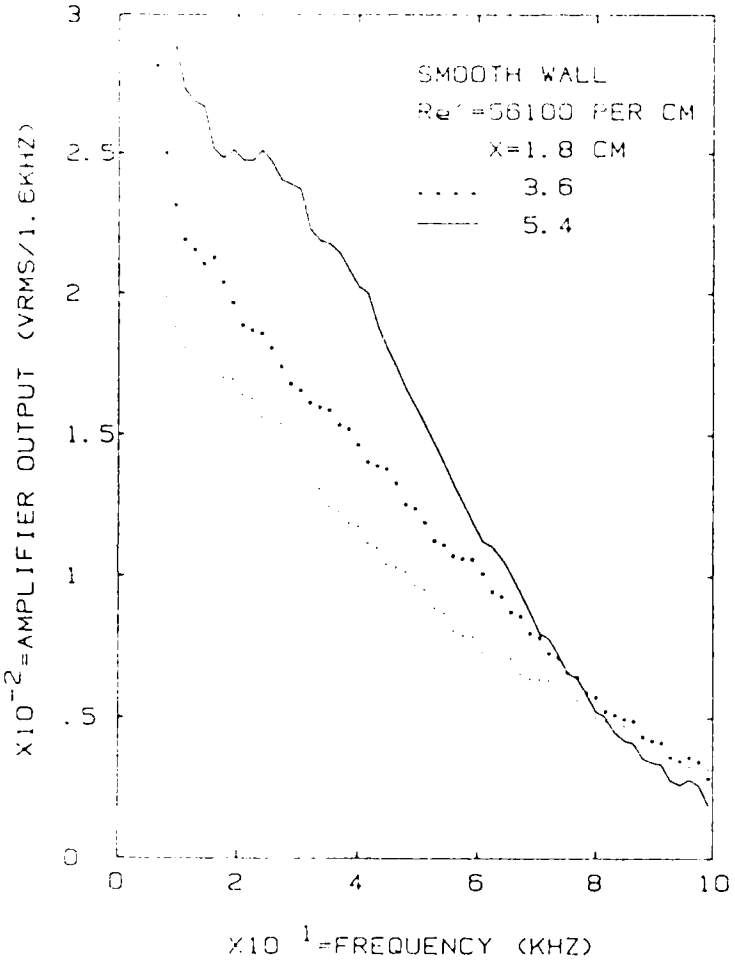

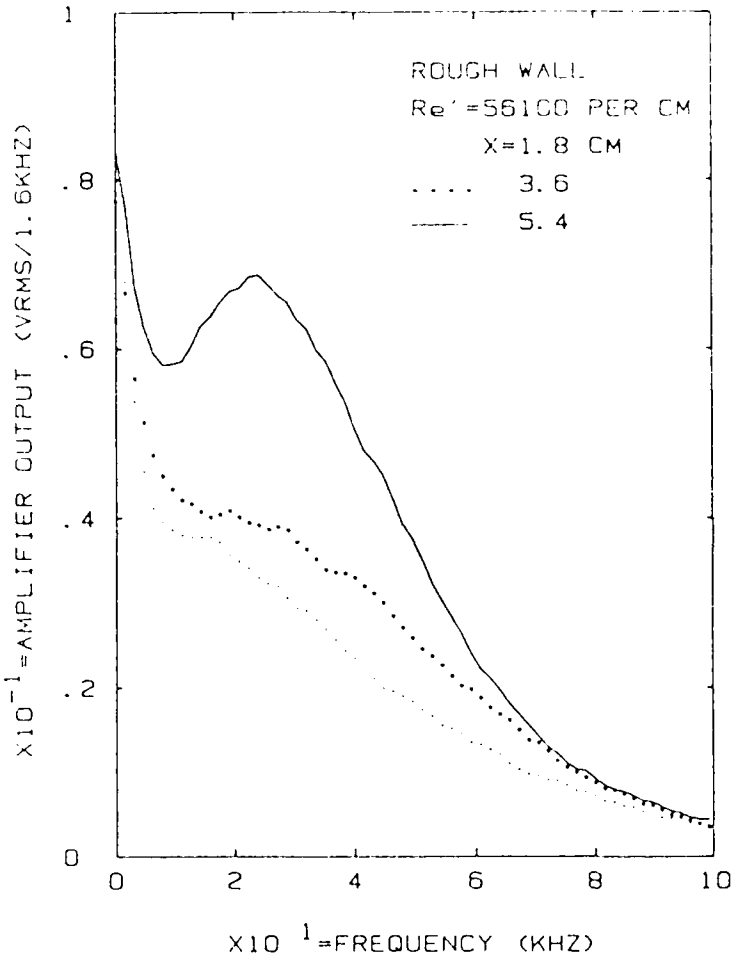

Figure 14. Typical fluctuation spectra, p_o = 600 torr.

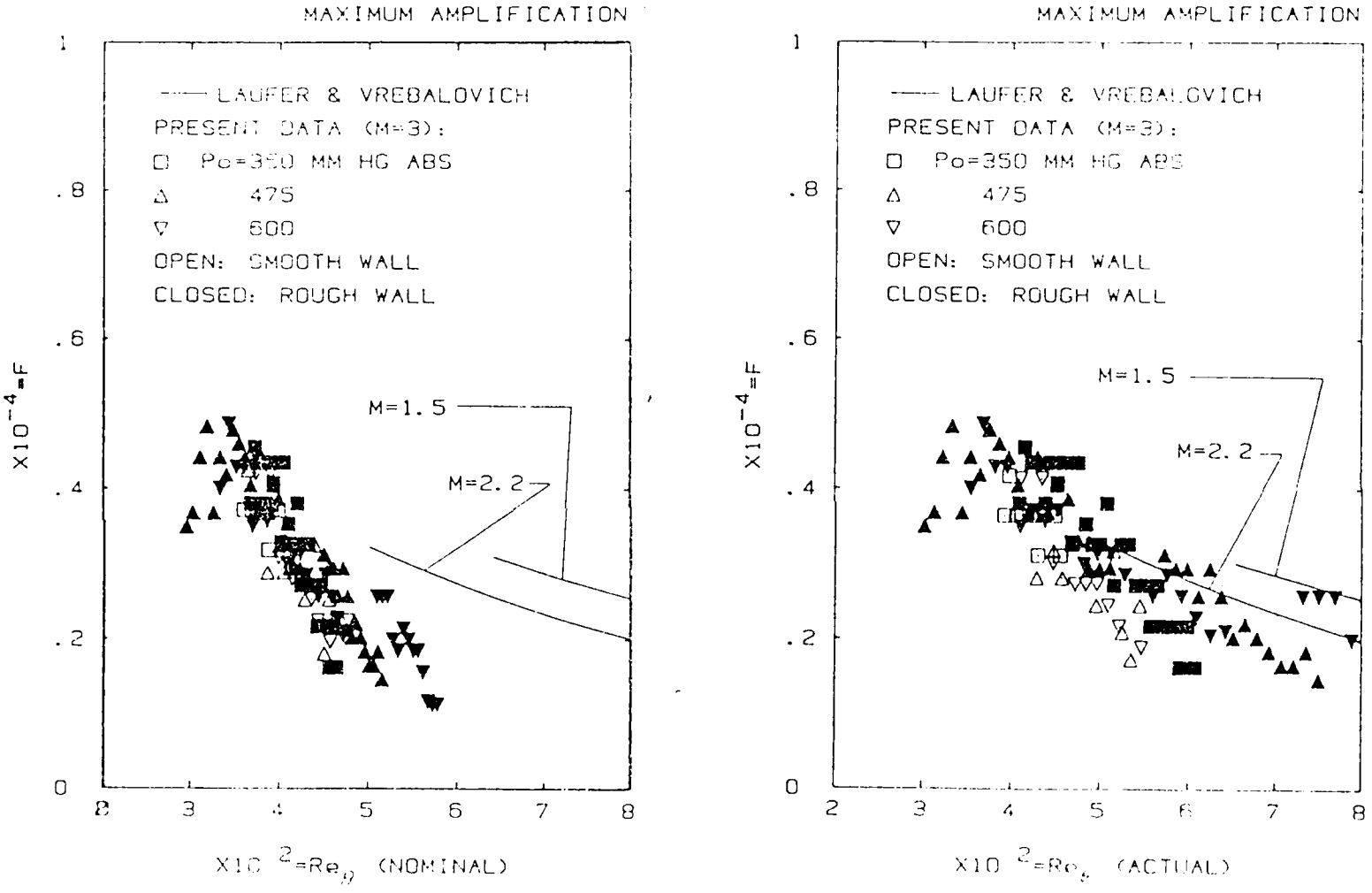

Figure 15. Maximum amplitude line obtained from the fluctuation spectra.

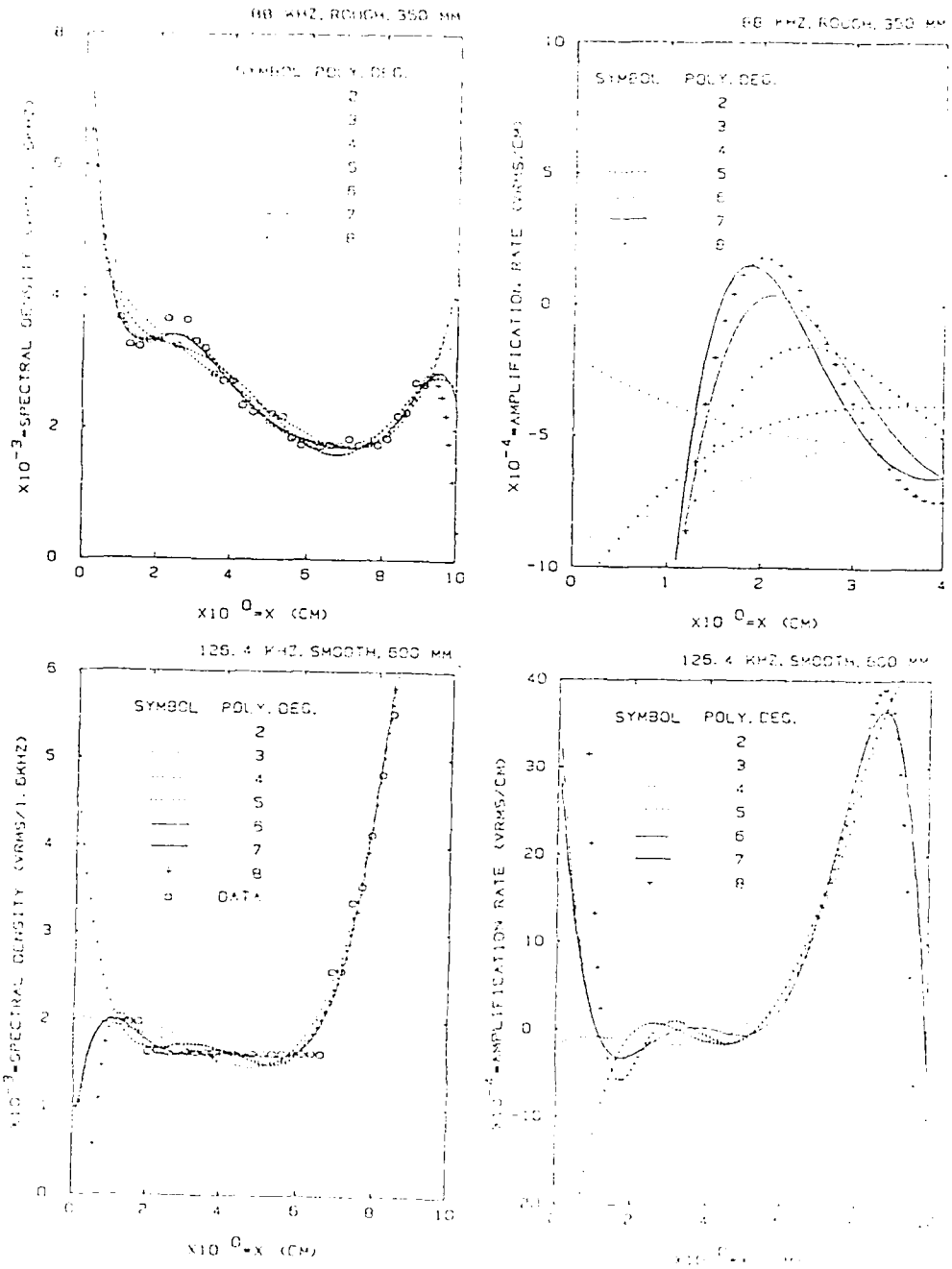

Figure 16. Effect of polynomial degree on least-squares fit (left) and the resulting amplification rates (right).

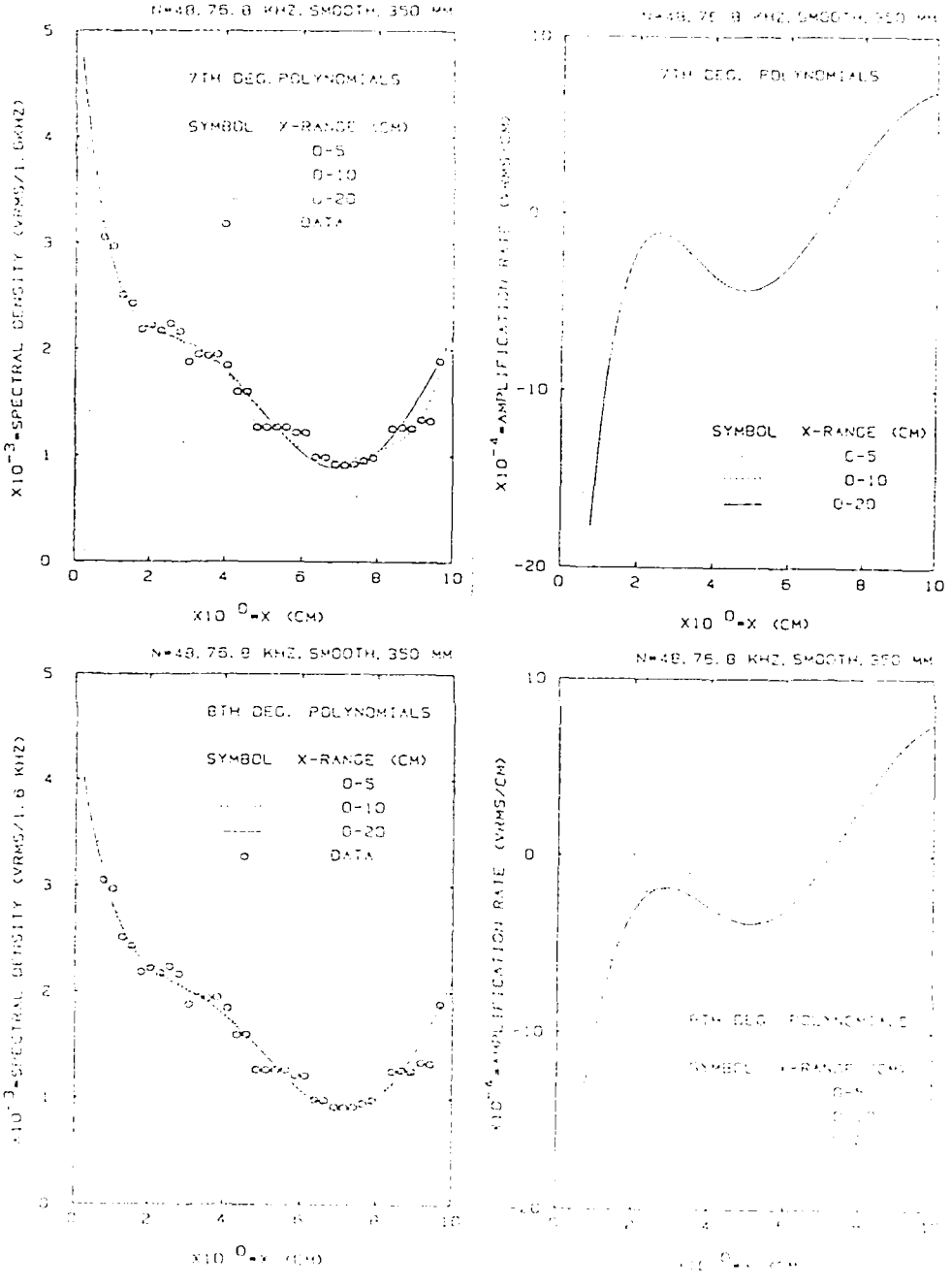

Figure 17. Effect of fitted data range for fixed polynomial degree on the amplitudes (left) and amplification rates (right).

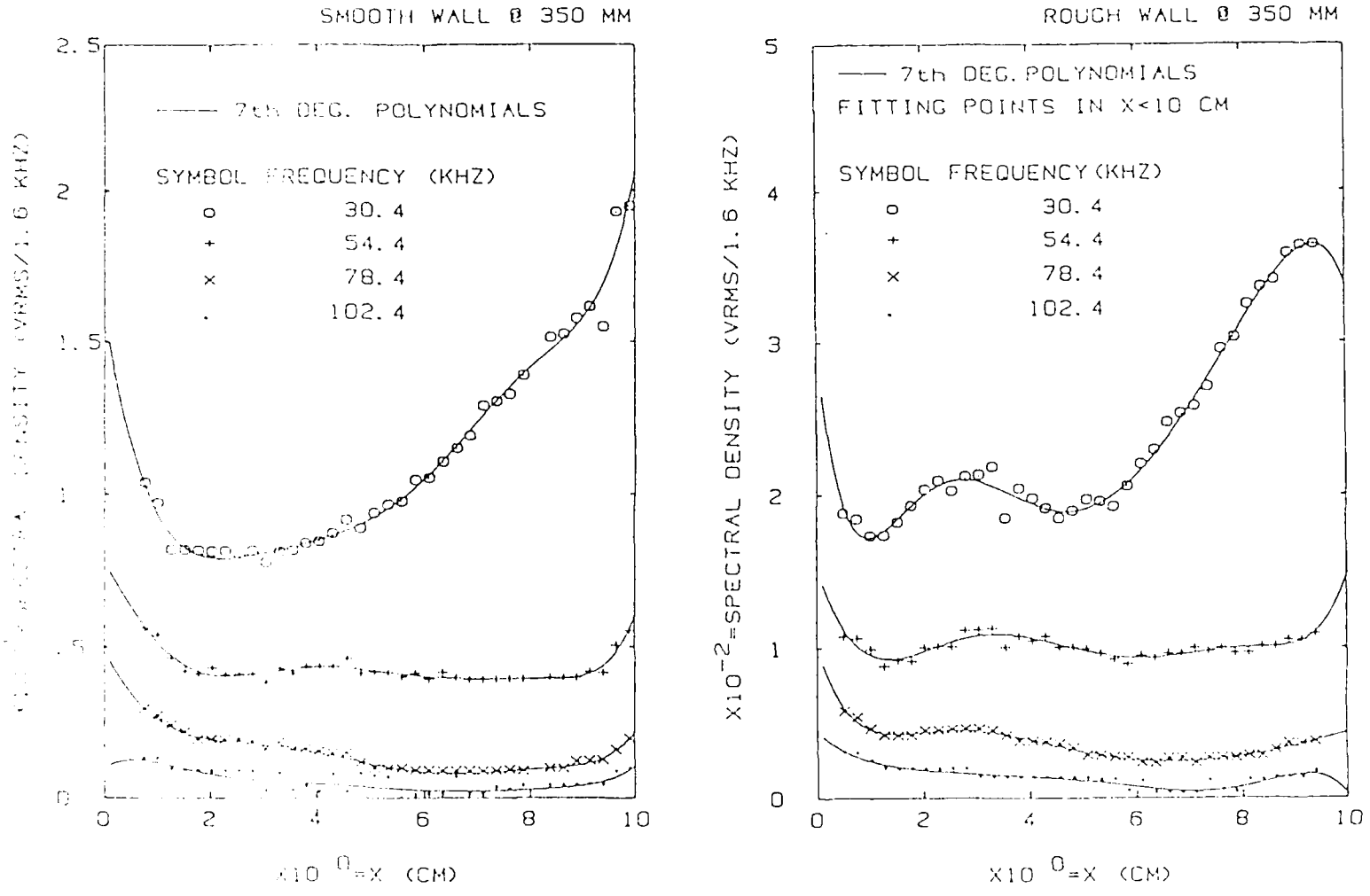

Figure 18. Typical amplitude variations for p_o = 350 torr.

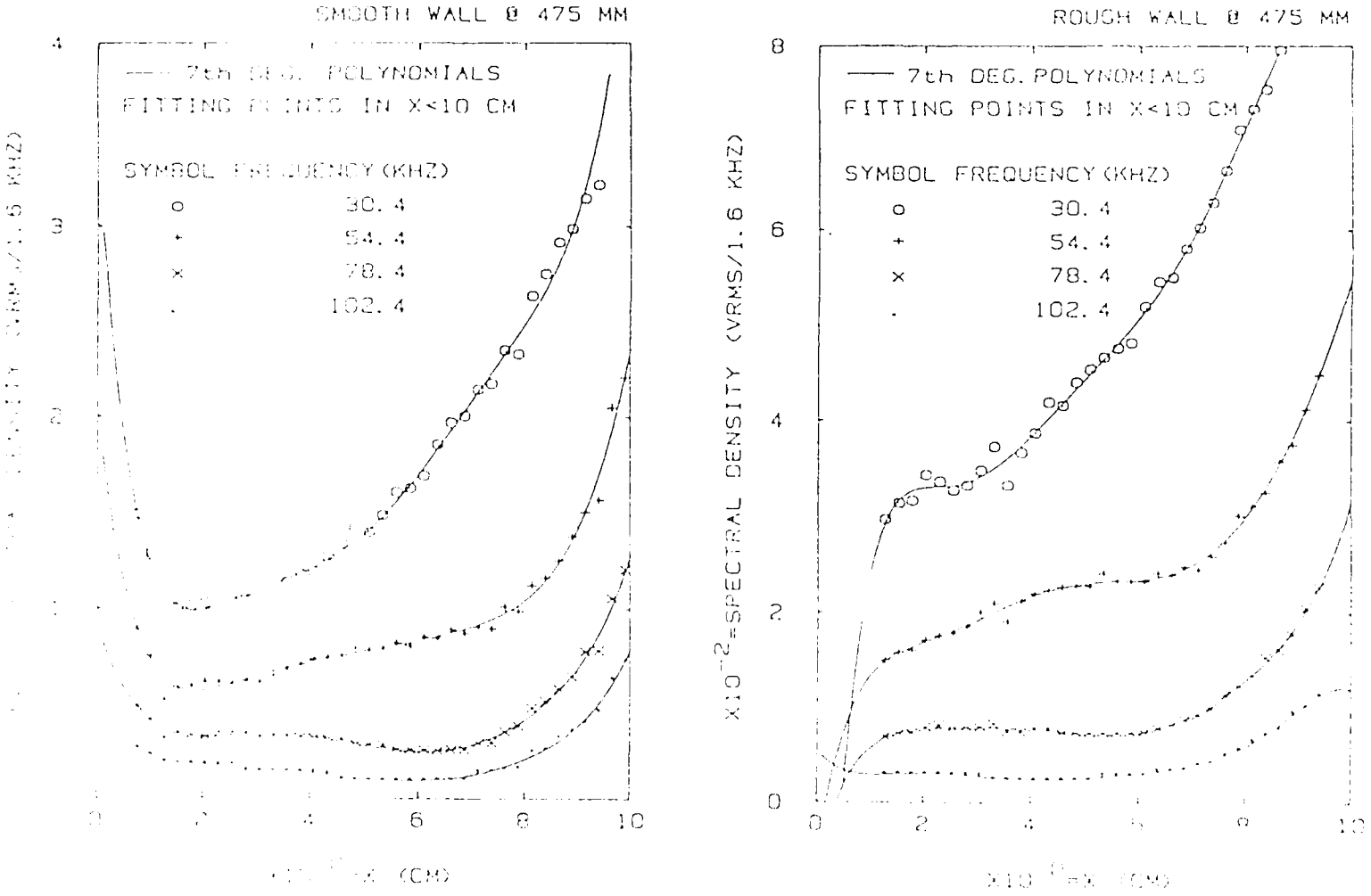

Figure 19. Typical amplitude variations for p_o = 475 torr.

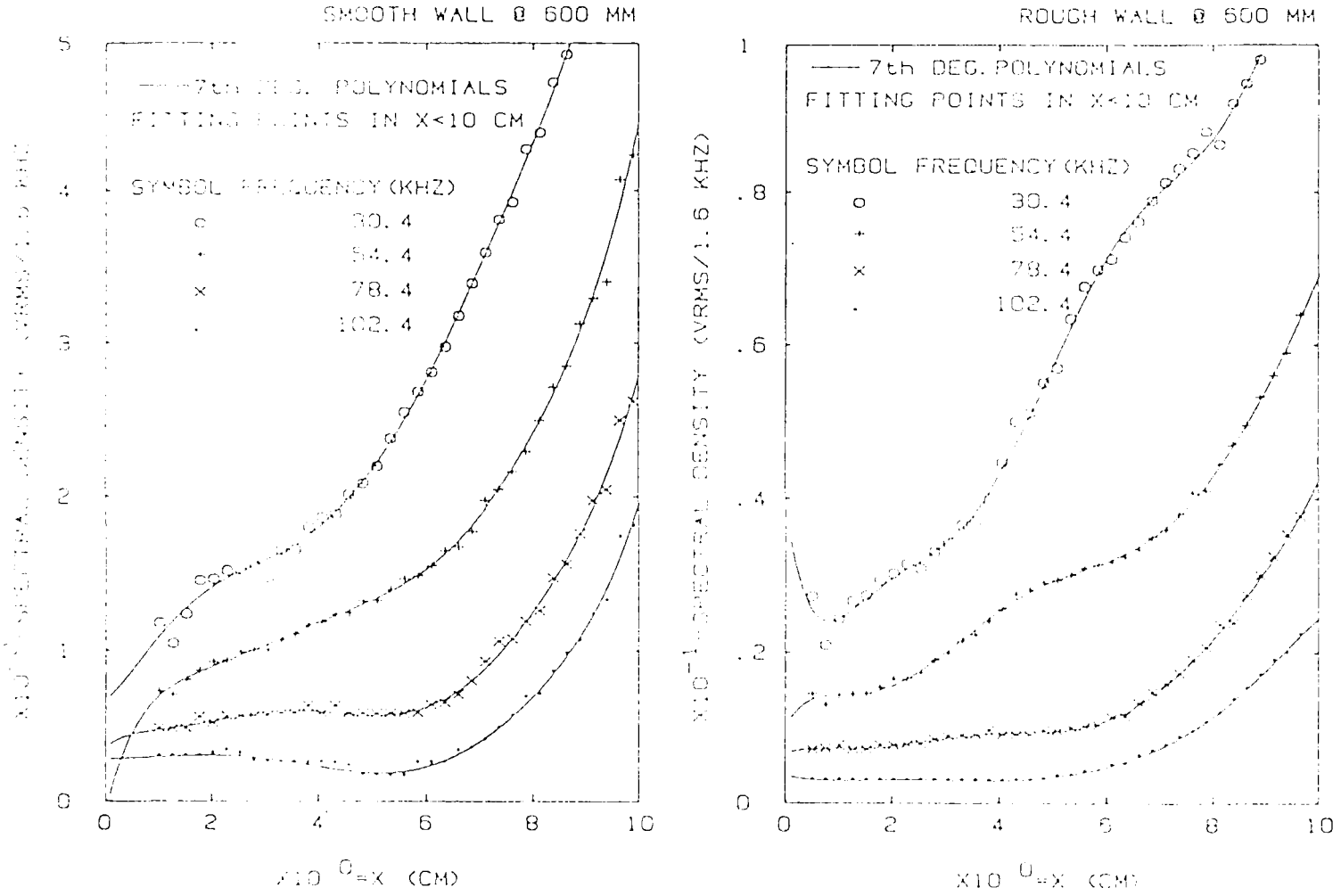

Figure 20. Typical amplitude variations for p_o = 600 torr.

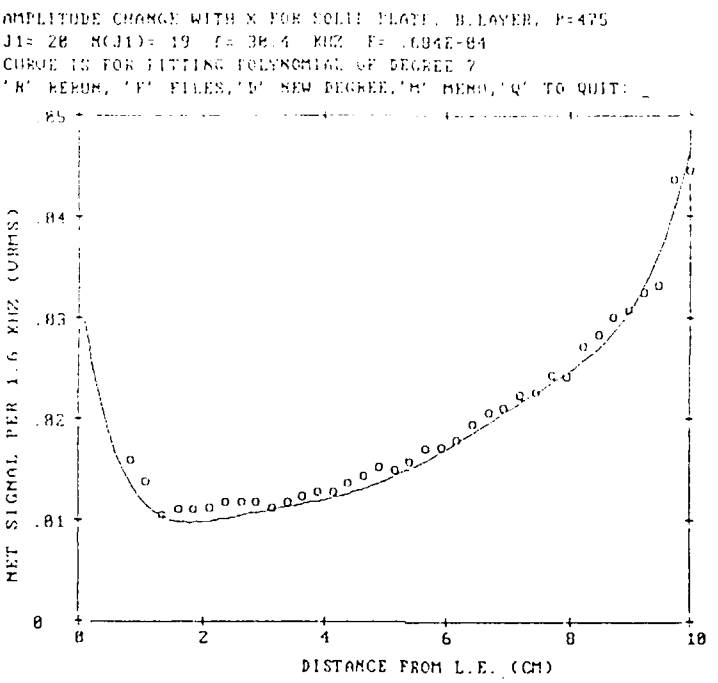

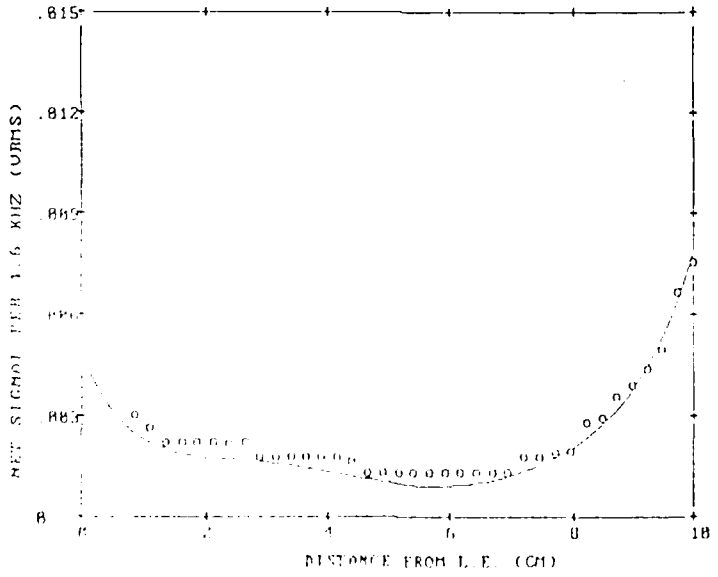

Figure 21. Typical computer CRT displays during the process of trying various polynomial degrees to attain the best possible curve-fit.

FIGURE LEGEND

Numbers are 1000F (F=n/d frequency)

SMOOTH WALL Po (MM):	350	475	600
f (KHZ)			
30.4	.101	.0684	.0532
54.4	.18	.122	.0952
78.4	.26	.176	.137
102.4	.339	.23	.179
ROUGH WALL			
30.4	.103	.0699	.0544
54.4	.185	.125	.0974
78.4	.267	.18	.14
102.4	.348	.236	.169

SYMBOLS

30.4 ·····

54.4 ·····

78.4 · - · - ·

102.4 ——

Figure 22. Key to Figures 23-25.

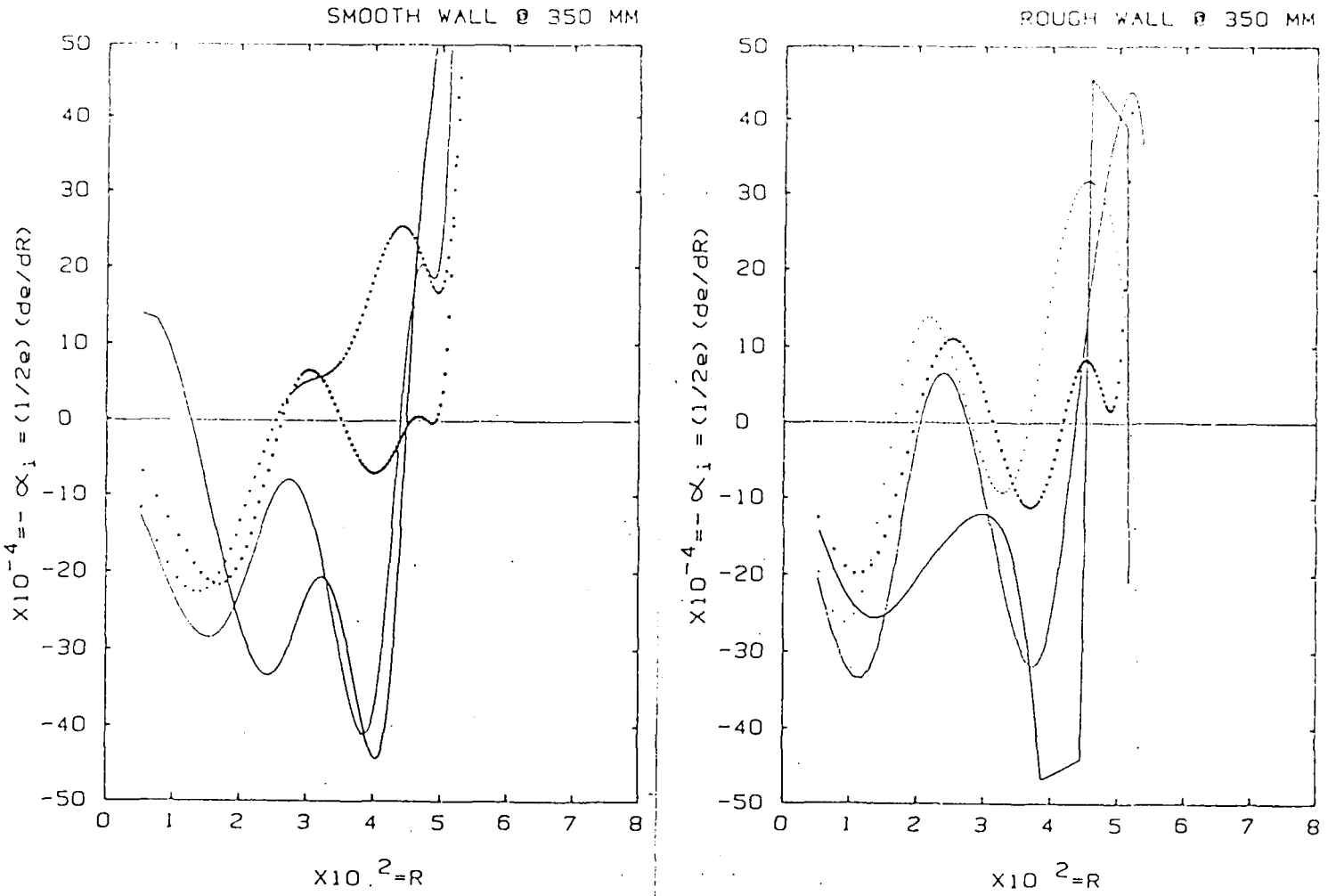

Figure 23. Effect of frequency on the amplification rates, p_o= 350 torr.

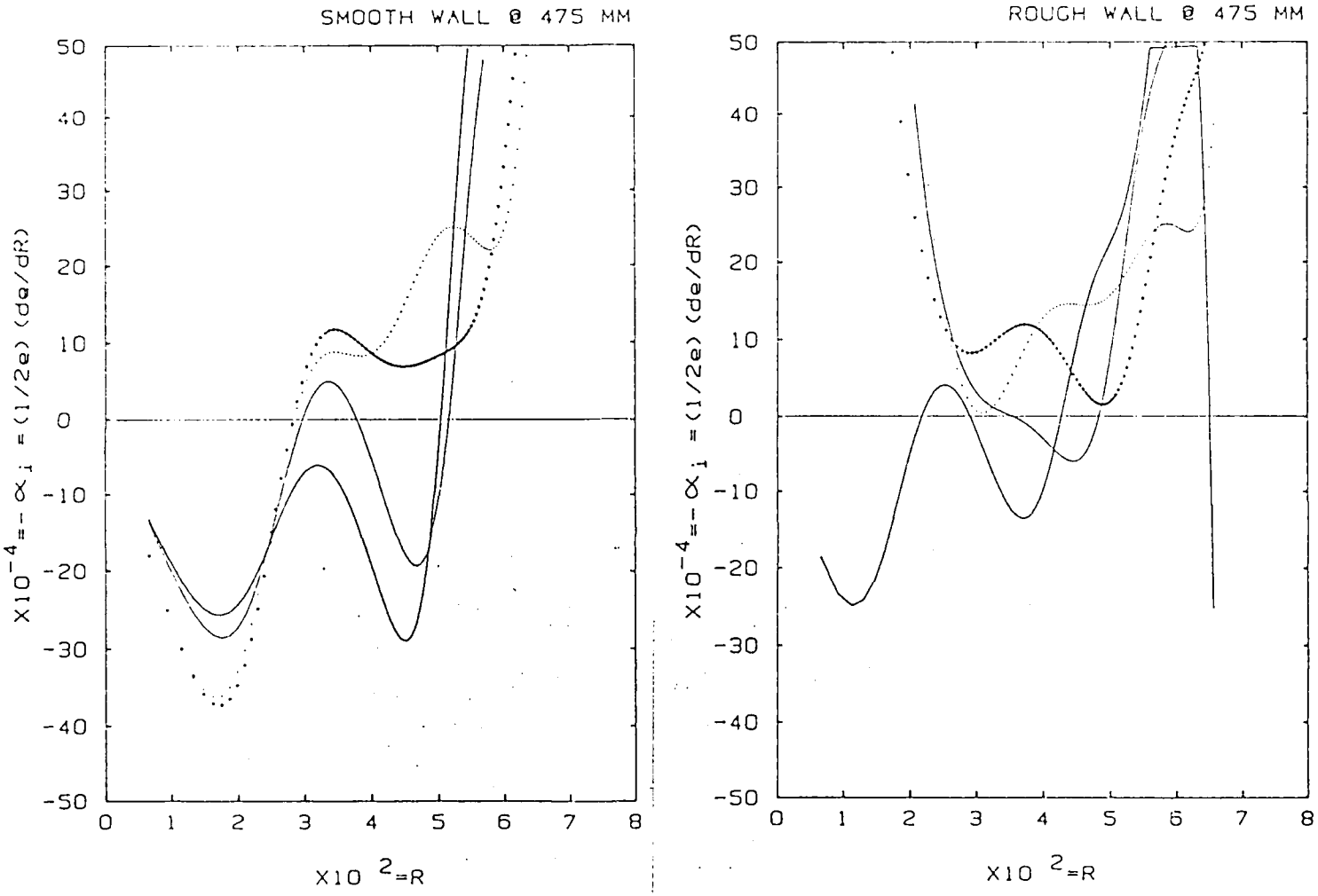

Figure 24. Effect of frequency on the amplification rates, p_o= 475 torr.

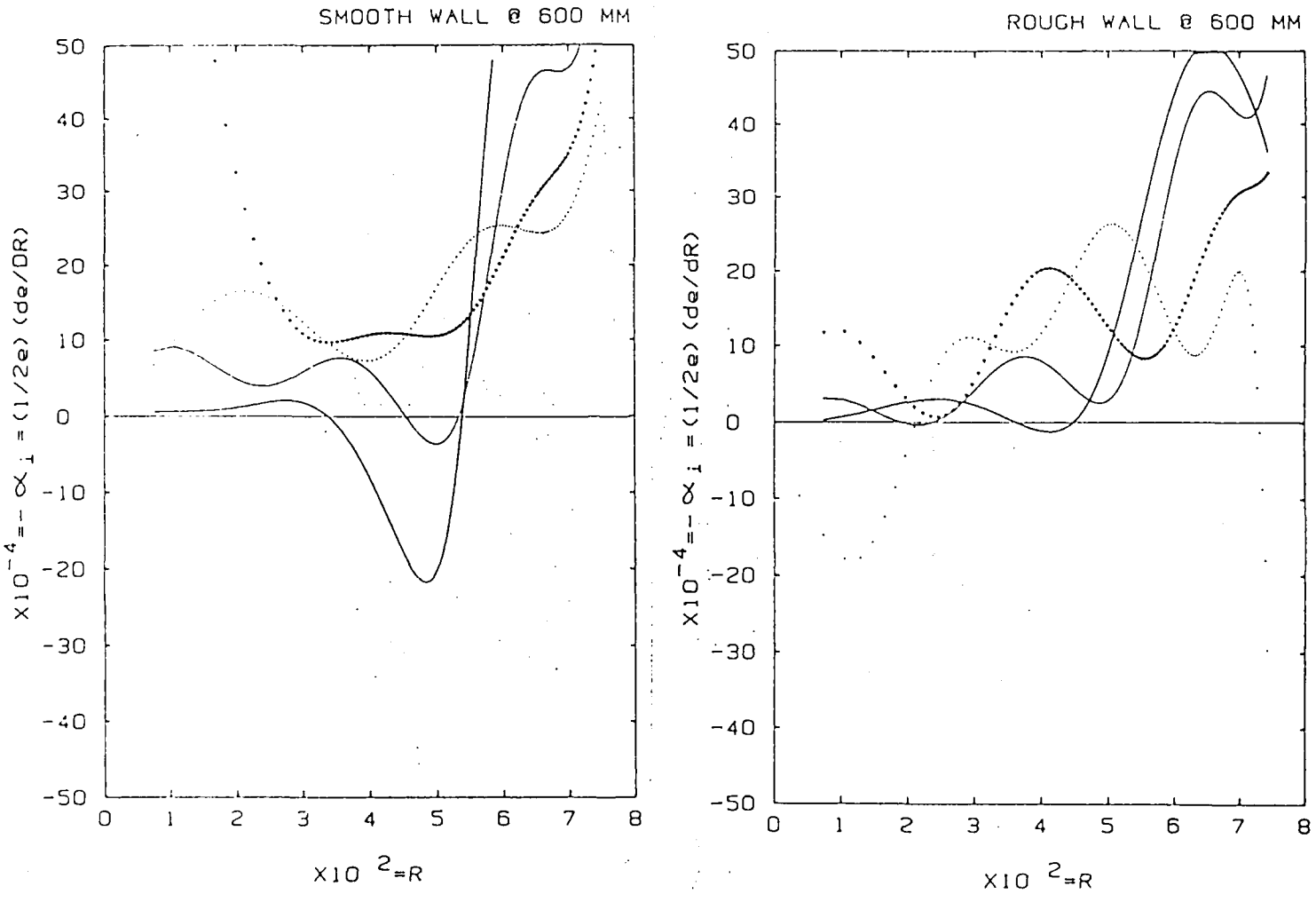

Figure 25. Effect of frequency on the amplification rates, P_0= 600 torr.

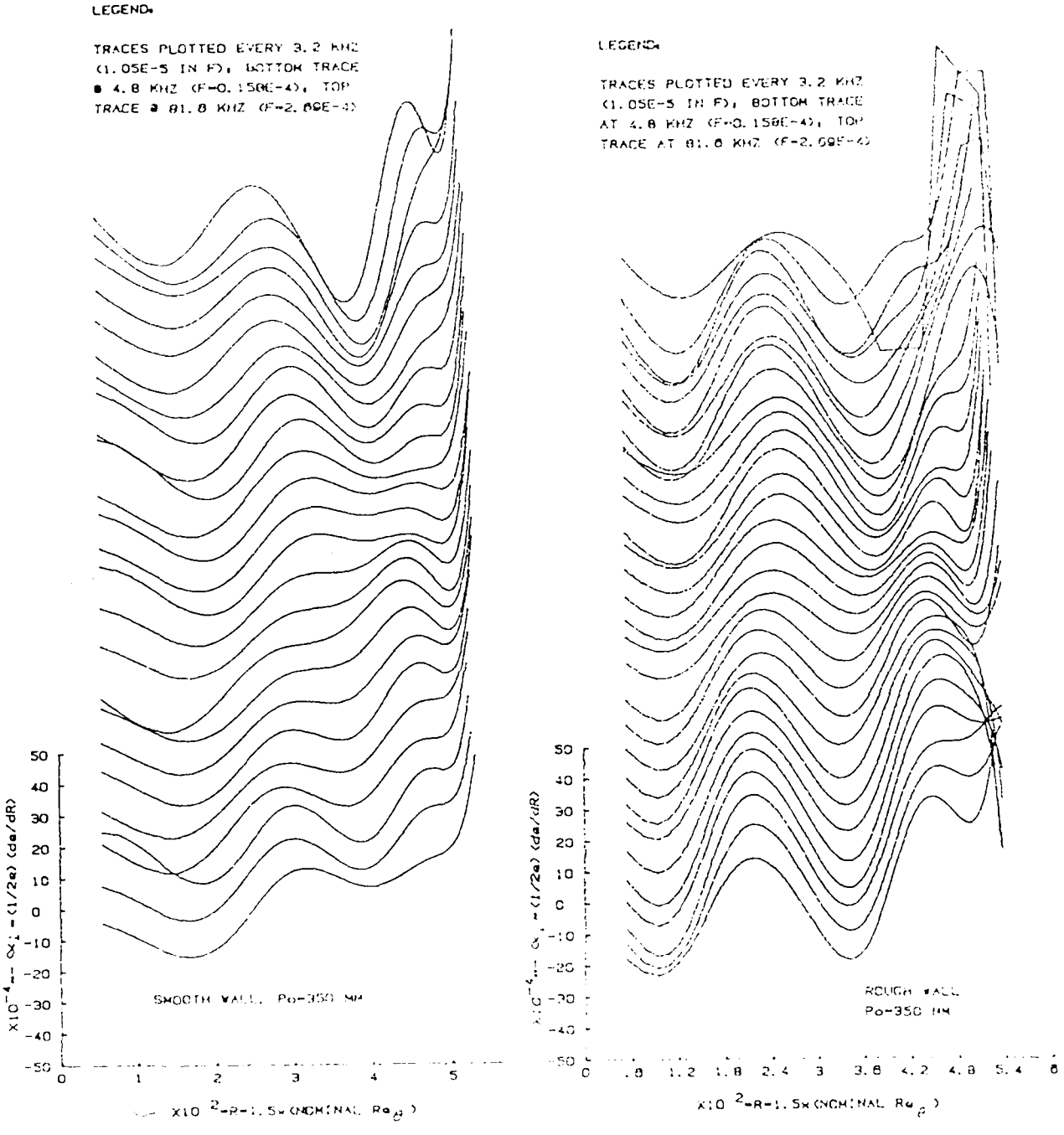

Figure 26. Amplification-rate summary vs Re_θ , p_o=350 torr.

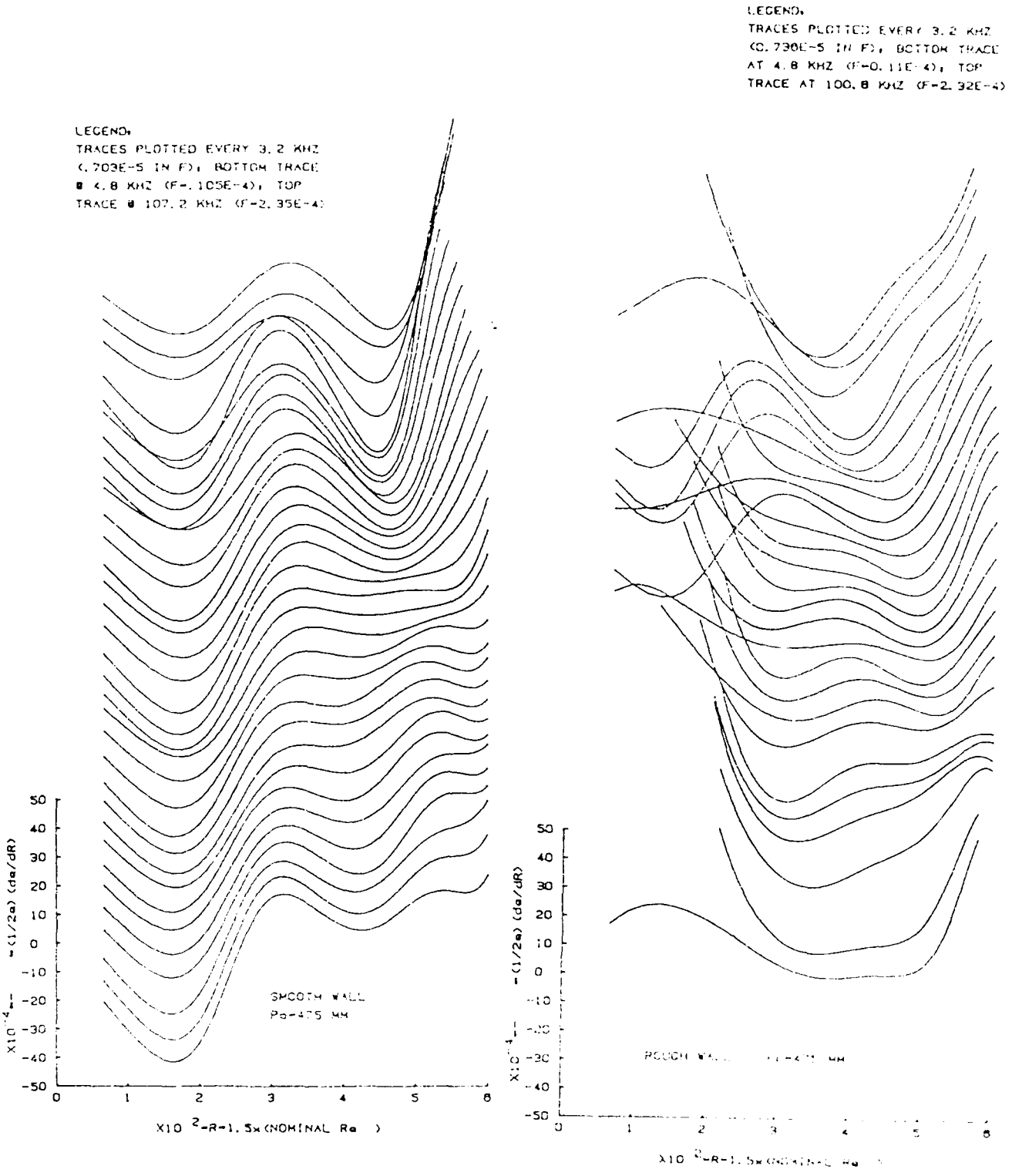

Figure 27. Amplification-rate summary vs Re_θ , p_o= 475 torr.

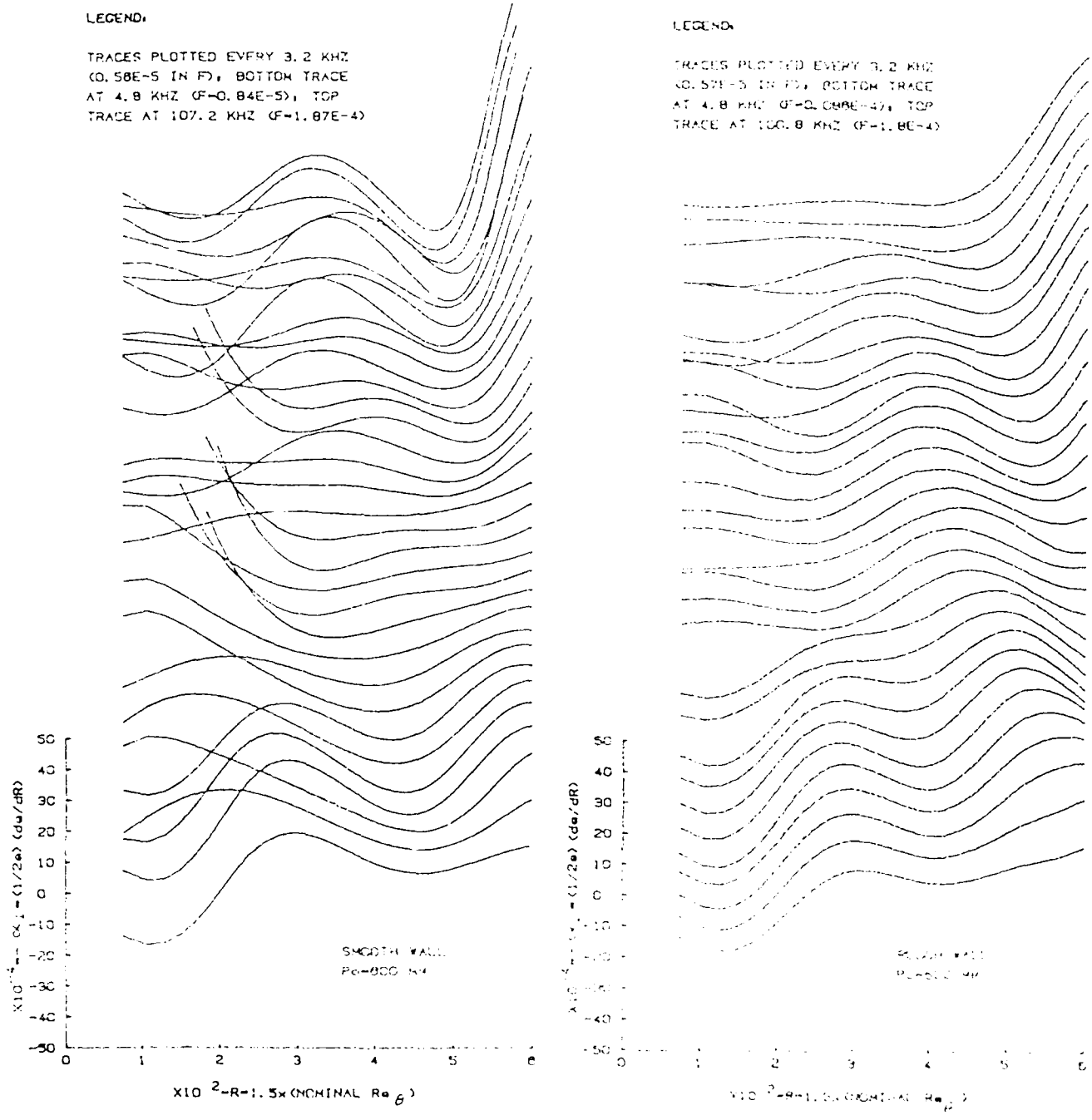

Figure 28. Amplification-rate summary vs Re_θ , p_o= 600 torr.

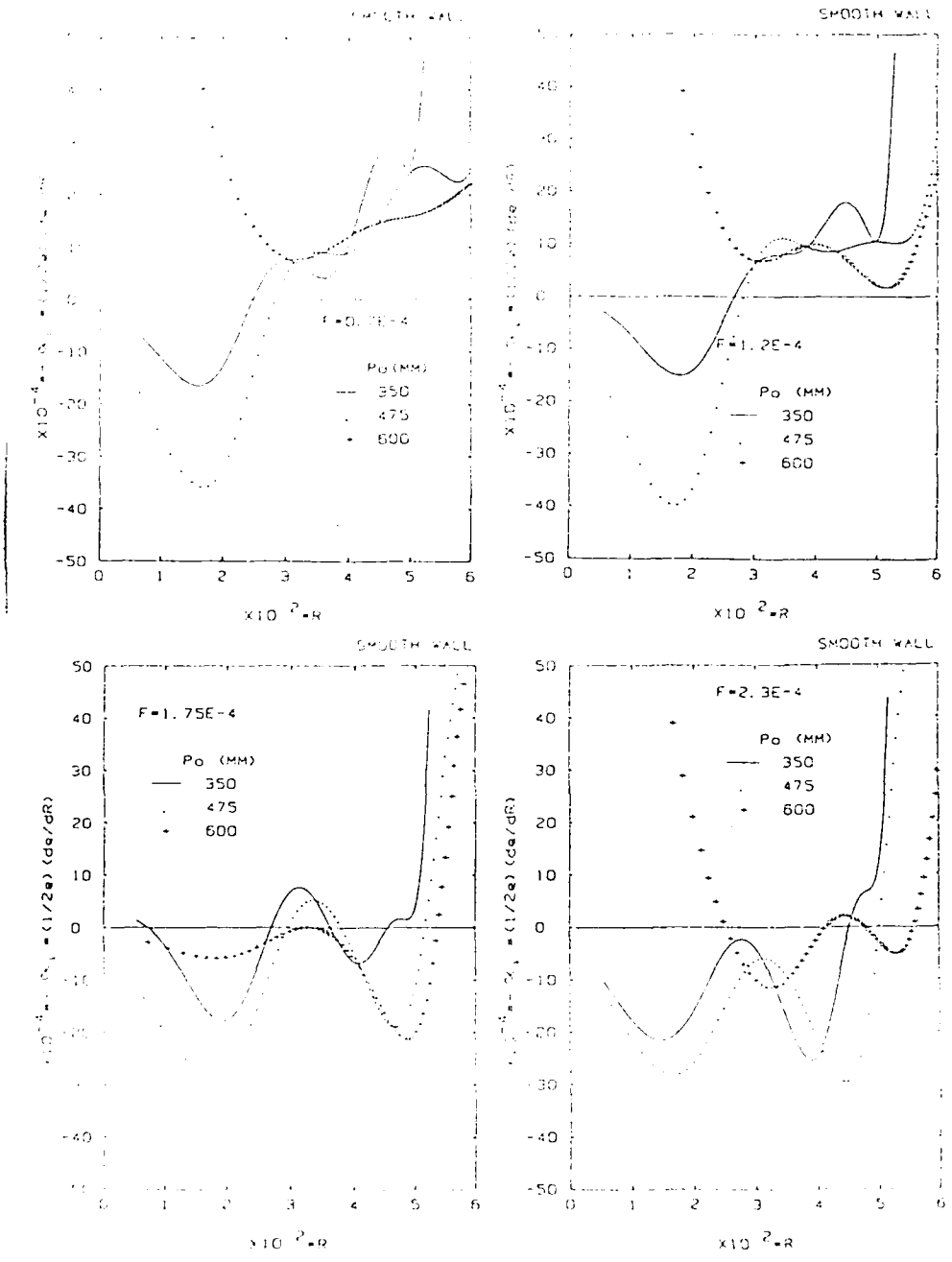

Figure 29. Effect of p_o on the amplification rates for the smooth wall.

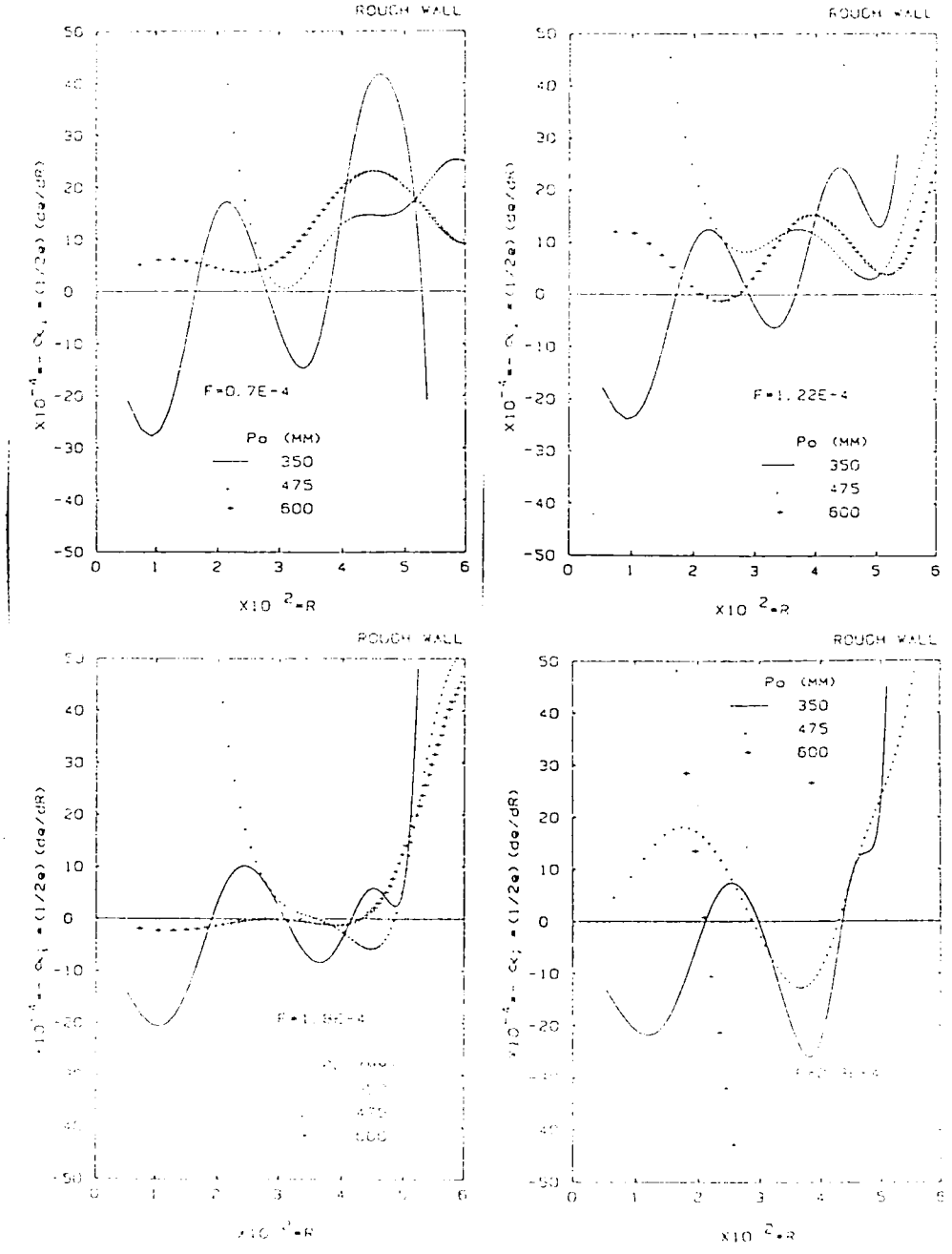

Figure 30. Effect of p_0 on the amplification rates for the rough wall.

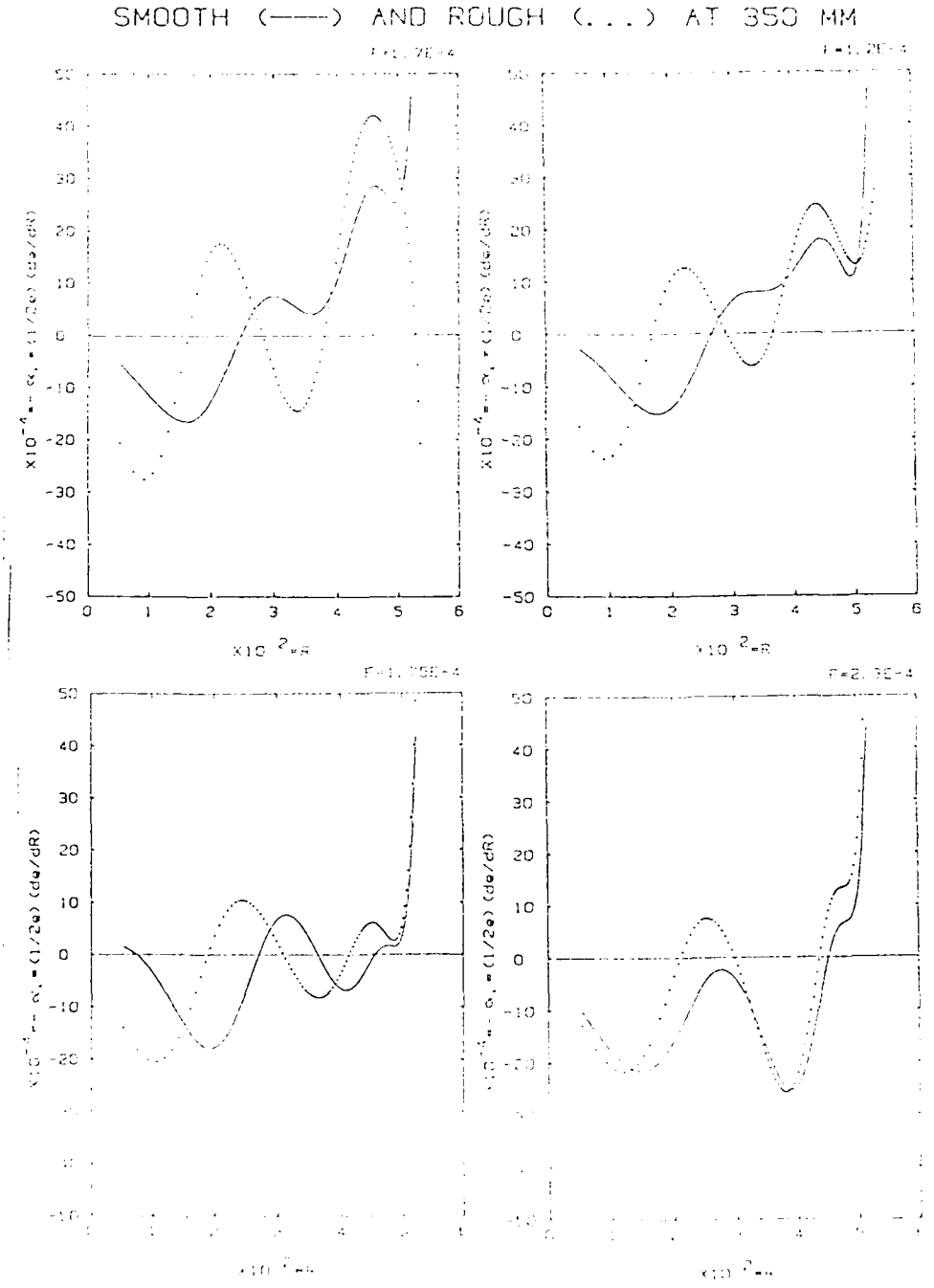

Figure 31. Effect of roughness on the amplification rates, p_o = 350 torr.

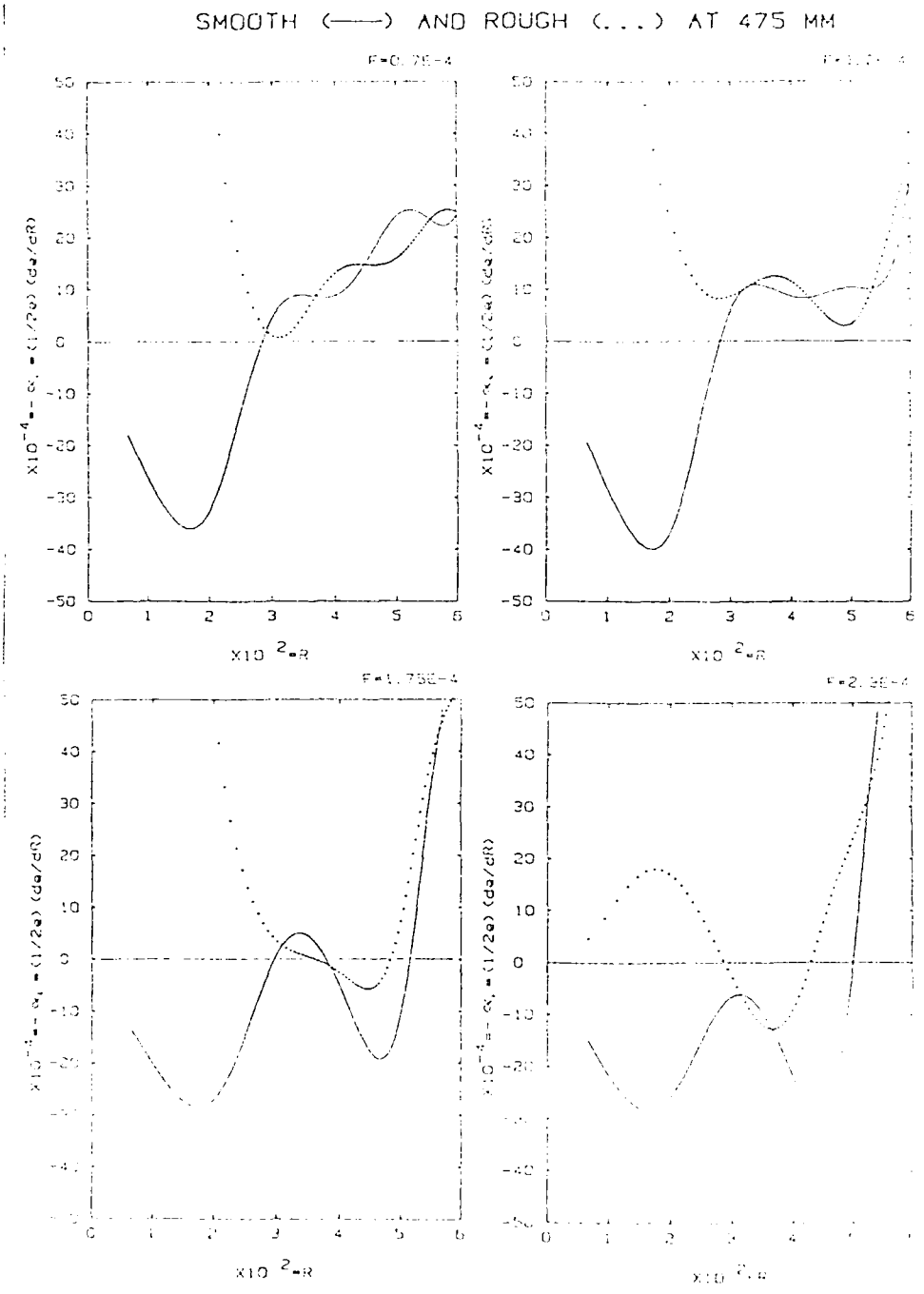

Figure 32. Effect of roughness on the amplification rates, p_o = 475 torr.

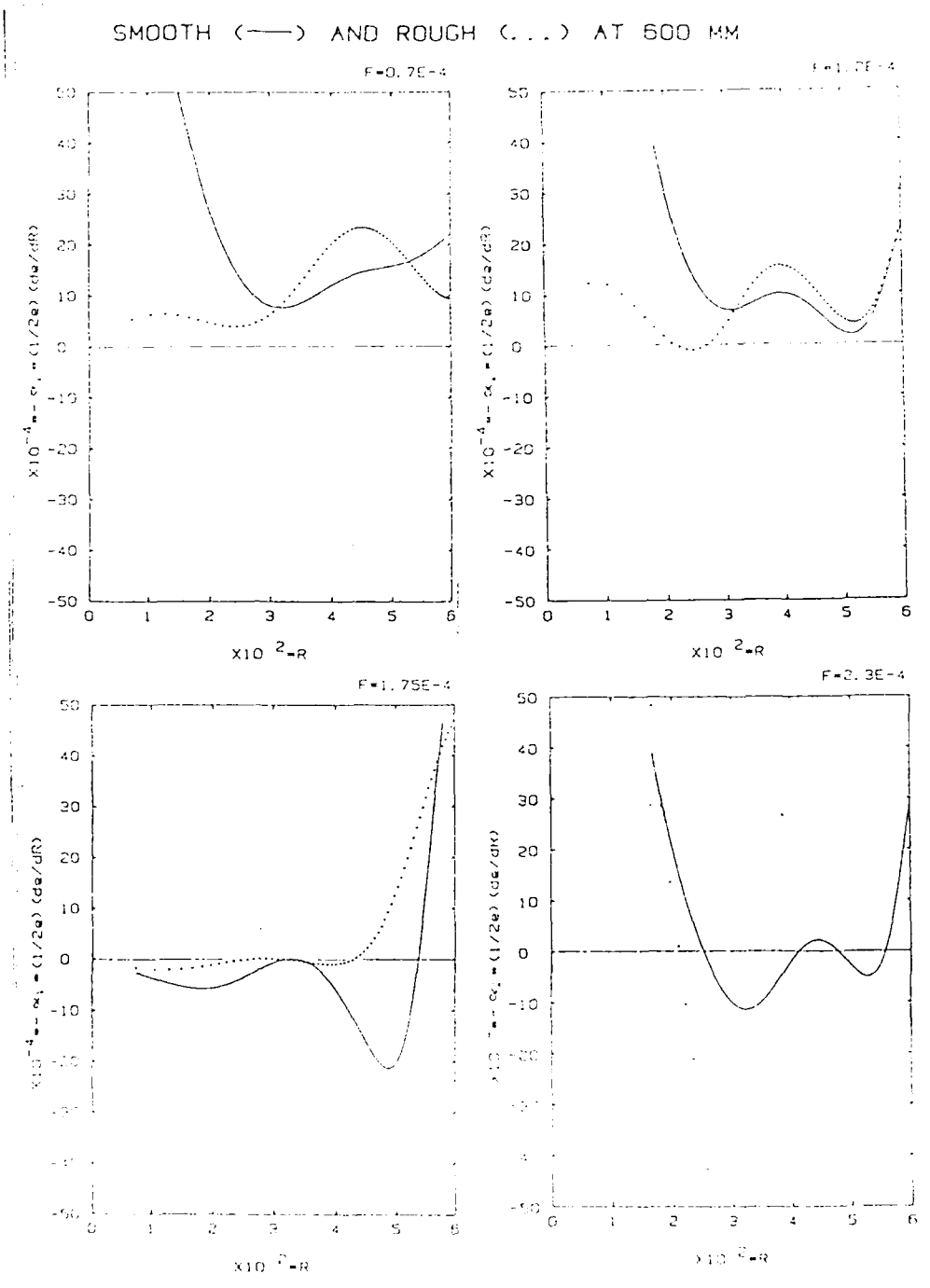

Figure 33. Effect of roughness on the amplification rates, p_0 = 600 torr.

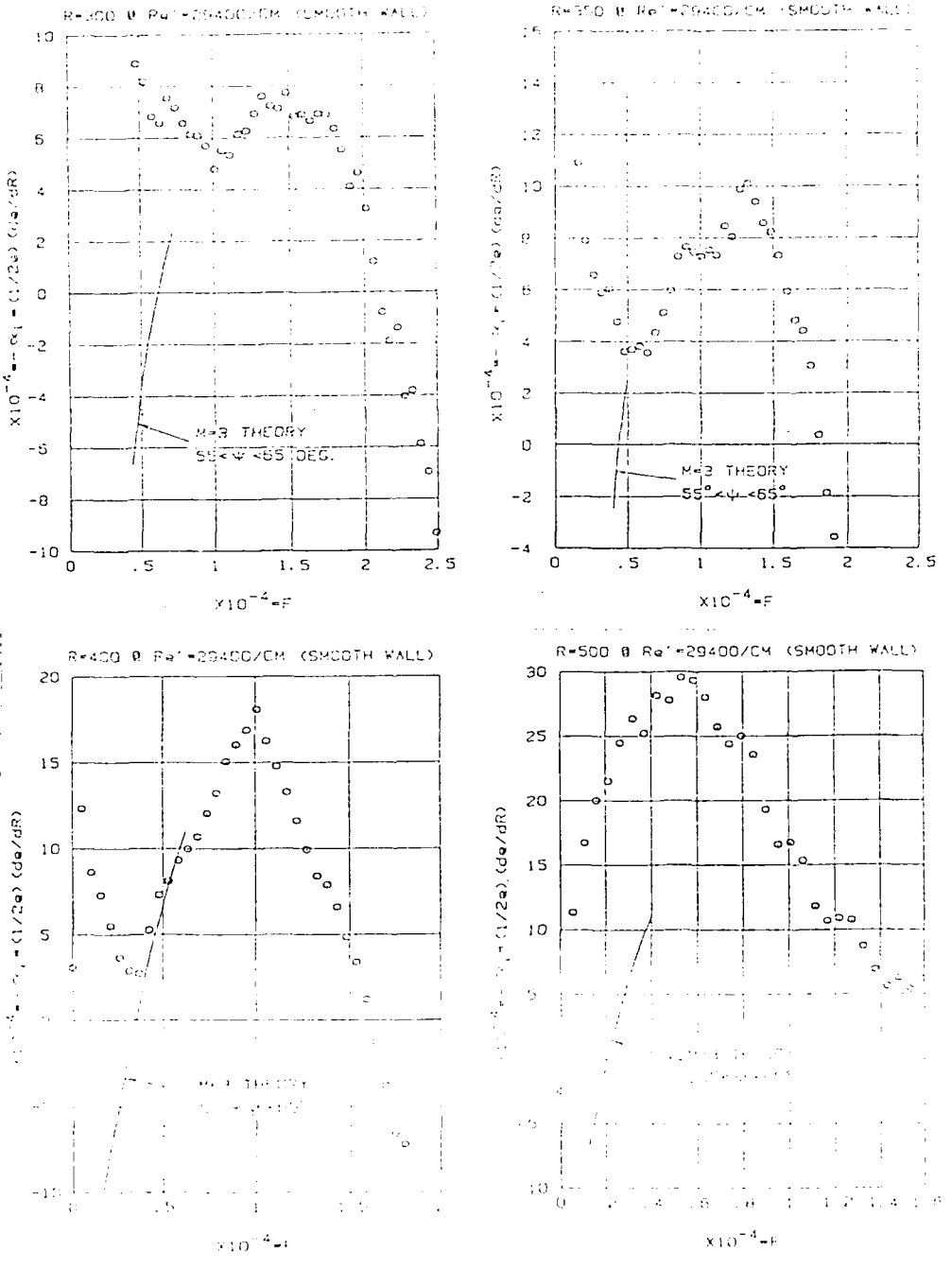

Figure 34. Selected smooth-wall amplification spectra, low R.

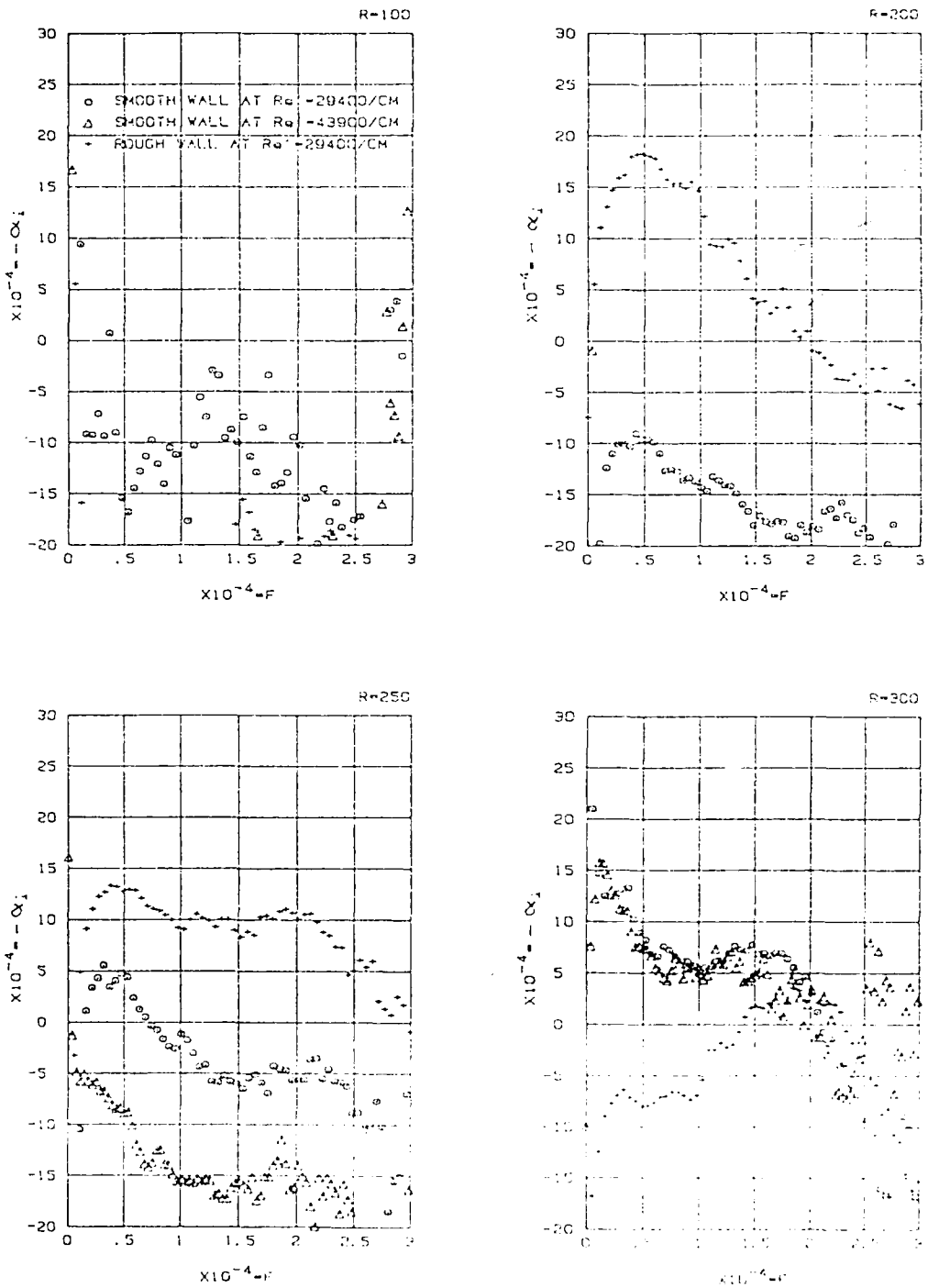

Figure 35. Typical amplification spectra in the "linear" region.

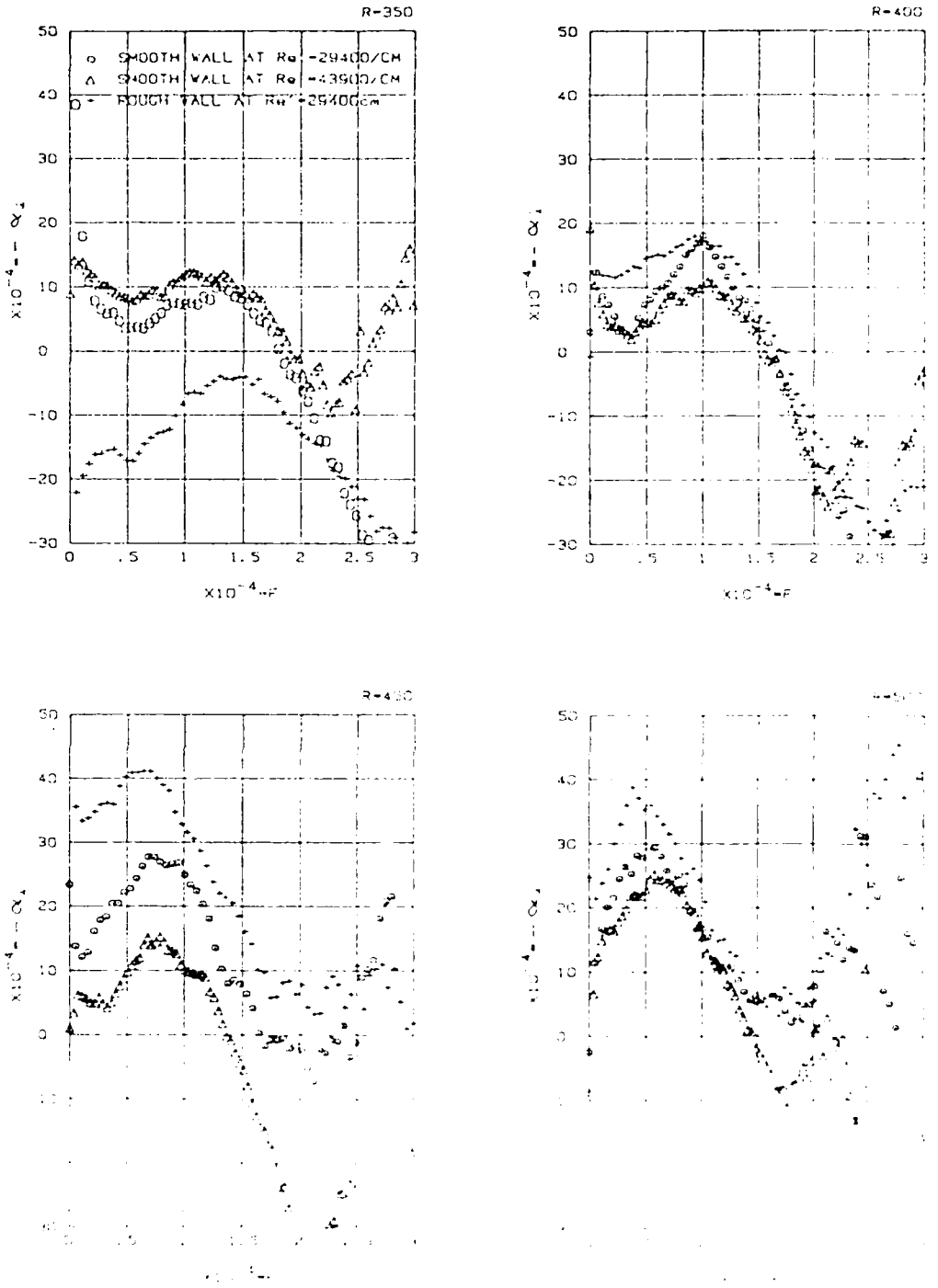

Figure 36. Typical amplification spectra approaching the transition zone.

PRESENT DATA (M=3):

o Po=350 MM HG (Re'=29400/CM)

Δ Po=475 MM HG (Re'=43900/CM)

□ LAUFER & VREBALOVICH
(M=2.2, Re'=29,500/CM)

Open symbols: lower neutral branch
Filled symbols: upper neutral branch

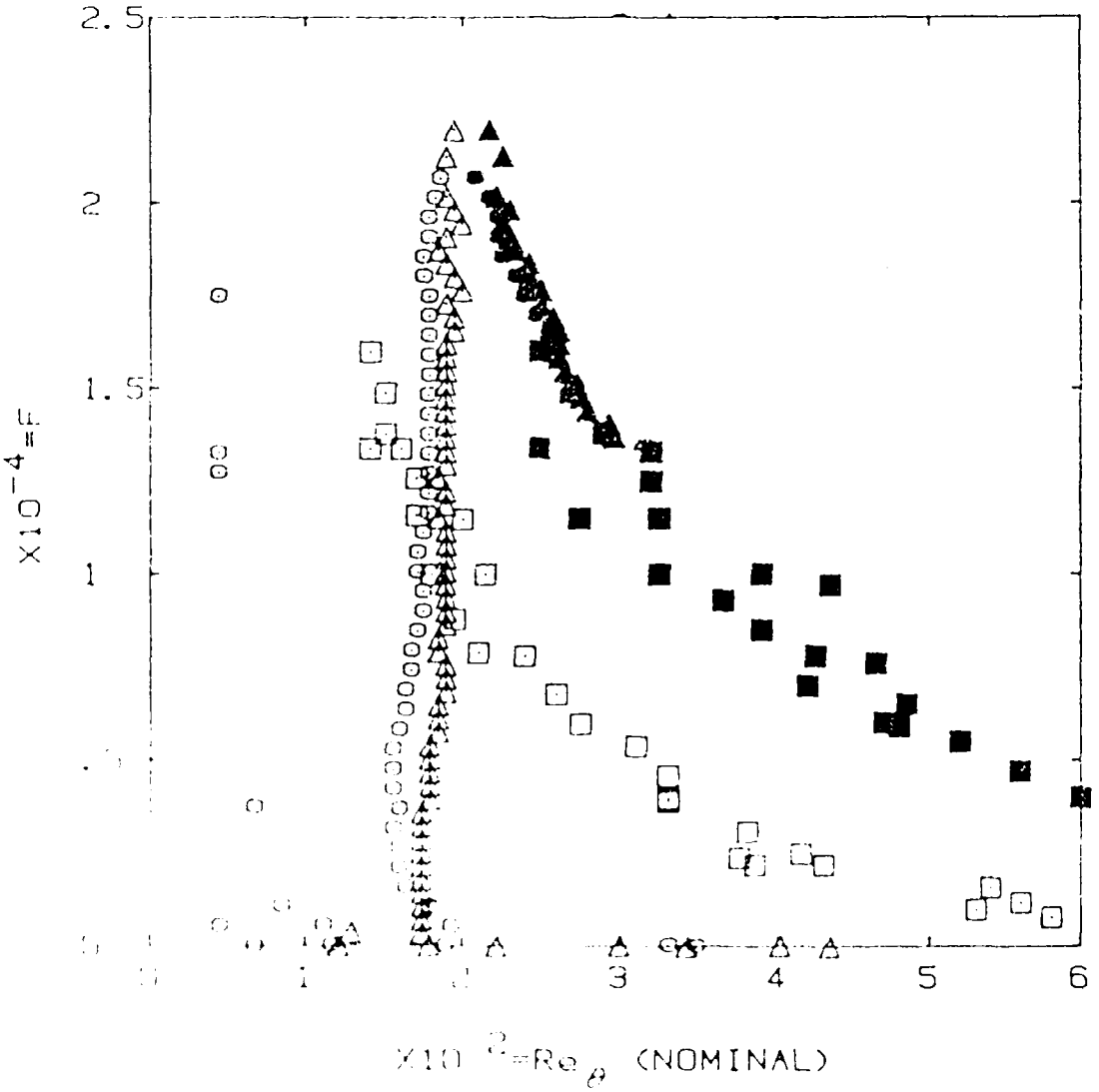

Figure 37. Stability diagram for smooth wall.

SYMBOL KEY FOR STABILITY DIAGRAMS:

SYMBOL	MEANING
o	LOWER NEUTRAL BRANCH
Δ	UPPER NEUTRAL BRANCH
+	AMPL. RATE MAXIMA
.	AMPL. RATE MINIMA

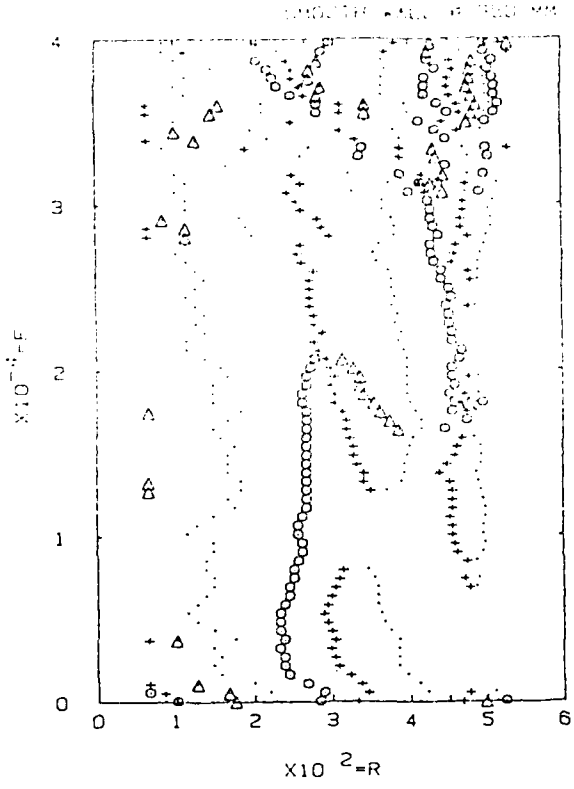

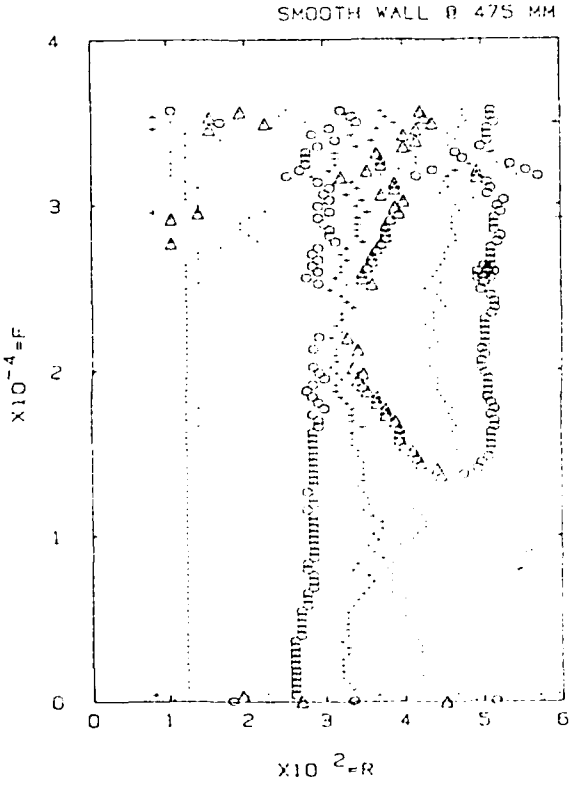

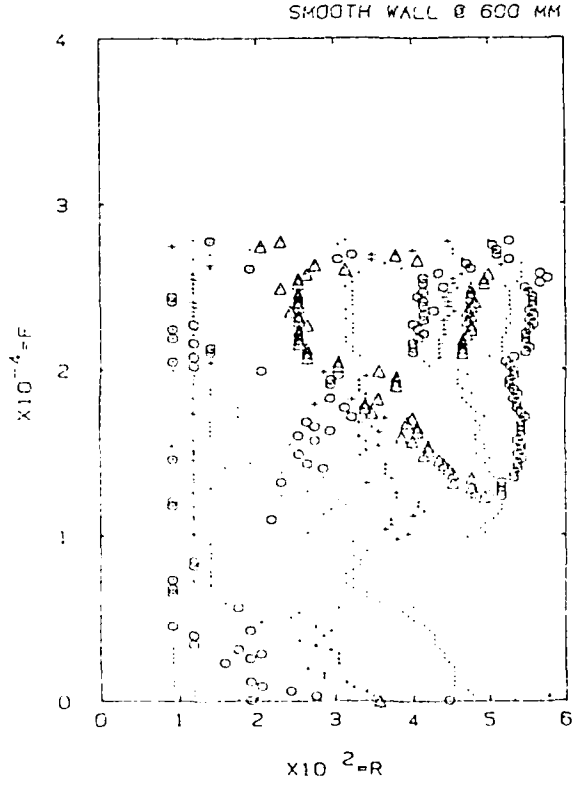

Figure 38. Extended stability diagrams for the smooth wall (all points included)

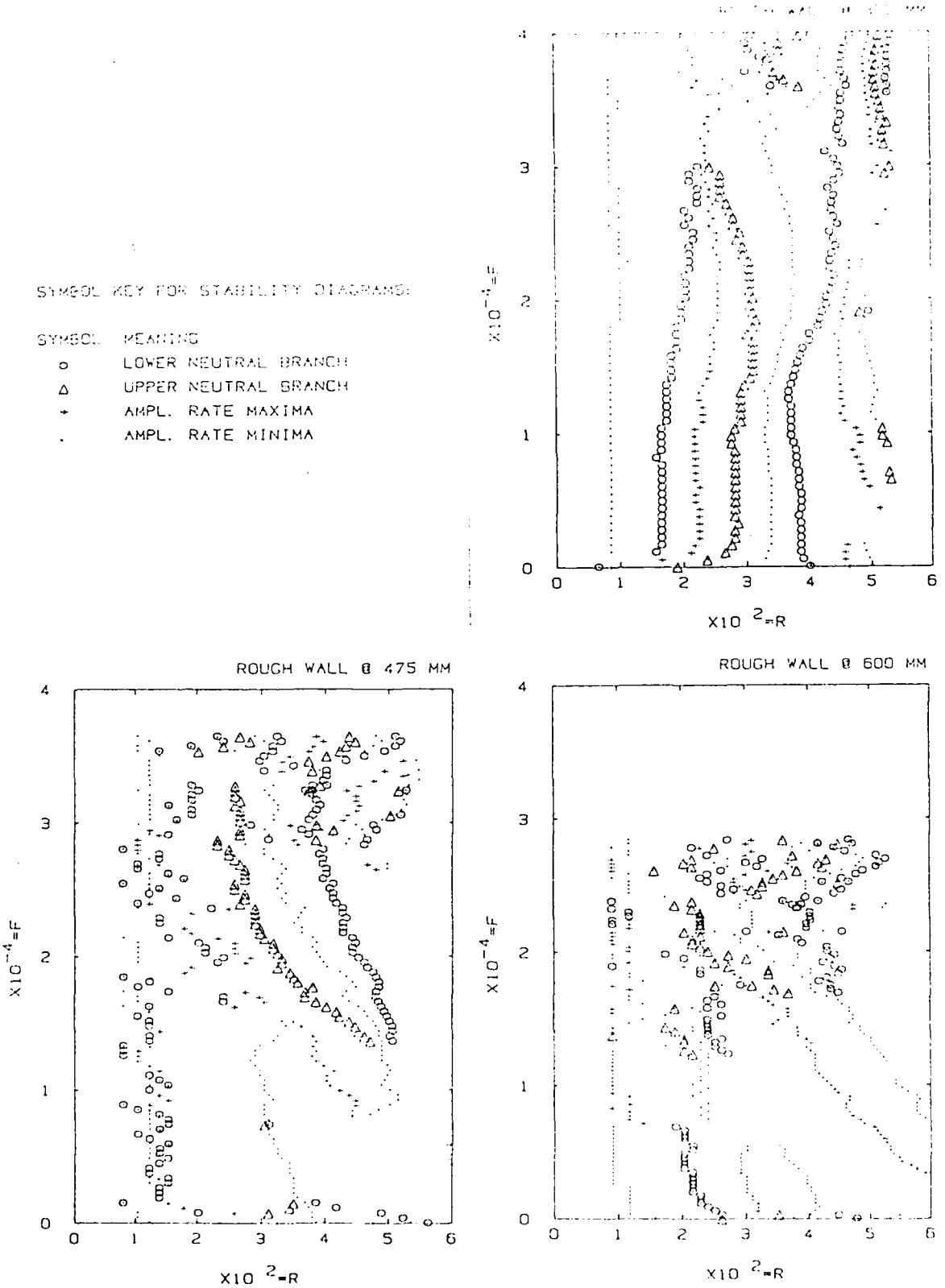

Figure 39. Extended stability diagrams for the rough wall (all points included):

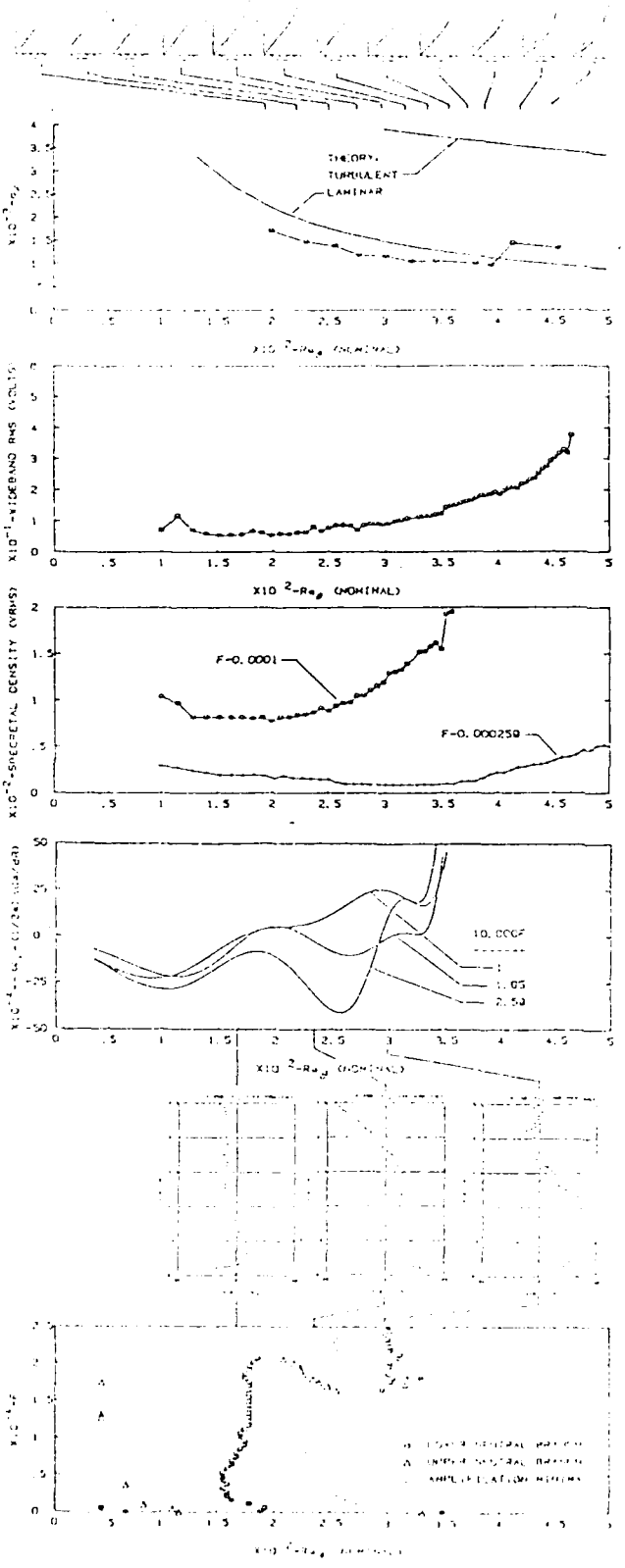

Figure 40. Summary overview at p_o= 350, smooth wall: (a) Velocity profiles, (b) friction coefficient, (c) wideband rms amplitude variation, (d) Amplitude variations at selected frquencies, (e) Typical amplification rates,(f)Typical amplification-rate spectra, (g) stability diagram. All are plotted vs the nominal Re .

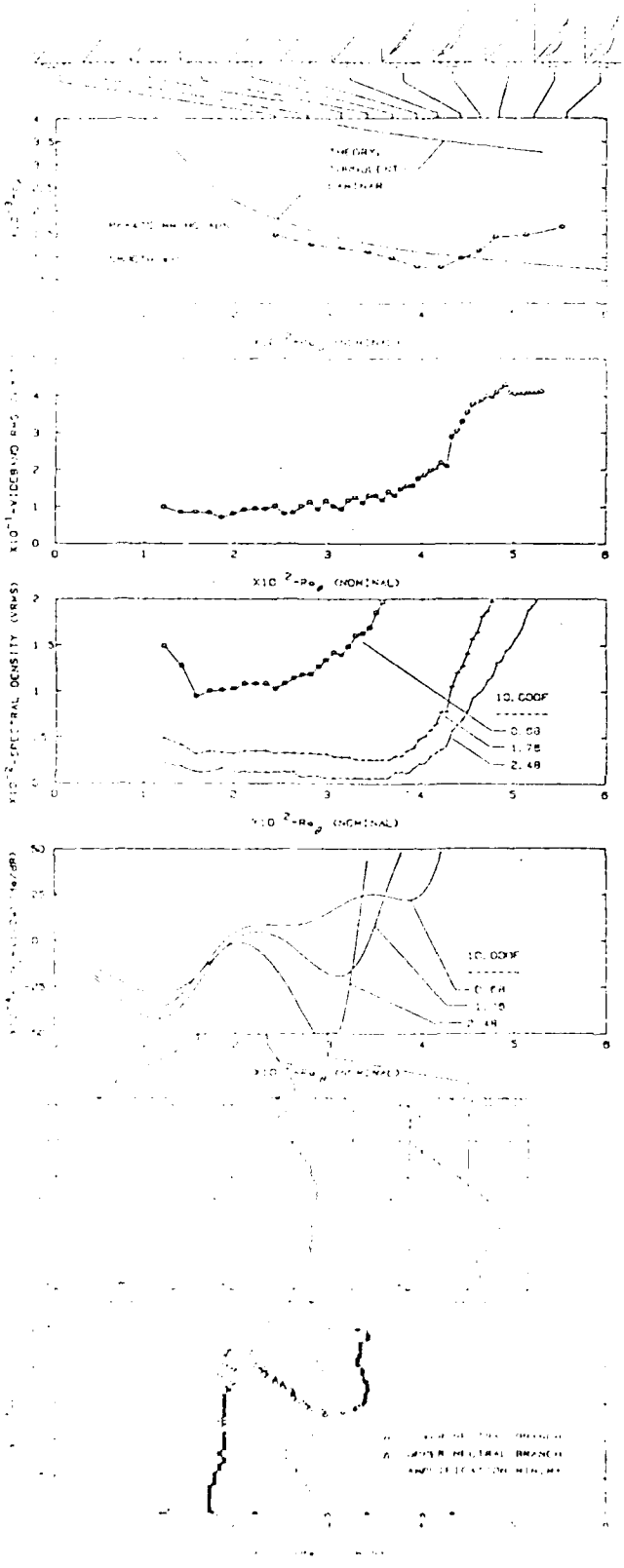

Figure 41. Summary overview at p_0= 475, smooth wall: (a) Velocity profiles, (b) friction coefficient, (c) wideband rms amplitude variation, (d) amplitude variations at selected frequencies, (e)Typical amplification rates, (f) typical amplification-rate spectra, (g) stability diagram. All are plotted vs the nominal Re .

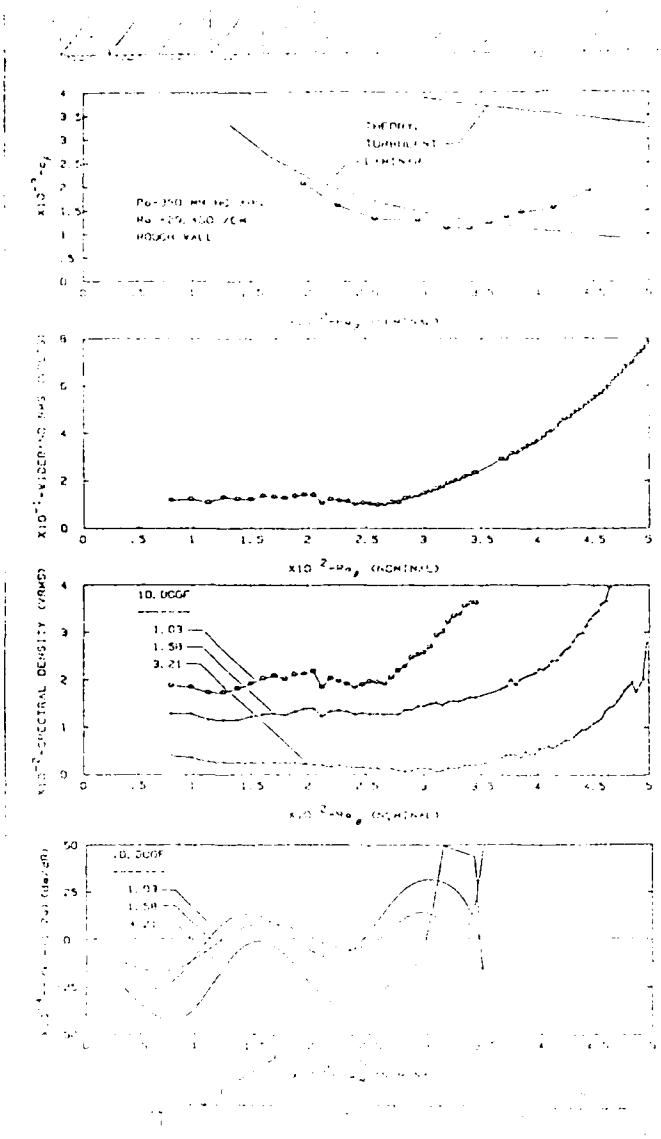

(a)

(b)

(c)

(d)

(e)

(f)

(g)

Figure 42. Summary overview at p_o = 350, rough wall: (a) Velocity profiles, (b) friction coefficient, (c) wideband rms amplitude variation, (d) amplitude variations at selected frequencies, (e)Typical amplification rates, (f) typical amplification-rate spectra, (g) stability diagram. All are plotted vs the nominal Re .

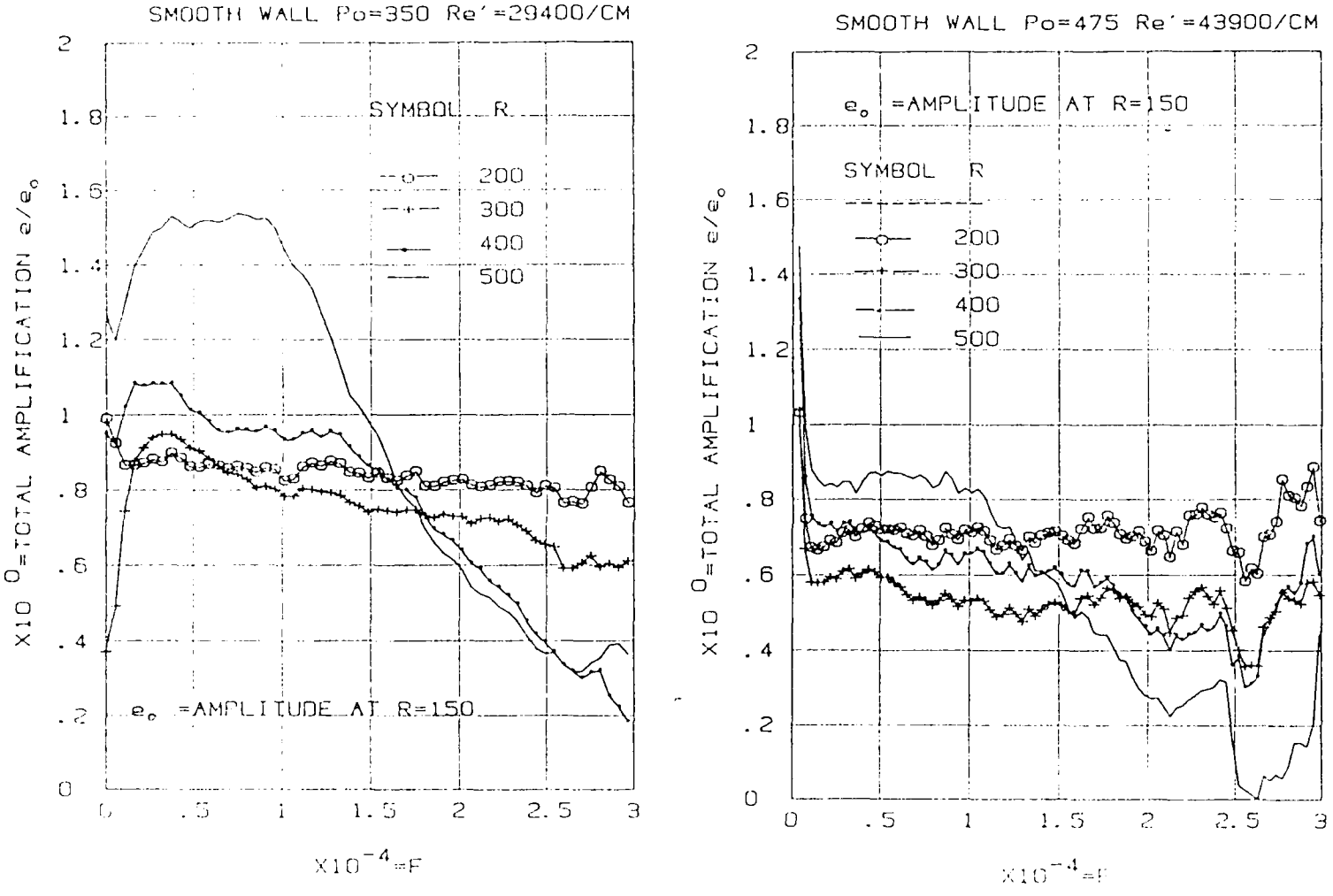

Figure 43. Total amplification achieved within the boundary layer at p_0 = 350 (left) and 475 (right), smooth wall.

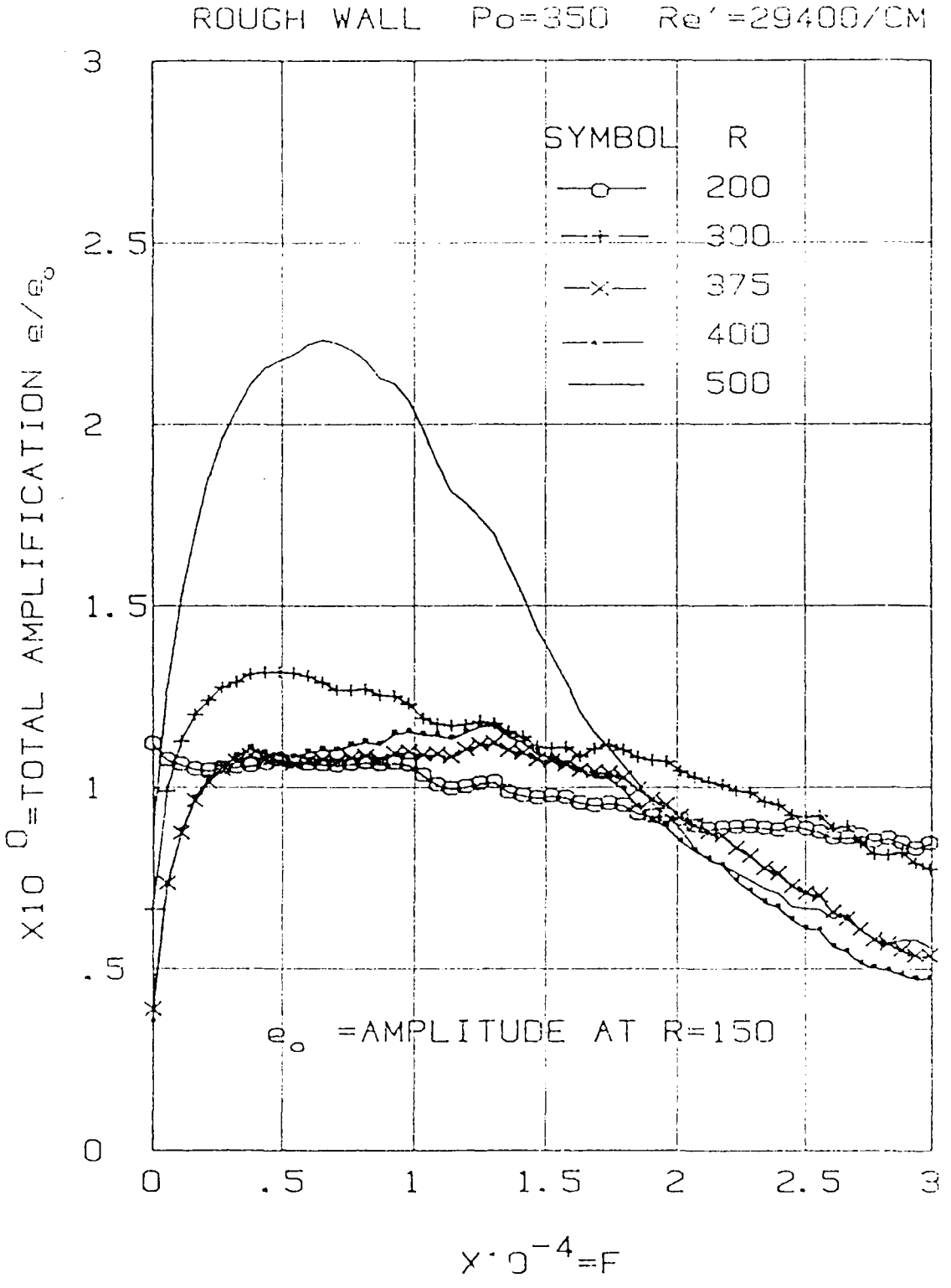

Figure 44. Total amplification achieved within the boundary layer at p_o=350, rough wall.

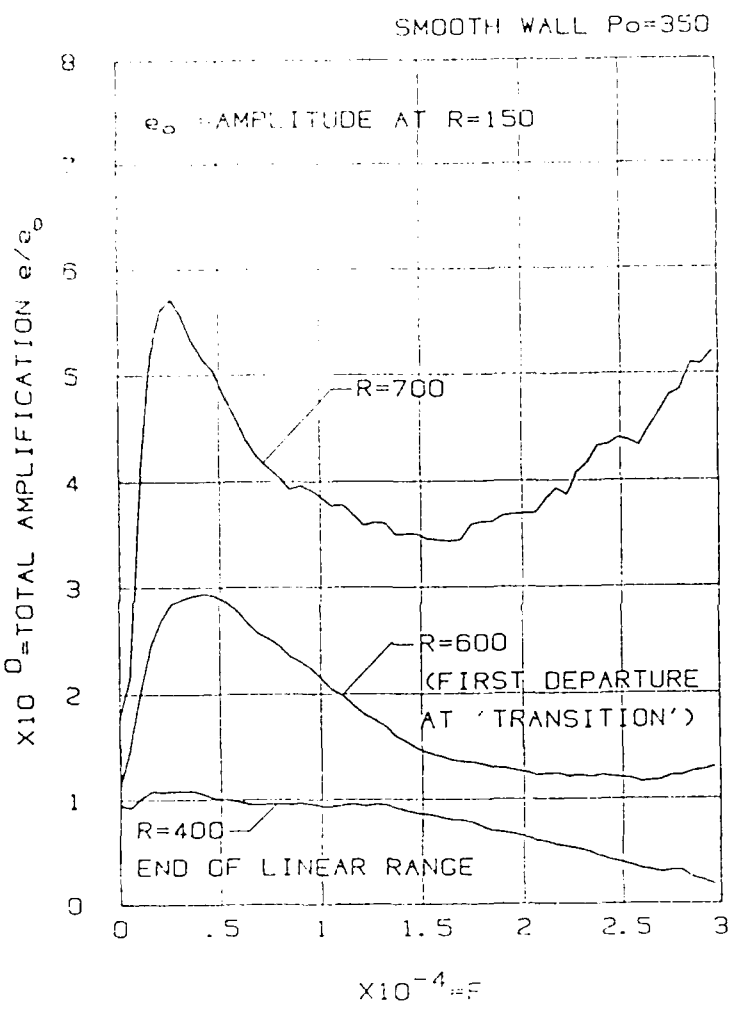

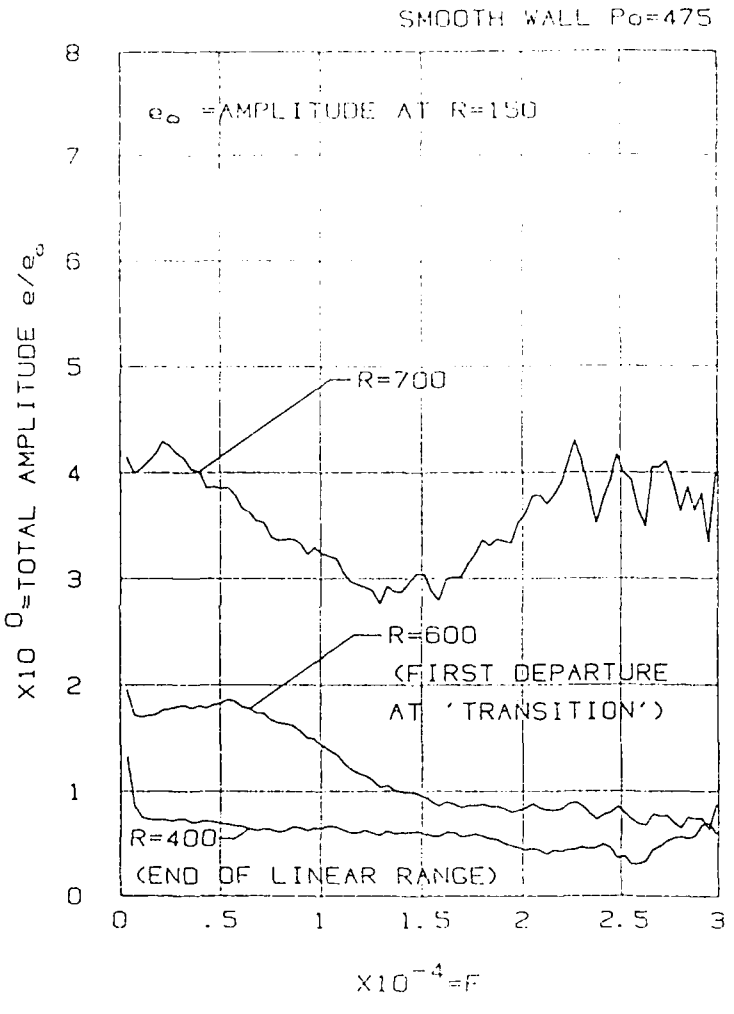

Figure 45. Linear, non-linear and transitional amplification within the boundary layer (smooth wall).

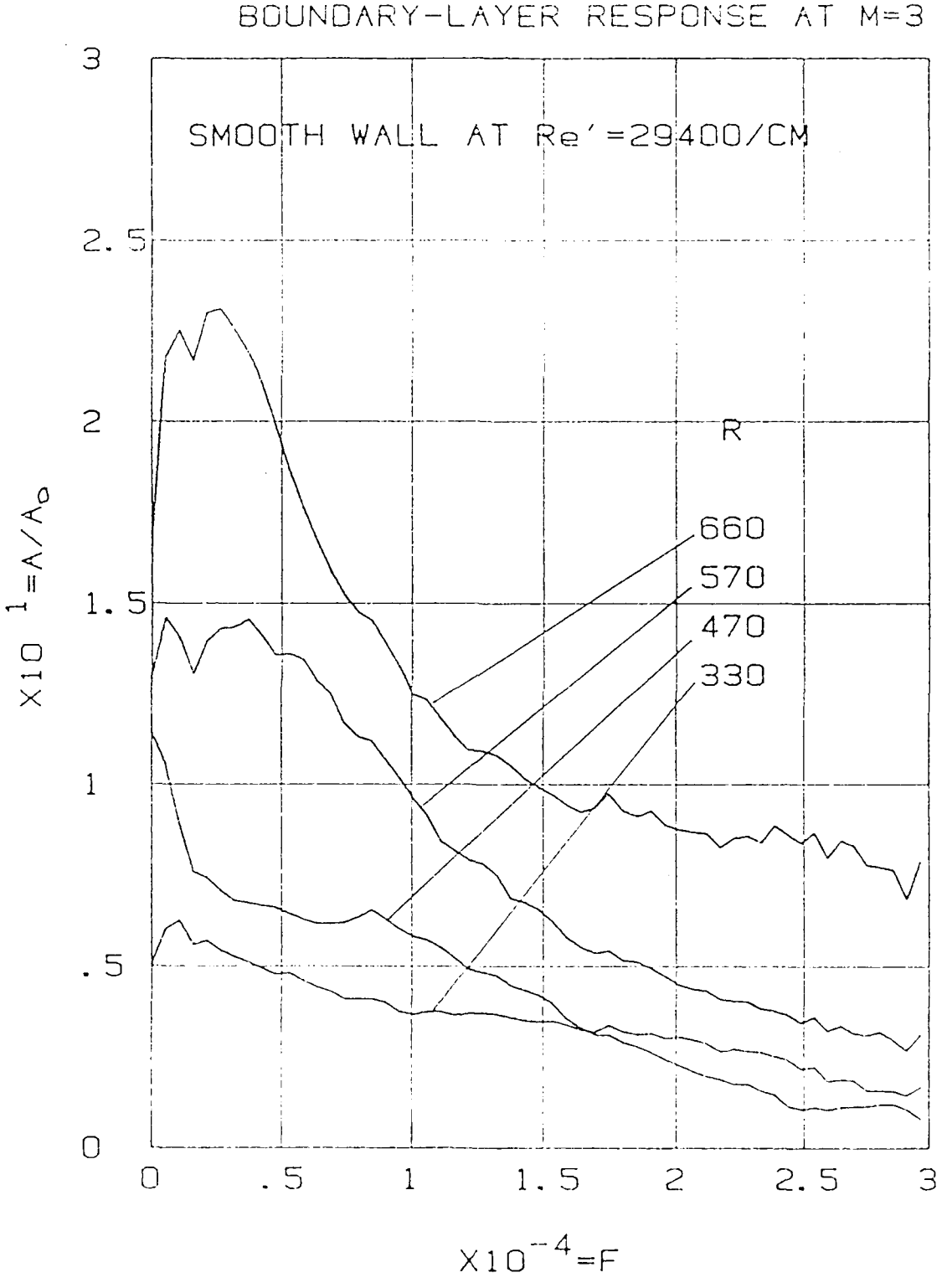

Figure 46. Spectrum of stream disturbance amplification achieved by the boundary layer at p_o = 350 torr (smooth wall)

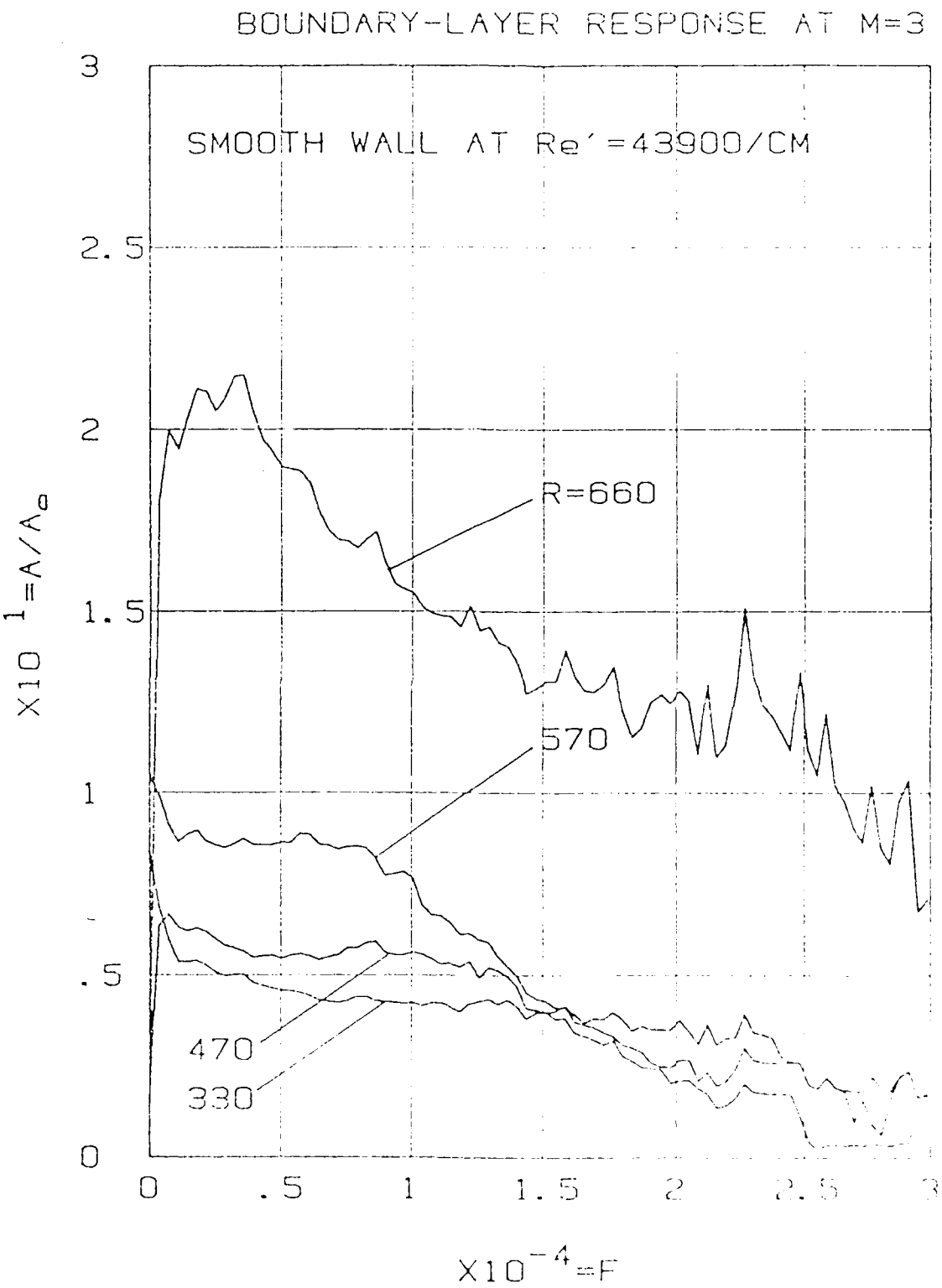

Figure 47. Spectrum of stream disturbance amplification achieved by the boundary layer at p_o= 475 torr (smooth wall).

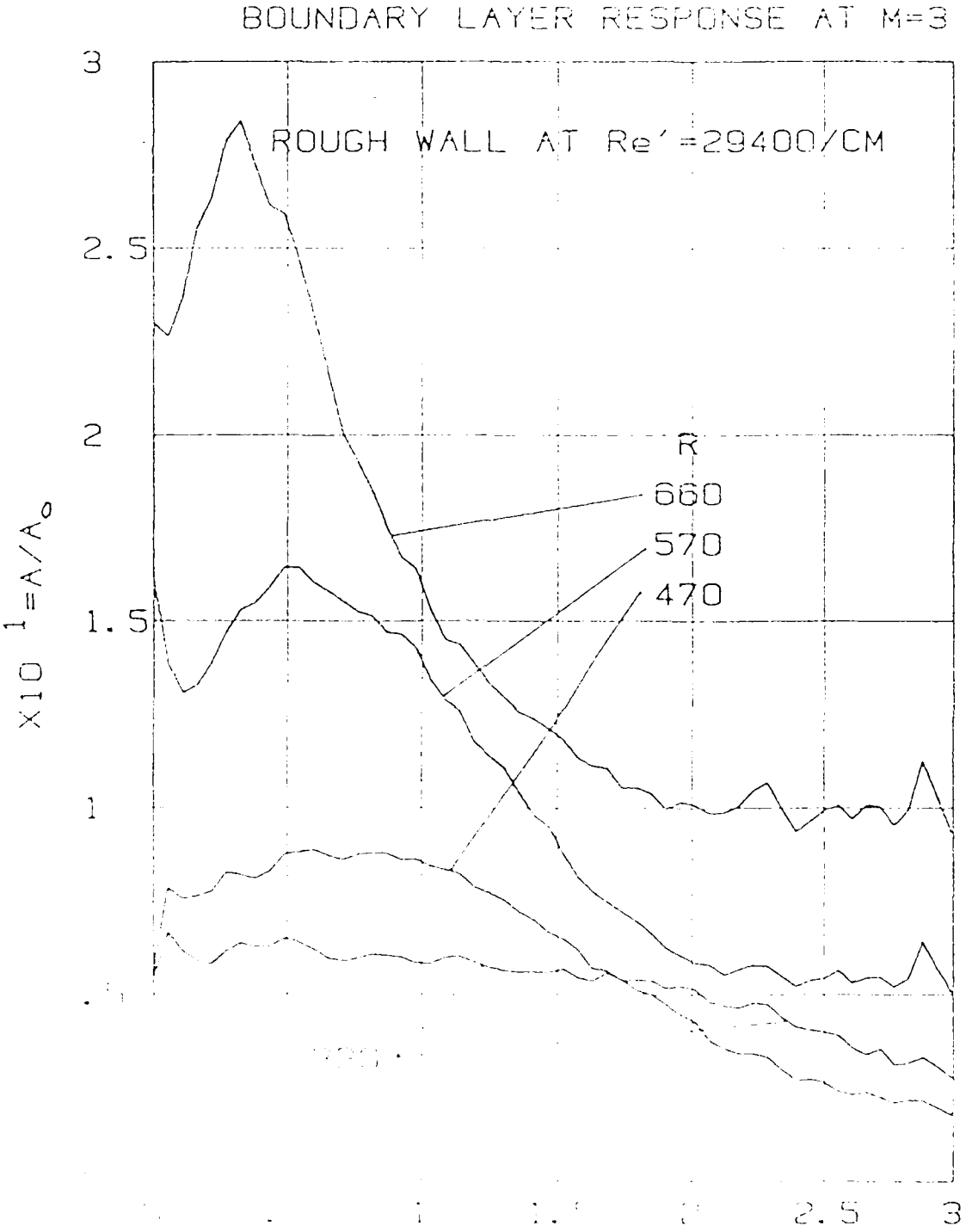

Figure 4a. Spectrum of stream disturbance amplification achieved by the boundary layer at [illegible] torr [illegible] wall.

END

5-87

DTIC